

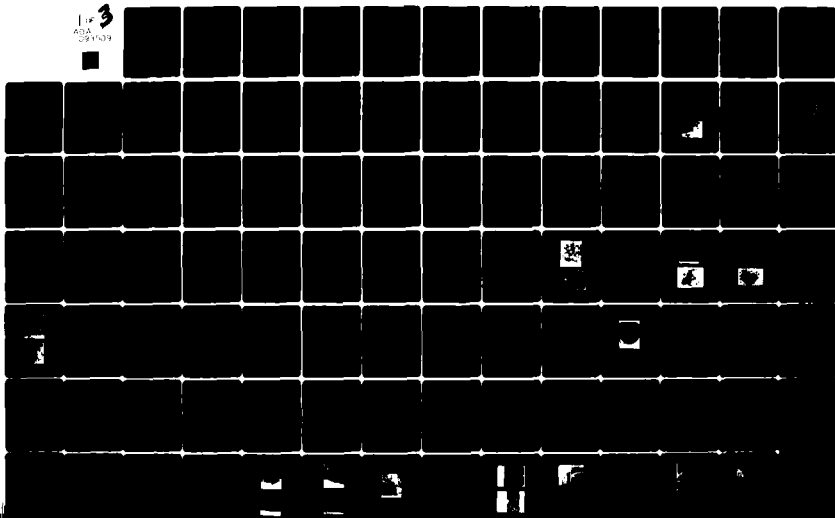
AD-A093 509

AIR FORCE WRIGHT AERONAUTICAL LABS WRIGHT-PATTERSON AFB OH F/6 11/6
THE EFFECT OF DEFECTS ON THE FATIGUE INITIATION PROCESS IN TWO --ETC(U)
SEP 80 J M HYZAK
AFWAL-TR-80-4063

UNCLASSIFIED

NL

1 of 3
ADA
SEP 1989





AFWAL-TR-80-4063

LEVEL

2

AD A093509

THE EFFECT OF DEFECTS ON THE FATIGUE INITIATION
PROCESS IN TWO P/M SUPERALLOYS

Jack M. Hyzak, Capt, USAF
Metals Behavior Branch
Metals and Ceramics Division

DTIC
JAN 5 1981
C

September 1980

TECHNICAL REPORT AFWAL-TR-80-4063

Final Report for Period November 1977 - November 1979

Approved for public release; distribution unlimited

DDC FILE COPY

MATERIALS LABORATORY
AIR FORCE WRIGHT AERONAUTICAL LABORATORIES
AIR FORCE SYSTEMS COMMAND
WRIGHT-PATTERSON AIR FORCE BASE, OHIO 45433

81 1 05 023

NOTICE

When Government drawings, specifications, or other data are used for any purpose other than in connection with a definitely related Government procurement operation, the United States Government thereby incurs no responsibility nor any obligation whatsoever; and the fact that the government may have formulated, furnished, or in any way supplied the said drawings, specifications, or other data, is not to be regarded by implication or otherwise as in any manner licensing the holder or any other person or corporation, or conveying any rights or permission to manufacture, use, or sell any patented invention that may in any way be related thereto.

This report has been reviewed by the Office of Public Affairs (ASD/PA) and is releasable to the National Technical Information Service (NTIS). At NTIS, it will be available to the general public, including foreign nations.

This technical report has been reviewed and is approved for publication.



THEODORE NICHOLAS, Project Engineer
Metals Behavior Branch
Metals and Ceramics Division



NATHAN G. TUPPER, Chief
Metals Behavior Branch
Metals and Ceramics Division

"If your address has changed, if you wish to be removed from our mailing list, or if the addressee is no longer employed by your organization please notify AFWAL/MLLN, W-PAFB, OH 45433 to help us maintain a current mailing list".

Copies of this report should not be returned unless return is required by security considerations, contractual obligations, or notice on a specific document.

SECURITY CLASSIFICATION OF THIS PAGE (When Data Entered)

12

229

REPORT DOCUMENTATION PAGE

READ INSTRUCTIONS
BEFORE COMPLETING FORM

14

1. REPORT NUMBER
AFWAL-TR-80-40637

2. GOVT ACCESSION NO.
AD A093509

3. RECIPIENT'S CATALOG NUMBER

6

4. TITLE (and Subtitle)
THE EFFECT OF DEFECTS ON THE FATIGUE INITIATION
PROCESS IN TWO P/M SUPERALLOYS

9

5. TYPE OF REPORT & PERIOD COVERED
Final Report
November 1977-November 1979

6. PERFORMING ORG. REPORT NUMBER

10

7. AUTHOR(s)
Jack M. Hyzak Capt, USAF

8. CONTRACT OR GRANT NUMBER(s)

9. PERFORMING ORGANIZATION NAME AND ADDRESS
Materials Laboratory (AFWAL/MLLN)
AF Wright Aeronautical Laboratories, AFSC
Wright-Patterson Air Force Base, Ohio 45433

16

10. PROGRAM ELEMENT, PROJECT, TASK
AREA & WORK UNIT NUMBERS

2307 P1 02

17 P1

11. CONTROLLING OFFICE NAME AND ADDRESS
Materials Laboratory (AFWAL/MLLN)
AF Wright Aeronautical Laboratories, AFSC
Wright-Patterson Air Force Base, Ohio 45433

12. REPORT DATE
July 1980

13. NUMBER OF PAGES
229

14. MONITORING AGENCY NAME & ADDRESS (if different from Controlling Office)

11 Sep 80

15. SECURITY CLASS. (of this report)

Unclassified

15a. DECLASSIFICATION/DOWNGRADING
SCHEDULE

16. DISTRIBUTION STATEMENT (of this Report)

Approved for public release; distribution unlimited.

61 J2F

17. DISTRIBUTION STATEMENT (of the abstract entered in Block 20, if different from Report)

18. SUPPLEMENTARY NOTES

19. KEY WORDS (Continue on reverse side if necessary and identify by block number)

Defects	Low Cycle Fatigue	AF2-1DA
Inclusions	Crack Initiation	Creep-Fatigue
Porosity	AF-115	Superalloys

20. ABSTRACT (Continue on reverse side if necessary and identify by block number)

A metallurgical investigation was performed to determine the effect of defect size, shape, and population on the fatigue initiation process in two high strength P/M superalloys, AF-115 and AF2-1DA. The specific alloy heats tested had contrasting defect populations; the AF-115 alloy contained a large population of spherical pores, and a lesser number of elliptical ceramic inclusions and plate-like hafnium oxide inclusions, and the AF2-1DA material contained only a small population of the elliptically shaped inclusions.

(over)

392662 DM

20. Abstract (Cont'd)

Strain controlled fatigue tests were performed on uniform section specimens at 760°C, 649°C, and 22°C using both continuously cycling and cyclic dwell waveforms.

Microscopic examination of the failed specimens showed that for the high temperature tests there was a transition in the nucleation site of the cracks that caused failure from a surface to a subsurface location as the strain range was reduced. This surface-subsurface transition (SST) occurred at approximately the same strain range for both alloys. An explanation for this phenomenon is developed by first considering individually the crack initiation and crack propagation phases of the fatigue process, and hypothesizing that crack initiation is controlled by localization of plastic strain, and crack propagation is a function of the environment and the stress intensity at the crack tip. The results indicated that at high strain ranges the crack propagation phase of fatigue life was most critical and, therefore, defect size and population were most important. At the lower strain ranges, the initiation phase of life was more critical in the overall fatigue process and defect shape was shown to be of primary concern.

Finally, a significant creep-fatigue interaction is shown to occur for specimens tested at elevated temperature with a tensile dwell cycle while those specimens tested with a compressive dwell cycle failed in the same manner as the continuously cycling tests. The fatigue data are analyzed to show the effects of cyclic dwell cycles on both the crack initiation and propagation phases of the fatigue process.

Accession For		<input checked="" type="checkbox"/>
NTIS Grant		<input type="checkbox"/>
DTIC TAB		<input type="checkbox"/>
Unannounced		
Justification		
BY _____		
Distribution/		
Availability Codes		
Dist	Avail and/or	Special
A		

FOREWORD

This technical report was prepared by the Metals Behavior Branch, Metals and Ceramics Division, Materials Laboratory, Air Force Wright Aeronautical Laboratories, Wright-Patterson Air Force Base, Ohio. The research was conducted under Project No. 2307, "Solid Mechanics". Task 2307P102, "Failure Prediction in Metals". This report includes work performed during the period July 1976 to September 1979. The research was performed by Capt. Jack M. Hyzak.

The high temperature strain control testing was performed by Mar-Test Inc. under Materials Laboratory contract F33615-76-C-5245. The author gratefully acknowledges the valuable discussions with Messrs. Stentz, Conway, and Berling of Mar-Test Inc.

The author also wishes to sincerely thank Dr. W. H. Reimann, Mr. N. G. Tupper, Dr. T. Nicholas, Dr. V. J. Russo, Dr. A. F. Grandt, and Mr. L. N. Hjelm of the Materials Laboratory for encouragement, support, and technical assistance throughout the course of this study. The technical assistance of Lt. S. Doerr of AFML is also gratefully acknowledged.

I would also like to sincerely thank my thesis advisor, Professor Mel Bernstein of the Department of Metallurgy and Material Science, Carnegie-Mellon University for his guidance and encouragement. Also, Professors J. C. Williams, A. W. Thompson, and J. L. Swedlow of Carnegie-Mellon University contributed valuable discussions.

Thanks is also due to Dr. N. T. Ashbaugh of Systems Research Laboratories, Dr. G. R. Leverant of the Southwest Research Institute, and Prof. S. Antolovich of the University of Cincinnati for very valuable discussions. The help of Dr. John Cammett of Metcut Research Associates in providing technical assistance with the residual stress measurements and interpretation of the data is also gratefully acknowledged. The personnel of Systems Research Laboratories are also thanked for their assistance, especially R. Bacon, R. Omlor, R. Brodecki, C. Conway, and E. Keppler.

AFWAL-TR-80-4063

TABLE OF CONTENTS

SECTION	PAGE
I INTRODUCTION	1
II LITERATURE REVIEW	5
1. Introduction	5
2. Microstructure	6
3. Overview	11
4. Deformation Modes and Initiation Mechanisms	13
5. Oxidation	17
6. Defects	20
7. Creep-Fatigue Interactions	25
8. Analytical Modeling of High Temperature Fatigue	28
9. Summary	29
III MATERIALS	30
1. Processing	30
2. Microstructure	33
3. Defects	38
4. Summary	40
IV EXPERIMENTAL PROCEDURES	44
1. Fatigue Testing	44
2. Metallographic Examination	48
V TEST RESULTS	51
1. Tensile Properties	51
2. Fatigue Test Results	56
3. Summary	64

TABLE OF CONTENTS (Cont'd)

SECTION	PAGE
VI CRACK INITIATION MODES - ELEVATED TEMPERATURE CONTINUOUSLY CYCLING FATIGUE	66
1. Overview - Fatigue Origins	66
2. Surface Initiation - High Strain Range	68
3. Subsurface Initiation - Low Strain Range	92
VII LOW DEFECT AF-115	102
1. Materials Characterization	102
2. Fatigue Behavior	102
VIII INITIATION MECHANISMS - SPECIAL TESTS	107
1. Environmental Tests	107
2. Residual Stress	110
3. Strain Ratio	112
4. Low Frequency Tests	114
5. Crack Initiation Life	114
6. Summary	117
IX ELEVATED TEMPERATURE - CYCLIC DWELL TESTS	118
1. AF-115 Tensile Dwell Tests	118
2. AF2-1DA Tensile Dwell Tests	125
X INITIATION MODES - ROOM TEMPERATURE TESTS	134
1. AF2-1DA	134
2. AF-115	139
XI TEM THIN FOIL ANALYSIS	145
1. Elevated Temperature	145
2. Room Temperature	154

TABLE OF CONTENTS (Concluded)

SECTION	PAGE
XII DISCUSSION	158
1. Introduction	158
2. Surface-Subsurface Transition (SST)	158
3. Effect of Temperature on Initiation Mechanisms	180
4. Creep-Fatigue Interaction	183
XIII SUMMARY	189
XIV SUGGESTIONS FOR FUTURE WORK	197
REFERENCES	199
APPENDIX A	207
APPENDIX B	208
APPENDIX C	212

LIST OF ILLUSTRATIONS

FIGURE	PAGE
1 Schematic Illustration of Stage I and Stage II Fatigue Crack Growth (Laird, Reference 7)	7
2 a) TEM Replica Image of the AF2-1DA Microstructure Showing the Cuboidal Morphology of the Cooling γ' ; b) TEM Micrograph of the Cooling γ' and Fine Spheroidal Aging γ' in the AF-115 Alloy	8
3 a) $L1_2$ Unit Cell; b) Arrangement of Atoms in $L1_2$ Closed-Packed Plane	10
4 a) SEM Micrograph of the AF-115 Microstructure Showing the Large Unsolved γ' and the Smaller Cooling γ' ; b) Optical Micrograph of Carbides Outlining Prior Powder Particle Boundaries	34
5 a) SEM Micrograph of the AF2-1DA Microstructure Showing the Morphology of the Grain Boundary γ' and the Cooling γ' , as Well as the Carbide Distribution; b) TEM Superlattice Reflection of the Cooling γ' and Fine Aging γ' Particles	36
6 a) Optical Micrograph of the AF2-1DA Microstructure; b) Diffraction Pattern of a Twin in AF2-1DA $\langle 110 \rangle$ Zone Axis, $\{111\}$ Twin Plane	37
7 a) SEM Micrograph of a Pre-existing Argon Pore in AF-115; b) SEM Micrograph of a Nonmetallic Inclusion in AF-115	39
8 a) Representative Distribution of Pores and Non-metallic Inclusions in AF-115; b) SEM Micrograph of a Hafnium Oxide Inclusion	41
9 Representative Distribution of Nonmetallic Inclusions in AF2-1DA	42
10 Fatigue Waveforms Used in the Test Program	45
11 Uniform Section Smooth Bar Fatigue Specimen	47
12 TEM Replica Grid Used to Locate Specific Features While in the Microscope	49
13 Illustration of the Range of Metallographic Observations Made in Failed Specimens	50

LIST OF ILLUSTRATIONS (Continued)

FIGURE	PAGE
14 0.2% Yield Strength vs Temperature for a) As HIP AF-115, b) HIP Plus Forged AF-115	54
15 0.2% Yield Strength vs Temperature for AF2-1DA	55
16 Continuously Cycling Fatigue Data for AF-115, AS-HIP	57
17 Continuously Cycling Fatigue Data for AF-115 HIP Plus Forged	58
18 Comparison of the Fatigue Behaviors of the AS-HIP and HIP Plus Forged Conditions of AF-115, 760°C	59
19 Cyclic Dwell Tests, AF-115, 760°C	61
20 Continuously Cycling Fatigue Data for AF2-1DA	62
21 Cyclic Dwell Tests, AF2-1DA, 760°C and 649°C	63
22 Comparison of the Fatigue Behaviors of AF-115 and AF2-1DA, 760°C and 20 cpm	65
23 Summary of the Surface-Subsurface Transition (SST) in the Site of the Dominant Fatigue Origins at Elevated Temperatures	67
24 Location of the Dominant Fatigue Origins for the Elevated Temperature AF-115 tests	69
25 Location of the Dominant Fatigue Origins for the Elevated Temperature AF2-1DA tests	70
26 SEM Micrographs of Typical Stage II Surface Crack Initiation Sites on AF2-1DA Fracture Surfaces	71
27 a) High Magnification Micrograph of a Stage II Fatigue Origin on an AF2-1DA Fracture Surface; b) Distorted Fracture Surface Near a Stage II Crack Origin, 760°C	72
28 Defect Cavity at the Origin of a Stage II Fatigue Crack in AF2-1DA	73
29 Polished and Etched Cross-Section of a Failed AF2-1DA Specimen. a) Surface Crack Propagating Normal to the Tensile Axis; b) Crack Initiating at a Small Surface Inclusion	75

LIST OF ILLUSTRATIONS (Continued)

FIGURE	PAGE
30 a) Surface Crack Possibly Having Originated at an MC Carbide in AF2-1DA; b) Subsurface Cracking at an Inclusion in AF2-1DA After Testing at a High Strain Range	76
31 TEM Image of Two Stage Carbon-Platinum Replica Showing a) A Crack Initiating at an Inclusion; b) At Higher Magnification, the Crack Avoiding Large γ' Precipitates	78
32 a) SEM Micrograph of a Cracked Inclusion Cavity; b) TEM Replica Showing the Crack Path	79
33 TEM Replica Images of Surface Cracks in AF2-1DA	81
34 SEM Micrograph of the Stage II Crack Propagation Region on a Fracture Surface Showing Intact Cuboidal γ' Precipitates	82
35 SEM Micrograph of a Stage I Initiation Facet on the Fracture Surface of an AF2-1DA Specimen	84
36 a) Surface Crack Along a Twin Boundary in AF2-1DA; b) Slip Lines Parallel to the Twin Boundary	85
37 Intergranular Surface Initiation in AF2-1DA at 760°C and 0.2 cpm	86
38 Crack Initiation at AF-115 at a Near-Surface Pore	88
39 a) Stage II Crack Initiated at a Near-Surface Pore; b) Crack Initiation Along the Equator of a Pore	89
40 Crack Initiation in AF-115 Originating at a Near-Surface Defect. a) Hafnium Oxide Inclusion; b) Nonmetallic Inclusion	91
41 a) Subsurface Crack Initiation as Observed on the Fracture Surface of a AF2-1DA Specimen; (b Higher Magnification of the Crack Origin, a Nonmetallic Inclusion	93
42 a) Internal Crack Initiation at an Inclusion Cavity in AF2-1DA; b) A Stage I Facet at the Defect's Edge	94
43 Fatigue Crack Originating at an Internal Cavity in Stage I Mode (Shown by Arrow)	95

LIST OF ILLUSTRATIONS (Continued)

FIGURE	PAGE
44 a) TEM Replica Image of the Stage I Initiation Region Shown in Figure 43; b) Higher Magnification of the Planar Slip Bands Originating at the Defect	97
45 Near-Surface Elongated Cavity Devoid of Crack Initiation	98
46 a) Subsurface Initiation Site on the Fracture Surface of an AF-115 Specimen; b) SEM Back-Scattered Electron Image of the Fatigue Origin	99
47 a) Crack Initiation as the Result of Inclusion-Matrix Decohesion; b) Stage II Propagation from a HfO_2 Inclusion	101
48 Fatigue Behavior of Low Defect AF-115 Compared to the Primary Heat of AF-115	103
49 a) Stage II Surface Crack Initiation in AF-115-LD; b) Subsurface Crack Initiation at an Inclusion Cavity	105
50 a) Stage I Surface Crack Initiation in the AF2-1DA High Vacuum Test above the SST; b) SEM Micrograph of the Stage II Early Crack Propagation Region	108
51 Fatigue Hysteresis Loops. a) Initial Cycle, $A = +1$; b) High Strain Range Stable Loop, $A = +1$; c) Low Strain Range Stable Loop, $A = +1$; d) Low Strain Range Stable Loop, $A = \infty$	113
52 Cracks on the Surface of an AF2-1DA Specimen Fatigued to 10% of It's Expected Life	116
53 Surface and Internal Cracking in a Tensile Dwell Specimen, Arrows Indicate Some of the Internal Cracks	119
54 a) Intergranular Crack Initiation from an Internal Defect; b) Grain Boundary Cavitation Cracking, Arrow Indicates the Tensile Axis	120
55 a) Internal Cracking at Defects in a Cyclic Dwell Specimen Fatigued at $1.0\% \Delta \epsilon_t$; b) Internal Crack Nucleation at Defects and Along Grain Boundaries in a Tensile Dwell Specimen Fatigued at $0.80\% \Delta \epsilon_t$	122

LIST OF ILLUSTRATIONS (Continued)

FIGURE	PAGE
56 a) An Internal Crack Originating at a Pore on the Fracture Surface of a Failed AF-115 Tensile Dwell Test; b) Fracture Surface of an AF-115 Tensile Dwell Test with Many Internal Crack Nucleation Sites at Defects	123
57 Cross-Sectional View of the Microcrack Link-Up Process in Tensile Dwell Tests	124
58 a) Multiple Crack Initiation Ahead of a Major Surface Crack; b) Microcrack in this Cluster Apparently Free of Surface Oxide	126
59 Internal Grain Boundary Cracking in an AF2-1DA Tensile Dwell Test, Tensile Axis (T.A.) as shown	127
60 Grain Boundary Cavitation Cracking in an AF2-1DA Tensile Dwell Test	128
61 Fracture Surface of an AF2-1DA Tensile Dwell Test with Regions of Internal Crack Initiation	130
62 Intergranular Internal Initiation Sites on a Tensile Dwell Fracture Surface	131
63 Schematic Illustration of the Stress Biases in Stable Hysteresis Loops of a) Tensile and b) Compressive Dwell Tests	132
64 Optical Micrograph Showing the Intense Planar Slip in the Central Portion of a Room Temperature Fatigue Specimen	135
65 a) Optical Micrograph of Stage I Surface Cracking; b) SEM Micrograph of the Middle Crack in the Figure Above	136
66 a) Surface-Offset Associated with Stage I Surface Cracking; b) TEM Replica Image of γ' Shearing in a Planar Slip Band	137
67 a) Stage I Crystallographic Facets at the Origin of Crack Initiation for a Room Temperature Test; b) A high Magnification SEM Image of the Stage I Facet Showing Striation Formation	138
68 a) Intense Slip Planes in Selected Near-Surface Grains at a Total Strain Range of 0.60% b) Cracking Along Slip Planes in One Grain Pictured in Figure 68a	140

LIST OF ILLUSTRATIONS (Continued)

FIGURE	PAGE
69 a) Stage I Cracking Originating at a Near-Surface Pore in AF-115; b) A High Magnification SEM Image of the Stage I Facet Morphology	141
70 a) Cross-Sectional View of a Stage I Crack Originating at a Near-Surface Pore in AF-115; b) TEM replica image of the Cracked Region Between the Pore and the Surface Edge in the Above Figure Showing Planar Shear Bands Parallel to the Stage I crack	142
71 Shearing of the γ' in Planar Slip Bands Shown in Figure 70b, TEM Replica	143
72 a) Dislocation Density of As-Received AF2-1DA; b) Cracked γ' Precipitates in As-Received AF2-1DA	146
73 a) Dislocation Density of 0.60% $\Delta\epsilon_t$ Test at 760°C b) Array of Dislocations Along the Trace of the (111) Plane, [110] Z.A.	147
74 a) Band of Dislocations Originating at a Carbide, [110] Z.A.; b) Higher Magnification of the Above Showing the Dislocations Preferentially Located in the γ Phase [110] Z.A.	148
75 a) High Dislocation Density of 0.90% $\Delta\epsilon_t$ Test at Elevated Temperature [110] Z.A.; b) Lower Dislocation Density Under Same Test Conditions as Above, [110] Z.A.	150
76 a) [001] Superlattice Reflection of γ' Precipitates Showing Dislocation Concentration After Fatiguing at 0.90% $\Delta\epsilon_t$, [110] Z.A.; b) Bright Field Micrograph of Dislocations Shearing γ' Precipitate along the Trace of the (111) Plane, [110] Z.A.	151
77 a) Band of Dislocations Along the Trace of the ($\bar{1}\bar{1}1$) Plane at Elevated Temperature, [001] Z.A.; b) Array of Dislocations Located Preferentially in the Matrix Phase, [100] Z.A.	152
78 a) Wavy Slip Character of High Temperature Test at 1.1% $\Delta\epsilon_t$, [110] Z.A.; b) Higher Magnification of Above Showing Lower Dislocation Density of the Larger Cooling γ' Precipitates, [110] Z.A.	153

LIST OF ILLUSTRATIONS (Concluded)

FIGURE	PAGE
79 a) Planar Slip Character of the Room Temperature Deformation at 1.1% $\Delta\epsilon_t$, [001] Z.A.; b) Dark Field Superlattice Reflection Showing Shearing of the γ' Precipitates at Room Temperature Along the Traces of the (111) Plane, [110] Z.A.	155
80 Intense Planar Deformation Apparently Originating at a Carbide at Low Strain Range, [110] Z.A.	156
81 Crack Initiation Life Versus Normalized Stress Range (Harkegard, Reference 65)	167
82 Summary of the Observations of Secondary Cracking in AF-115 and AF2-1DA at Elevated Temperature	170
83 Crack Growth Data for AF2-1DA at 649°C, 0.17 Hz, A = 0.82 (R = 0.1) (Reference 126)	172
84 Illustration of a) An Internal Crack in Round Bar; b) A Surface Flaw in an Infinite Body	174
85 AF2-1DA Cyclic Dwell Data Plotted as Maximum Tensile Stress Versus Cycles to Failure	186
86 AF-115 Cyclic Dwell Data Plotted as Maximum Tensile Stress Versus Cycles to Failure	187
87 Summary Illustration of the Fatigue Processes for Both Superalloys Above and Below the SST	191
88 Change in Slip Behavior with Temperature a) Planar Slip at Room Temperature; b) Wavy Slip at Elevated Temperature	193
89 Schematic Illustration of the Failure Process in Tensile Dwell Tests, Microcrack Initiation and Link-Up	195

AFWAL-TR-80-4063

LIST OF TABLES

TABLE	PAGE
1 AF-115 - Chemical Analyses; Wt. Percent	31
2 Chemical Composition - AF2-1DA; Wt. Percent	33
3 Tensile Properties	52
4 Yield Strength Data	53

AFWAL-TR-80-4063

SECTION I

INTRODUCTION

It has been well established in the literature that microstructural defects significantly affect fatigue crack initiation. In fact, it has been generally accepted that in engineering alloys, crack initiation occurs at some pre-existing defect (References 1,2). Defects can be: micropores which are introduced in casting or atomization processes; inclusions, both metallic and nonmetallic; and microstructural features, such as carbides and brittle second phases. In general, defects can be any discontinuity in the microstructure which acts to raise the local stress level. As a result, localized areas of plastic deformation can be generated in regions adjacent to the defects even at nominal stresses well below the yield stress of the material. This influence is important in the fatigue process because fatigue crack initiation occurs as the result of localized plastic deformation (Reference 2). Therefore, the greater the plastic strain concentration effect of the defect, the greater should be its influence on crack nucleation.

Although defects have such an enormous influence on crack initiation, few experimental studies have been performed to systematically determine the effects of defect size, shape, and population on fatigue. It is true that certain trends have been established throughout the literature, such as the observation of de Kazinczy (Reference 3) that surface defects appeared to be more detrimental than those in the interior of the specimen. These observations, however, have rarely been the subject of further research. As a result, it is the purpose of this investigation to determine the relative effects of defect size, shape, and population on the crack initiation life of a representative engineering material.

Typically, fatigue crack initiation life in the plastic strain regime has been determined by testing smooth bar specimens of either the uniform section or hourglass shape geometry in strain control. This type of testing technique is used to simulate the cyclic behavior of material in the vicinity of a stress concentration in engineering

structures (Reference 4). Fatigue, even in a test specimen, however, entails more than just crack initiation as described by Coffin (Reference 4) there are really three stages of the fatigue process: first, nucleation and early growth of cracks within the plastic zone developed at the maximum strain concentration; second, crack propagation of a stable crack through the plastic zone; third, propagation of the crack in the elastic zone with the crack generating its own plastic zone until fracture results. In this study, since uniform section specimens were fatigued over a range of plastic strain levels, the first two stages of the fatigue process, initiation and propagation through the plastic zone, influenced the life to failure. Some attempts were made to experimentally separate the initiation and propagation portions of the life, but due to many constraints, especially testing in an oxidizing atmosphere, this was not practically possible.

Since the total fatigue lives were determined by two dissimilar events, crack initiation and crack propagation, it was maintained throughout the program that the effect of defects on each of these two processes needed to be understood, and as a result, the relative influence of each phase of the fatigue process on the total life also had to be established. This basic approach to the problem, although obvious in retrospect, was critical in the success of the program. It is the author's opinion that much of the ambiguity of past results has been related to the fact that crack initiation and propagation were treated as one event.

Since the analysis did involve the consideration of crack initiation and propagation in the elastic-plastic range, there were obvious limitations encountered in treating the problem quantitatively. Elastic-plastic strain analysis and nonlinear fracture mechanics are both analytical tools pertinent to fatigue in the plastic strain regime; however, our capabilities did not extend into developing approximate computer solutions to account for plastic behavior. As a result, most of the quantitative comparison of strain concentrations or crack propagation behavior has been based on elastic analysis, and subsequent

extension of the trends to the elastic-plastic case has been necessarily restricted to a qualitative understanding. It is believed, however, that these analyses are valuable contributions to the understanding of the fatigue process.

As has been previously mentioned, the purpose of this study was to determine the effect of defect characteristics on the fatigue behavior of an engineering alloy. The requirements in choosing an alloy system were that the alloy could be tested over a range of experimental conditions; and that the alloy would contain defects of varying size and population which were uniformly distributed through the material. As a result, two high strength power metallurgy (P/M) nickel-base superalloys were chosen for this investigation. These alloys fulfilled the first criterion in that they could be tested over a range of temperatures in which the deformation behavior would be expected to change from planar slip at room temperature to wavy slip at elevated temperature (above approximately 750°C), and the alloys would also be subject to time-dependent damage, oxidation and creep, in the elevated temperature regime. The range of defects in these alloys was also well suited for the program. Since these alloys are made by powder metallurgy techniques, they would be expected to contain nonmetallic inclusions and gas porosity, in addition to other inclusions which would be the result of the specific chemical compositions. In this study, the major portion of the testing was done on alloy 115 with a high defect concentration and on alloy 2-1DA with a low defect concentration. Additional tests were also performed on a second heat of alloy 115 which had a low defect concentration similar to the 2-1DA alloy. This test program, therefore, provided the means to determine the influence of varying the defect characteristics on the fatigue behavior of a single alloy, along with the opportunity of comparing the results of different alloys in the hopes of establishing generic behavior patterns.

As mentioned, both superalloys were tested in the high temperature regime (649-760°C) where time dependent damage mechanisms were expected to influence the fatigue process. Since there is so much concern in

the literature concerning possible creep-fatigue interactions in high strength nickel-base superalloys (Reference 5), it was decided to perform several cyclic dwell tests to investigate this phenomenon. These tests provided information on both the nature and the magnitude of the influence of creep damage on the fatigue life. These tests also afforded an opportunity to determine the effect of defects in yet another test condition.

In summary then, the purpose of this investigation was primarily to explain the effects of defect size, shape, and population on the fatigue behavior of an engineering alloy. It was determined that to most effectively do this, the influences of defects on both crack initiation and crack propagation had to be determined. For this reason, the concepts of plastic strain localization and fatigue crack stress intensity formed the basis of the study. Two P/M superalloys were chosen for this study; the alloys contained defects that differed in size, shape, and population. These two alloys were tested over a range of strain ranges and temperatures in order to determine the effect of deformation behavior on the defect-matrix interactions, and particular attention was given to the existence of a creep-fatigue interaction with the incorporation of a cyclic dwell period at high temperature.

SECTION II

LITERATURE REVIEW

1. INTRODUCTION

As with other complex alloy systems, the mechanisms of high temperature crack initiation in nickel-base superalloys result from a combined interaction of deformation processes, microstructure, and environment. Deformation builds up at varying rates, depending on the temperature and loading conditions, usually exploiting the weakest element, either microstructure (grain boundary, twin boundary, a precipitate) or defect (inclusion, pre-existing pore). In this investigation, the effect of P/M defects on the fatigue behavior of superalloys will be studied over a wide range of temperatures and fatigue conditions. As a result, the nucleation mechanism can vary considerably from planar slip initiation at the specimen's surface to intergranular cracking in the interior of the specimen. At high temperatures, in particular, the initiation mode can be influenced by time-dependent damage mechanisms such as oxidation and creep, in addition to the already complex interactions of slip and microstructure which occurs at room temperature. In this section, the basic metallurgy associated with nickel-base superalloys will be described, and an overview of the varied modes of crack initiation in superalloys will be presented. In addition, a more detailed characterization of the parameters which can control initiation including slip behavior, oxidation, defect character, and creep deformation will be provided. Those interested are also directed to several review articles which, however, may treat the subject somewhat differently (References 1, 6).

Throughout this section and in the entire report, references will be made to the varied types of initiation that occur for different alloy systems. The terms Stage I and Stage II cracking will be used frequently to characterize particular observations. The differences between those two types of cracking are illustrated in Figure 1. Stage I cracking is a shear mode of propagation which occurs along macroscopic slip planes oriented for maximum shear, usually at an angle near 45° to the tensile axis. Since these cracks lie along a certain slip plane orientation, they

are termed crystallographic cracks. Stage II cracking, however, is a tensile mode of propagation which follows along the plane of maximum tensile stress, normal to the tensile direction. These cracks are macroscopically noncrystallographic although the microscopic mechanism for Stage II cracking has been described as involving alternating slip on crystallographic slip planes (Reference 8). Classically, cracks in structural alloys begin in a Stage I mode followed by a transition to Stage II propagation after some growth, as depicted in Figure 1. This generalization, however, does not always apply to nickel-base superalloys as will be described.

Finally, many nickel-base superalloys will be referred to in this report by their trade names. A listing of the more commonly referenced alloys is included in Appendix A along with the alloys' nominal compositions.

2. MICROSTRUCTURE

The nickel-base superalloy system is complex and in many ways unique. For this reason the initiation mechanisms for superalloys may differ from those previously reported for other systems. Nickel-base superalloys rely on a complicated combination of up to 15 important alloying elements to provide a very large volume fraction of γ' precipitate in a γ matrix for high temperature strength. In the more modern alloys, such as the AF-115 and AF2-1DA compositions used in this study, the volume fraction of γ' precipitate exceeds 60%. Figure 2a is a SEM micrograph of AF2-1DA showing the large number of orderly arranged cuboidal γ' precipitates within the grains, and Figure 2b is a high magnification TEM micrograph of AF-115 also showing the cuboidal γ' as pictured in Figure 2 along with finer spheroidal γ' between the cuboidal particles. It is difficult to imagine a greater percentage of precipitate in an alloy, and it is this large volume fraction of γ' precipitate that makes the superalloy system unique.

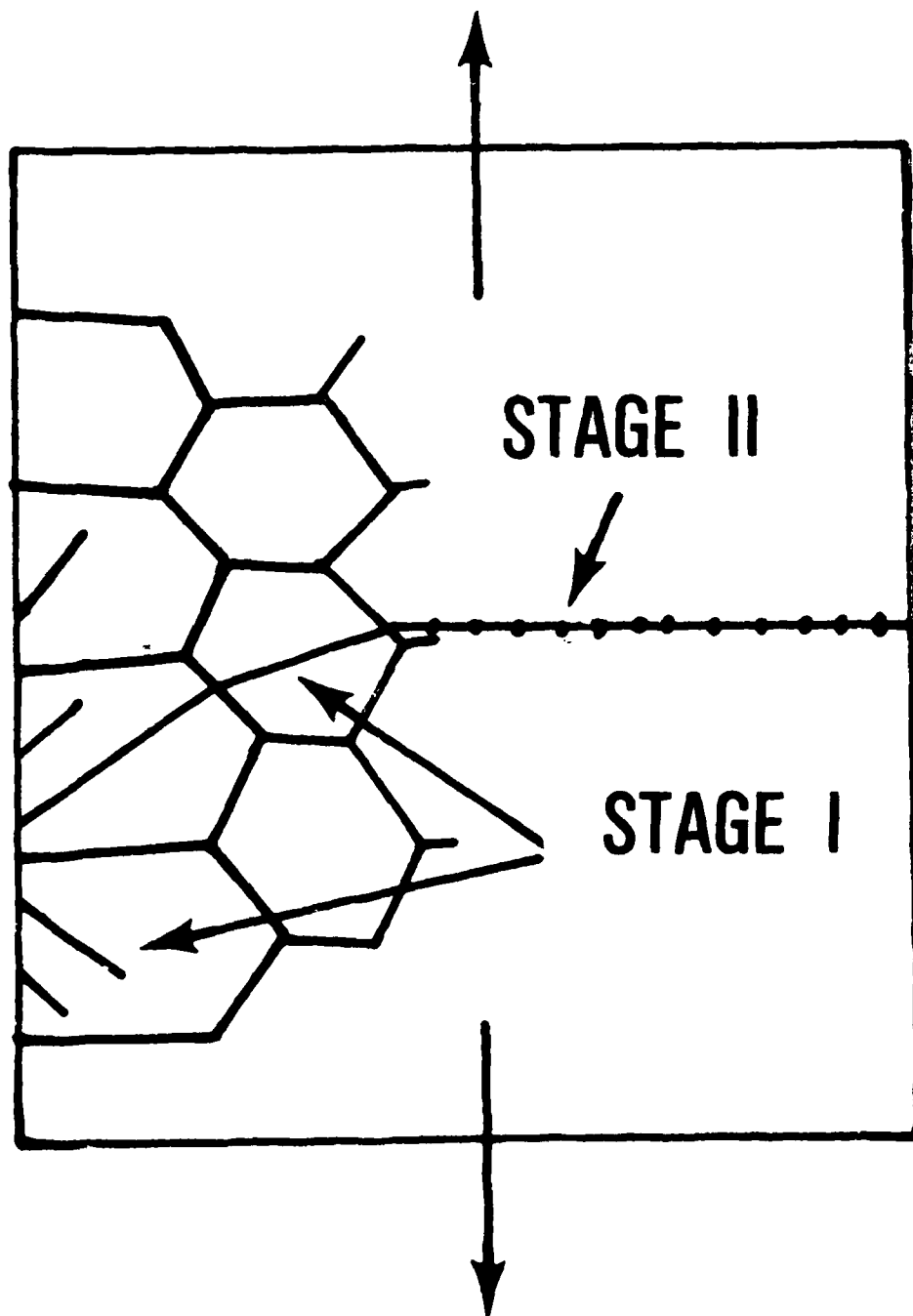
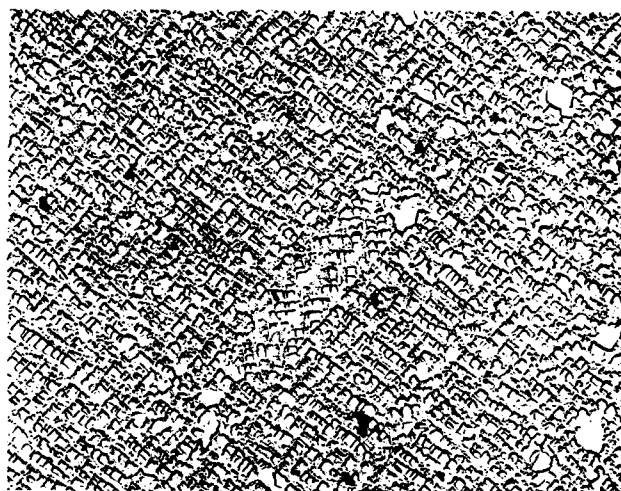
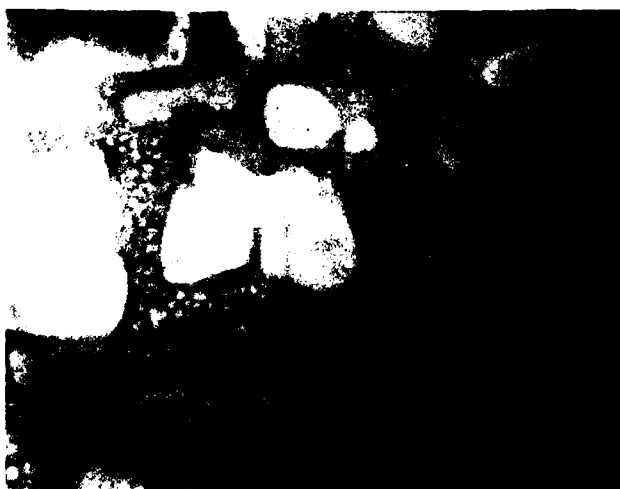


Figure 1. Schematic Illustration of Stage I and Stage II Fatigue Crack Growth (Laird, Reference 7)



(a)

3.4 μm



(b)

0.5 μm

Figure 2. a) TEM Replica Image of the AF2-1DA Microstructure Showing the Cuboidal Morphology of the Cooling γ' ; b) TEM Micrograph of the Cooling γ' and Fine Spheroidal Aging γ' in the AF-115 Alloy

The γ' phase is a coherent, ordered FCC precipitate having the $L1_2$ crystal structure which is shown in Figure 3. The composition of the γ' phase is Ni_3Al with cobalt and iron substituting for nickel, and titanium and columbium for aluminum. The trend in alloy development has been to add increasing amounts of aluminum and titanium to increase the volume fraction of the strong γ' precipitate in order to increase high temperature strength. The γ' precipitate is a particularly effective strengthener at high temperature in that its yield strength increases with temperature (References 23, 24). This unusual behavior is addressed in more detail in a later subsection.

The matrix phase, γ , is FCC, and it depends on solid solution alloying for strength. The solid solution elements in γ are usually aluminum, tungsten, molybdenum, chromium, cobalt, iron, vanadium, and titanium. The first four of these elements is the most effective strengthener.

There are also a number of other phases that can be present in nickel-base superalloys including carbides, borides, nitrides and topologically closed packed (TCP) phases (Reference 9). These phases can be beneficial or detrimental to the mechanical properties. The carbides, for example, are included to provide grain boundary strength and, therefore, to improve rupture properties. The TCP phases which are hard platelike phases such as σ , μ , and Laves, however, have lower rupture strength and ductility and are to be avoided.

Carbides can be of several kinds; the most commonly encountered are MC carbides where titanium, columbium, tantalum, vanadium, molybdenum, and tungsten form with carbon. These carbides form just below freezing and are very stable. $M_{23}C_6$ carbides are also frequently observed in nickel-base superalloys at grain boundary locations. These carbides form from MC carbides at temperatures between 982°C and 760°C. They are commonly rich in chromium with tungsten and molybdenum substitutes.

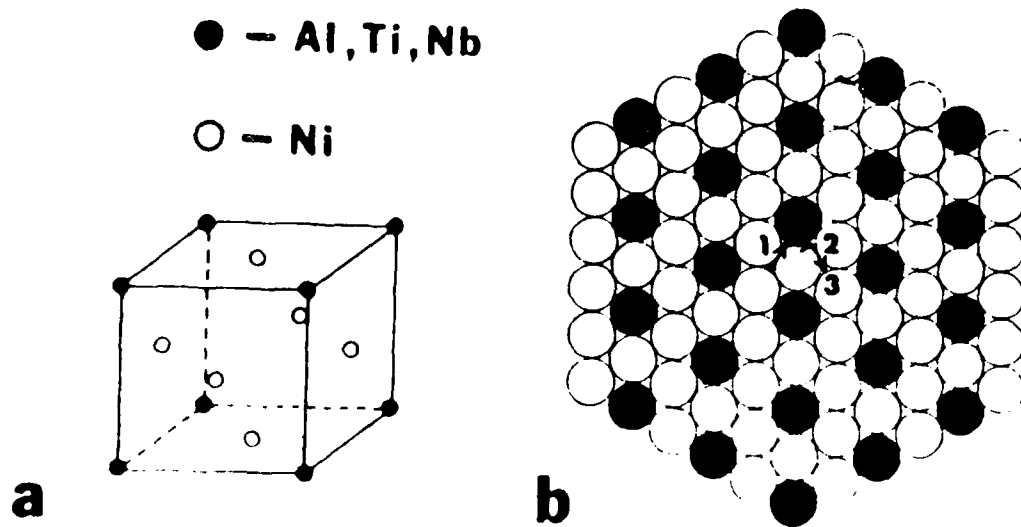


Figure 3. a) $L1_2$ Unit Cell; b) Arrangement of Atoms in $L1_2$ Closed-Packed Plane

3. OVERVIEW

As has been stated, the modes of initiation in nickel-base superalloys can vary considerably with changes in temperatures and microstructure. To help appreciate the range of nucleation mechanism that can control the fatigue life, a brief overview of the literature will be presented. A more detailed analysis of the factors which control initiation will then be addressed in following sections.

A classic study by Wells and Sullivan (References 10, 11, 12) described the crack initiation process in Udimet 700 over a range of temperatures. At room temperature and up to 649°C, localization of slip in discrete bands led to slip band crack initiation at the free surface. At 760°C, surface cracking became predominantly intergranular, due to the reduction in grain boundary strength, and there was a concomitant 80% reduction in life compared to room temperature results. At 927°C, the failure was again intergranular. The rate-controlling mechanism, however, was shown to be the nucleation and coalescence of voids as in a creep test.

A similar study was performed by Sabol, et al. (Reference 13), on Udimet 500 at 649°C, 816°C, and 982°C. At the lowest temperature, crack initiation occurred by planar slip preferentially at surface carbide particles, which crack during testing. Crack initiation occurred at grain boundaries or interdendritic carbide particles at 816°C, and totally at grain boundaries at 982°C.

In another study on Udimet 700, Organ and Gell (Reference 14) investigated the effect of cyclic frequency on the fatigue life at 760°C. They reported a 100-fold increase in life with a frequency change from 2 to 600 cpm. At the lowest frequencies, crack initiation occurred at surface-connected grain boundaries and propagation was initially intergranular. With an increase in frequency, intergranular notches produced by oxidation and creep deformation became less important. There was then a transition to subsurface crack initiation at coherent annealing twin boundary intersections or at hard phases located at grain

boundaries, and to Stage I crack propagation. With a further increase in frequency from 600 to 6×10^5 cpm, the fatigue life was reduced by a factor of seven and Stage I remained as the predominant mode of cracking. The reduction in life was attributed to the concentration of plastic deformation in fewer and fewer planar bands.

The influence of temperature and frequency was also studied by Leverant and Gell (Reference 15) on Mar-M200 single crystals. They found that at lower temperatures and higher frequencies, cracks initiated and propagated in a Stage I mode, while at the higher temperature and lower frequencies, cracks initiated and propagated in a Stage II mode. It was also observed that Stage II cracking often preceded Stage I propagation, in contrast to the opposite behavior usually noted for most alloys. An optimum frequency was also identified for maximizing fatigue life. Creep damage was detrimental at frequencies below the optimum, and intense planar slip was detrimental at frequencies above the optimum.

Gell and Leverant (Reference 16) also investigated the room temperature fatigue behavior of Mar-M200 in single-crystal and columnar-grained forms. It was found that the fatigue lives of these materials were greatly affected by the size of pre-existing cracks in MC-type carbides contained in the microstructure. The authors concluded from their observations that the carbide size distribution determined the number of matrix cracks, the number of cycles necessary to initiate each crack, the initial rate of propagation, and, as a result, the rate of crack link-up. It was also shown that casting micropores controlled initiation in Mar-M200 which was free of MC carbides (Reference 16). In this case, 0.20 mm size casting pores were the origin of the critical fatigue cracks, and when the pore size was reduced to 0.04 mm, an increase in fatigue life of a factor of five was obtained.

In summary, this brief review of crack initiation in nickel-base superalloys has shown that the mechanisms of cracking can range from Stage I planar slip to creep cavitation, and the site of initiation can vary from the surface to a location in the specimen's interior.

The controlling mode of nucleation has also been shown to be dependent on environment, alloy microstructure, defect population, and the interaction of temperature and cyclic frequency which influence deformation behavior. The details of how these factors affect the initiation process will now be addressed in more detail.

4. DEFORMATION MODES AND INITIATION MECHANISMS

Within the lower temperature range for superalloys, room temperature to about 649°C, the yield strength of nickel-base superalloys is relatively independent of temperature, and deformation is characterized by shear of both the γ and γ' phases by superlattice dislocations which consist of two $a/2 \langle 110 \rangle$ primary dislocations joined by an antiphase domain boundary (APB). Deformation is confined to the $\{111\}$ slip planes, and can be ideally described as mechanically reversible. This results in heterogeneous deformation localized in coarse planar slip bands (Reference 17). As the temperature is increased, thermal activation leads to a much more homogeneous array of dislocations due to enhanced cross slip and climb, with $a/2 \langle 110 \rangle$ and $a/3 \langle 112 \rangle$ dislocations shearing the γ' precipitate by diffusion controlled processes (Reference 18). The yield strength often reaches a maximum at about 650°C and begins to rapidly decrease at approximately 760°C. The particular functional relationship of yield strength with temperature, however, depends upon the volume fraction of γ' in the alloy and the strain rate (Reference 19). Leverant, et al. (Reference 18), have described the yield behavior of γ' strengthened superalloys in terms of the contributions of the γ and γ' phases. At low temperatures, the γ' particles are sheared by $a/2 \langle 110 \rangle$ superlattice pairs and the flow stress is controlled by the APB of the γ' . The mechanisms of γ' shearing in nickel-base superalloys have been thoroughly reviewed by Kear, et al (References 20, 21, 22). At higher temperatures and high strain rates where the flow stress of the alloy increases, both the APB and the flow stress for shear of the γ' make larger contributions to the strength. In fact, the yield stress of the γ' phase actually increases with increasing temperature to about 760°C. Finally, as temperature is increased beyond this point and the strain

rate is reduced, the yield strength of the alloy decreases as the intrinsic APB energy of the γ' is now lowered by diffusional processes. Here, $a/2 \langle 112 \rangle$ dislocations are generated in the γ phase and disassociate into $a/3 \langle 112 \rangle$ and $a/6 \langle 112 \rangle$ partials, the former then shear the γ' particles (Reference 11).

The unusual relationship of the flow stress of the γ' phase with temperature has been studied by Copley and Kear (Reference 23) and Thornton, Davies, and Johnston (Reference 24). The results showed that indeed the 1% yield stress for γ' increased approximately 200% over the temperature range of 25°C to 700°C. Above 700°C, however, the strength of the γ' decreased rapidly. Thornton, et al, (Reference 24) showed that the microplastic yield stress (10^{-6}) of the γ' did not vary over the same temperature range indicating that the frictional stress does not change substantially with change in temperature. The primary reason for the effect of temperature on the strength of γ' was, then, found to be due to the increased propensity of $\{100\}$ slip as the temperature was raised. Thornton, et al, (Reference 24) concluded that this causes the mechanism controlling the flow stress to change from exhaustion hardening to debris hardening. That is, at low temperature the yield process occurs largely by the free movement of dislocations on $\{111\}$ planes with very little dislocation-dislocation interaction. At higher temperature, however, due to the multiplicity of slip system $\{111\}$ and $\{100\}$ and the ease of cross-slip, the γ' crystal can never undergo plastic deformation in the easy glide mode. Strain hardening is increased by the proliferation of dislocation-dislocation interactions and the formation of dislocation dipoles and loops.

Several investigations have correlated the changes in crack initiation mode with change in deformation behavior (Reference 1, 25, 26). At lower temperatures, the formation of intense planar slip bands results in a heterogeneous distribution of deformation. This concentrated deformation, in turn, leads to the development of surface-initiated Stage I crystallographic cracks. In general, fatigue cracks always begin at concentrations of plastic strain, and because plastic deformation begins

preferentially at a free surface for defect free material (Reference 2), cracks originate there. The process of Stage I fracture in these alloys is not fully understood, but it is believed to involve both shear and normal stresses (References 27, 28). The reversed motion of planar dislocations during cyclic straining creates a large density of dislocation dipoles in the band, and it has been shown that this can lead to a local enhancement of the normal stress across the plane (Reference 29). In addition, the cyclic deformation may reduce the cohesive bond strength of the atoms across the slip band (Reference 16). The critical influence of the local normal stress across the slip plane has been explained as being responsible for the observations of such features as cleavage type river lines and equiaxed dimples on the fatigue facets (Reference 29). The observations of growth striations on the fracture surface, however, suggest a different model based on the plastic blunting process (Reference 7).

As temperature increases, the deformation becomes much more homogeneous for superalloys, with a lessening of intense planar slip. This condition leads to more frequent observations of Stage II cracking at microstructural defects (pores, inclusions, carbides) (Reference 15). Associated with Stage II cracking is the concept of crack initiation due to slip irreversibility. At high temperature where dislocations move out of the slip plane readily due to cross slip and climb, there is added dislocation-dislocation interaction, and therefore more of the cyclic deformation is irreversible (Reference 25). This can lead to localized concentrations of plastic strain around stress raisers, such as pores, and eventually crack initiation.

Leverant and Gell (Reference 15) have investigated the phenomenon of localized slip intensity by examining the fatigue behavior of Mar-M200 single crystals under various temperature-cyclic frequency conditions. Their observations showed that Stage I cracking was dominant at high frequencies (1058 Hz) and low temperatures (760°C and 843°C) while Stage II initiation occurred at low frequencies and higher temperatures. The authors explained these results by stating that it is likely that

planar bands of dislocations are generated at most frequencies at the tips of stress concentrations such as pores or existing cracks, but that the planar bands are unstable with respect to thermally activated recovery processes such as dislocation climb or cross slip. Therefore, to develop a Stage I crack, the crack must form along the slip band at a rate which exceeds the rate of dislocation recovery out of the bands. The conditions where both Stage I and Stage II cracks initiate from the same defects are considered to be those where the rate of dispersal of dislocations out of the planar bands is just equal to the rate of formation of Stage I cracks.

In a supporting investigation (Reference 18), the same authors determined the activation energy and activation volume associated with homogeneous plastic flow leading to Stage II initiation at 843°, 927°, and 1010°C. The values were comparable to the values for steady state creep in the same alloy at 760°C. The similarity of these activation parameters suggested that the same rate-controlling deformation mechanisms was operative in each case. Testing in vacuum, performed by other researchers, was also referenced to support the conclusion that the change in level or intensity of cyclic plastic deformation by varying cyclic frequency can, by itself, affect elevated temperature fatigue lives apart from the influence of frequency on environmental interactions.

In an analysis on the same subject, Wells (Reference 25) suggested that Stage I cracking is associated with the reversible motion of dislocations on the plane containing the crack, and the rate is thought to depend upon the range of shear displacement at the crack tip. Wells also concluded that since Stage II propagation clearly depends upon the irreversibility of crack type deformation, the transition from Stage I to Stage II propagation may be governed by the onset of more wavy slip at the crack tip as the result of thermally activated cross-slip and climb.

These observations and theories of crack initiation are somewhat different than those expressed in classical reviews of crack nucleation

for pure metals and single phase alloys (References 106, 119). In these systems, the formation of cracks has usually been associated with the presence of intrusion-extrusion pairs and the development of persistent slip bands. In addition, wavy slip in the single phase alloys has been shown to enhance the formation of persistent slip bands and, therefore, wavy slip increases the localization of strain and hastens crack initiation. In fact, Avery and Backofen (Reference 30) have shown in the Cu-Al system that slip band cracks initiated more rapidly in wavy slip rather than planar slip materials. In contrast, however, wavy slip connotes more homogeneous deformation and less strain localization for high strength precipitation strengthened alloys, such as the nickel base superalloys (Reference 1). This is because superalloys do not develop well defined dislocation cell substructures, and as a result, persistent slip band formation and crack nucleation are suppressed (Reference 2). It is, therefore, apparent that the initiation mechanisms for superalloys should be different from those described in the classical studies of single phase materials since strain localization occurs under different conditions. It is also clear that the terms "planar" and "wavy" are not sufficient to characterize slip behavior since both of these deformation modes can either accelerate or retard strain localization. As Williams, et al (Reference 31), have suggested, deformation also needs to be defined as homogeneous or heterogeneous, and it seems that this distinction is as important as the difference between planar and wavy slip, since in fatigue it is the concentration of plastic strain that is critical to the initiation process. Another reason why the more classical theories of crack initiation based on single phase materials do not seem to apply to the superalloys is that the large number of pores, inclusions and other microstructural discontinuities accelerate strain localization and therefore they control the fatigue process.

5. OXIDATION

At high enough temperatures, oxidation effects can govern fatigue crack initiation at free surfaces. These effects, which include passivation of slip steps, stabilization of grain boundary cavities, intergranular oxidation, and scale formation can be advantageous

or detrimental. Coffin (Reference 4) has been a strong advocate of the theory that the reduction in the fatigue life of nickel-base superalloys as temperature is increased is due to environmental effects, more specifically to oxidation, rather than to a creep-fatigue interaction. The findings of several investigators, including White (Reference 32) and Achter (Reference 33), have shown an increase in fatigue life over most of the ranges of life for materials tested in vacuum. Research by Coffin (Reference 34) on the crack initiation mechanism of Udimet 500 at high temperature provided additional support; evidence was presented of surface ridging and pronounced grain boundary penetration due to oxidation, a denuded γ' zone adjacent to the oxide, and cracking of the oxide. The ridging was selective, and was presumed to occur on those boundaries where high stresses existed. The author viewed this process as being analogous to stress-corrosion cracking.

Research on A286 (Reference 35), an iron-base superalloy, identified highly localized surface oxidation as the nucleation site for fatigue cracks under low cycle fatigue (LCF). Other experiments (Reference 36) conducted on A-286 and Udimet 500 at 816°C revealed that the strong frequency effect found in air was seen to disappear when the tests were performed in a vacuum of 10^{-8} Torr; initiation was transgranular in vacuum and intergranular in air.

Surface oxidation is detrimental to fatigue because it can cause the formation of stress raisers, and, therefore, it can accelerate crack initiation. Paskiet, et al (Reference 37), have shown that pre-oxidation of a specimen at 982°C followed by fatigue testing at 760°C produced many surface intergranular cracks, whereas, testing of specimens without prior oxidation produced a single intergranular crack. Thus, preoxidized phases or grain boundaries served as incipient cracks. Fujita (Reference 38) has also proposed a model for accelerated oxidation of surface connected slip bands which serve as crack nuclei.

It has also been reported that the fatigue lives of specimens tested in air and vacuum converge at low stress ranges ($10^7 - 10^8$ cycles), and

it appears that for some materials at very long lives there is a cross-over point beyond which the lives in air are greater than that in vacuum. Danek, et al, (Reference 39) and Achter (Reference 40) have explained these results on the basis of two competing effects; at high stresses and short lives, oxygen absorption at the crack tip accelerates the rate of crack growth in air, while at low stresses, a thicker oxide is formed which is thought to strengthen the metal. However, Gell and Duquette (Reference 41) in their analysis on the same subject interpreted these results in terms of creep-oxidation interaction. They proposed that at high stresses and short lives, crack initiation and, in some cases, crack propagation is intergranular because of the high creep component in the cycle, and for tests run in air, oxidation of grain boundary phases accelerates the rates of intergranular crack initiation and propagation and reduces the fatigue life. But, as the stress is lowered, the creep component in the cycle is reduced, which favors a transgranular mode of cracking and longer life.

A dramatic observation was made by Gell and Leverant (Reference 26) of the beneficial effect of oxygen on the elevated temperature fatigue of nickel-base superalloys. They showed that there was a change from surface to subsurface initiation for Mar-M200 tested at 927°C as the strain range was reduced. It was reported that at the lower strain ranges, although most cracks initiated on the surface of the specimen, the cracks that led to failure initiated in the interior. The explanation proposed was that oxide formed in surface cracks, and prevented resharpening of the fatigue cracks (according to the plastic blunting model by Laird (Reference 7) to the same degree as they would without the oxide, and the rate of crack growth was, therefore, slowed. Cracks that initiated at a later time in the specimen's interior were believed to propagate more rapidly since they were effectively in a vacuum.

The effect of environment on the crack propagation phase of fatigue has also been well documented in the literature. In fact the environment has been shown to be one of the major factors controlling crack growth rates (Reference 42). Specifically for the nickel-base superalloys, previous research has documented the detrimental influence of oxidation

on the elevated temperature crack propagation behavior. Scarlin (Reference 43) has shown that the crack propagation rates for both Nimonic 105 and IN 738LC increased as the cyclic frequency decreased for high temperature tests in air. The data also showed an increase in crack growth rate in air compared to vacuum which led the author to conclude that oxidation was the controlling factor in increasing the propagation rates in air. James (Reference 44) has also studied the effect of oxidation on the nickel-base superalloys, Inconel 600 and Inconel 718. Elevated temperature crack growth tests were performed in air and in liquid sodium which had previously been shown to be an inert atmosphere for crack propagation tests (Reference 45). The results showed that the crack propagation rates in liquid sodium were lower than in air, especially in the lower ΔK regime. The improvement in properties in liquid sodium was associated with the presence of an oxygen free environment.

In summary, the literature has shown that environmental interactions can have an overwhelming effect on the fatigue behavior of nickel-base superalloys. In particular, both the initiation and crack propagation phases of fatigue are both influenced by the environment. For this reason, several temperatures and cyclic frequencies will be included in this study to determine if the environmental influences are more significant than those of the defect population, for the alloys tested.

6. DEFECTS

The effect of defects on fatigue can be overwhelming. In general, crack initiation in engineering materials usually occurs at some defect (References 1, 2). These defects can be microstructural inclusions such as carbides and borides, nonmetallic inclusions such as slag or refractor brick, or micropores. The defects can also be related to surface finish such as machining marks or gouges; these, however, will not be included in this discussion since the effect of microstructural defects is of primary concern in this study.

Many of the investigators that have been cited in this report have described the detrimental effect of defects (References 1, 2, 6, 16). The literature of cast and wrought, and directionally cast superalloys has documented the particularly harmful effects of MC carbides and microporosity. Significant life improvements have also been described when the size of these defects was reduced (Reference 16). Defects are also a cause of particular concern in P/M alloys because pores and nonmetallic inclusions can be easily introduced into the alloy material during the powder production process, and these defects can result in a significant reduction in mechanical properties (Reference 46). Researchers have described the influence of defects on the mechanical properties on P/M steels (References 47 through 51) and P/M titanium (Reference 52), and more recently research on the low cycle fatigue behavior of P/M superalloys has shown that inclusions and pores can be sites of crack initiation in these materials, too (Reference 53).

A considerable amount of research has been done on other alloy systems, besides the superalloys, looking at the problem of the effect of defects. Grosskreutz and Shaw (Reference 54) reported on the critical mechanisms in the development of fatigue cracks in 2024-T4 aluminum. In notched fatigue samples, they noticed that deformation began with the formation of fine slip, followed by intensification around inclusions. This intensified slip was accompanied by the production of small dislocation loops and dipoles. Fatigue cracks initiated at large ($> 1 \mu\text{m}$) impurity inclusions clusters, and no correlation could be found between the initiation event and the formation of fine slip, concentrated slip, or dislocation dipoles and loops. All of their evidence favored the view that fatigue cracks nucleated at the interface between surface inclusions and the matrix, probably by a debonding mechanism. This led the authors to state that the general production of slip bands so important in the fatigue of pure metals does not play a role in 2024 aluminum. Grosskreutz and Shaw (Reference 54) also concluded that the size of the nucleating inclusions or clusters was important; the larger ones were the most effective initiators. In addition, surface inclusions were found to be more detrimental than subsurface inclusions. This latter point will be important in the development of this investigation.

Bowles and Schijve (Reference 55), and Morris, et al, (Reference 56) investigated the role of inclusions in fatigue crack initiation of 2024-T3 and 2219-T851 aluminum, respectively. They also found that cracks initiated primarily at the inclusion-matrix interface. In the latter investigation, tensile fatigue straining was used and initiation occurred at those surface inclusions heterogeneously distributed in clusters.

In a review on the subject of the effect of oxide inclusions on the fatigue life of steels, Lankford (Reference 57) has reported that for hard inclusions of similar chemistry, there exists a trend of increasing crack nucleation propensity with increasing inclusion size. In addition, the average minimum (critical) inclusion size causing failure appears to increase with depth below the surface, so that surface inclusions are generally more detrimental than subsurface ones.

For 4340 steel, Lankford (Reference 58) also reported that inclusions were able to debond on the very first load cycle, and they can do so below the fatigue limit. Initiation was either "slipless" at higher strength levels or it was related to slip band formation in lower strength steels. Regardless of the mode of initiation, the common critical factor governing whether these small ($< 1 \mu m$) initial cracks would grow to Stage II engineering cracks was the requirement that a crack be associated with a debonded inclusion (Reference 58, 59). Cracks were also seen at bonded inclusions, but these did not grow.

De Kajinczy (Reference 3, 60, 61) has studied the effect of defects on the fatigue properties of cast steels. From his observations, relationships between the endurance limit and defect size which depend on the inverse square root of defect diameter, have been developed for surface and interior cavities. Although there was considerable amount of data generated for these steels concerning the location of dominant defects, no definite trend was discerned for surface or interior initiation. De Kajinczy did note, however, that defects at the specimen

surface had a larger notch effect than defects located in the interior; this, of course, is a similar finding with that of Grosskreutz and Shaw for an aluminum alloy.

Mitchel (Reference 62) has also reviewed the fatigue behavior of cast steels and he has concluded that fatigue performance is altered by the size, shape, and distribution of defects, as well as the strength and ductility of the matrix metal. In another comprehensive report, Mitchell (Reference 63) reported surface crack initiation in high hardness wrought steels, cast steels, nodular iron, and grey cast iron at inclusions, pores, graphite spherulites, and graphite flakes, respectively. He treated these defects analytically as "metallurgical notches" and was able to analyze the stress and strain concentrations around these defects using a Neuber notch analysis (Reference 64).

To begin to understand the effects of notches and other defects on the mechanical properties of structural alloys, many investigators have calculated the stress and strain concentrations around various geometrical discontinuities especially for the elastic cases. Peterson (Reference 65) has compiled a number of two dimensional elastic solutions for the stress concentrations around notches and pores. For the specific cases that are most pertinent to this investigation, the calculations have shown that surface and near-surface defects, such as pores, have a greater stress concentration factor, K_t , than do internal defects of the same shape. Also, not surprisingly, the K_t at the tip of an elliptical cavity has been calculated to be greater than the stress concentration at a round pore. Edmonds and Beevers (Reference 66) have also studied the effect of inclusions on the stress distribution in solids using photo-elastic techniques. Their results showed that the stress concentrations produced depend on the elastic modulus, and orientation of the inclusions. So, from these two reports it appears that defect shape, location, and orientation are critical in determining the stress concentrations at defects.

Although these studies are of significant value, they have not attempted to calculate the concentration of plastic strain at the various discontinuities, and it is this value which is most closely associated with crack initiation. Of course, the lack of knowledge of the redistribution of stresses and strains due to localized yielding at a stress concentration make this problem formidable. Harkegard (Reference 67), however, has published the results of a finite element analysis of elastic-plastic plates containing cavities and inclusions. In this work, he calculated the equivalent plastic strain ranges generated at these discontinuities. The results show that the plastic strain at the tip of a pore or elliptical cavity when subjected to a nominal stress approaching the yield stress can be several times as great as the elastic strain at yield. The precise value, of course, depends on the stress-strain characteristics of the particular alloy being studied. Harkegard also proposed a definition of crack initiation based on ductility exhaustion, and he showed that the threshold stress for crack nucleation from a pore is greater than that from an elliptical cavity.

In addition to the problem of determining the strain concentrations around defects, another important consideration in the fatigue of engineering alloys is the statistical nature of the nucleation event (Reference 68). It has been well established that the fatigue properties of metals are statistical in nature (Reference 69). In practical terms, this relates to a certain amount of scatter in the fatigue results due to many causes. Some of the scatter is inherent in the material itself and is due to local variations in composition and microstructure, while some is due to heat material variations and to differences in manufacturing practices (Reference 70). In materials in which defects control the initiation process, the size, distribution, and location of the defects would also be expected to significantly affect the fatigue scatter. References have already been cited which concluded that the size of the defects (Reference 54) and their location either on the surface or in the specimen's interior (References 3, 54) influenced the nucleation process. Swedlow and Sinclair (Reference 71) have also used analytical methods

to show that the interaction of the strain fields surrounding neighboring defects can magnify the localized plastic strain concentrations that would be expected from individual defects. In this case, the crack initiation lives would be expected to be significantly less than for the situation where there were no defect-defect interactions. Therefore, the statistical variations in defect size and distribution can apparently alter the fatigue behavior of an alloy.

In general, to improve the understanding of the statistical variability of fatigue in materials with defects, the range of interactions of defects with other defects, as well as with the microstructure, needs to be experimentally determined. Cracks have been shown to initiate at inclusion clusters in aluminum rather than at single inclusions (Reference 56); defects at the surface were shown to be more detrimental than those in the interior (References 3, 54); and cracks were found to originate at larger defects than at smaller one (Reference 54). These observations which have been previously cited in this report are examples of the information that is needed. This investigation will attempt to better define the mechanisms responsible for these observations, and it will also hopefully be able to present the implications of changes in defect size, shape, and population on the fatigue life.

7. CREEP-FATIGUE INTERACTIONS

Although the term creep-fatigue interaction has often been used in the literature to include any time-dependent damage mechanism including environmental attack, this section will deal only with the incorporation of classical creep deformation processes during fatigue. In high strength superalloys, creep-fatigue behavior has been studied by including in the fatigue cycle a dwell period at maximum stress or strain in both tension and compression. Although there is now much interest in this work, the literature on the metallurgical mechanisms of creep-fatigue interaction in superalloys is limited.

Research has been published; however for several stainless steels subjected to tensile hold periods at high temperature. Fiore and

Dierchs (Reference 72) have reported that a one minute tension hold period per cycle produced a significant reduction in cyclic life for several austenitic alloys. The decrease in life was attributed to localized deformation at grain boundaries. Wareing (References 3, 74) studied the effect of hold time on the fatigue behavior of 316 and 20/25/Cb stainless steel. He reported a reduction in life with the incorporation of a tensile dwell period and he related this to the production of creep damage in the bulk of the specimen. Wareing also reported that such reductions in life were not observed for hold period cycles where creep damage was not produced or was removed by sintering. Similarly, Dawson, et al (Reference 75) studied several austenitic steels and concluded that the reduction in life with the incorporation of a tensile dwell results from the formation and propagation of both surface and triple point cracks.

For superalloys, Wells and Sullivan (Reference 76) reported on the effect of dwell period on the LCF behavior of Udimet 700 at 760°C. They observed that holding at compressive strain is *more damaging than holding* at tensile strain. Internal creep cracks, however, were only present in the tensile hold specimens, and these internal cracks were along grain boundaries inclined 45° to the tensile stress axis. The authors proposed that creep cracks were initiated by a pileup of edge dislocations at a grain boundary particle as modeled by Barnby (Reference 77) and subsequent growth was controlled by vacancy diffusion as described by Gittus (Reference 78).

Most of the research on creep-fatigue deformation in superalloys, however, has been limited to analytically modeling the relationship of dwell period duration to cyclic life. Several authors have observed, as did Wells and Sullivan (Reference 76), that tests which incorporated a tensile hold period had significantly longer lives than did compressive hold tests when tests were compared at equal total strain ranges (References 79, 80) Hyzak and Bernstein (Reference 80) have explained this observation for the superalloy Rene 95 by taking into account the significant mean stresses that developed during the dwell cycles.

In this study, the data were shown to correlate well with the values of the maximum tensile stress and the tensile dwell period per cycle which suggested that creep deformation was controlling the life.

As with fatigue initiation, the mechanism of internal creep-fatigue initiation and propagation depends on many factors including stress level, temperature, dwell period, and microstructure. There are generally two types of fatigue cracks that develop: triple point cracks (w-type) and grain boundary cavities (r-type). It has been reported by McLean (Reference 81) for the superalloys, Nimonic 80 and Nimonic 90, that triple point cracks form at high stresses and low temperatures, while grain boundary cavitation predominates at low stress levels and high temperatures. Cavitation cracking has been attributed to grain boundary sliding at ledges associated with grain boundary particle-matrix interfaces or to slip band impingement on grain boundaries (Reference 76). Fractographic examination of the elevated temperature fatigue of copper, brass, magnesium, and a copper-gold alloy has associated the formation of grain boundary cavities with microstructural particles (Reference 82), and in Udimet 700, cracking was said to have initiated at grain boundary carbides or borides due to interface separation or particle cracking (Reference 76).

It is generally agreed that once initiated, cavitation type crack growth on grain boundaries normal to tensile axis takes place by condensation of vacancies at voids (References 83, 84). This results in a process of void growth and coalescence leading to final failure.

Raj (Reference 85) has reviewed the analytical models for crack initiation in grain boundaries under conditions of steady-state and cyclic creep. The effects of grain size, inclusion size, temperature, frequency, and load level were systematically treated. Concerning the effect of creep-fatigue cycles, Raj stated that a stress reversal after steady state has been reached will produce stress levels which will be approximately twice as large as without a stress reversal. Since void nucleation probability varies exponentially as the normal stress squared, a stress reversal event can cause a large increase in the nucleation

rate of cracks. In addition, grain boundary inclusions were identified as the primary nucleation sites because the interface energy at inclusions is high and because sliding produces stress concentration at inclusions.

In summary, little has been determined experimentally about the creep-fatigue interactions in nickel-base superalloys especially in the presence of a high defect concentration. It does appear, however, that superalloy behavior is unusual since tensile dwell tests have been shown to last longer than compressive dwell tests when the tests were compared at equal total strain ranges.

8. EMPIRICAL REPRESENTATIONS OF HIGH TEMPERATURE FATIGUE

In addition to the research that has concentrated on defining the metallurgical mechanisms of crack initiation in nickel-base superalloys, there has been extensive work performed which has been directed at formulating predictive methods for describing crack initiation. Some of the more prominent approaches include Strain Range Partitioning developed by Manson, et al, (Reference 86) Coffin's Frequency-Modified Model (Reference 87), the Ostergren variation of the Frequency-Modified Model (Reference 88), and the Damage-Rate Approach of Majumdar (Reference 89). The scope of this work has been reviewed in several recent publications, and therefore, the models will not be discussed individually (Reference 90, 91).

Although most of the approaches have some physical basis for their development, they are necessarily very empirical in nature. As a result, they do not provide much information as to the metallurgical micro-mechanisms that are responsible for initiation which, as has been stated, is the emphasis of this investigation. In a recent review on the subject, it was concluded that none of the existing equations can adequately predict LCF life in nickel-base superalloys in the regime where time-dependent damage affects the life. It is this author's opinion that much of the problem in predicting the LCF life of superalloys stems from the fact that the number of cycles-to-failure of a test specimen is treated as the crack initiation life, instead of separating

out an actual initiation phase and a crack propagation phase. Unfortunately, this is very difficult in most cases, but one empirical expression should not be expected to model several dissimilar processes that occur in varying proportions in a smooth bar crack initiation test. In fact, it has been recommended that future work examine the applicability of a crack propagation model to this problem since crack propagation has been shown to comprise the major portion of the LCF life for many materials (Reference 92). Based on these data, this investigation will attempt to determine the effects of defect characteristics separately on the crack initiation and crack propagation phases of fatigue.

9. SUMMARY

This review has documented how different metallurgical factors can affect the crack initiation process in metals, with particular attention to nickel-base superalloys. The nickel-base superalloys have also been shown to be a somewhat unique alloy system in that they do not follow some of the generalized fatigue mechanisms previously described for single phase alloys. The environment, slip character, defect population, and creep deformation have each been shown to dominate the initiation mechanism for certain superalloys under specific testing conditions. Since the alloys in this investigation will be tested at particularly high temperatures for high strength superalloys, each of the preceding factors can conceivably control the fatigue behavior. Particular attention, however, will be given to the effect of P/M defects on the crack initiation and crack propagation phases of the fatigue process. The details of the experimental portion of this study will be described next, followed by a review of the test results.

SECTION III

MATERIALS

Two alloys were selected for this study, AF-115 and AF2-1DA. Both alloys are recently developed high strength powder metallurgy nickel-base superalloys. Such alloys require P/M technology in order to attain optimum properties since they contain a large concentration of alloying elements which would be prone to segregation during conventional cast and wrought processing. The combination of high alloy content, P/M processing, and involved heat treatments results in these alloys having complex microstructures containing uniform arrangements of greater than 60% volume fraction of the γ' (Ni_3Al) strengthening precipitate. The compositions and processing steps for both alloys are described herein, and a characterization of the resultant microstructures and defect concentrations is contained in the following section.

1. PROCESSING

a. AF-115

The AF-115 billet material for this program was processed from two vacuum induction melted ingot master heats; the chemistries of which are shown in Table 1. These master heats were then vacuum induction remelted into a single heat, which was subsequently argon atomized. Argon atomization is a process in which a stream of molten metal is mechanically disintegrated by a jet of high pressure argon gas. The individual droplets quickly solidify thus resulting in an alloy powder of near uniform composition. The final chemistry of this heat of powder is also shown in Table 1. The powder was then charged into a stainless steel canister and compacted by hot isostatic pressing (HIP). The pressing parameters used were 1190°C for 2 hours at 100 MPa. Some of the billet material was heat treated in the as-HIP condition while the remainder was forged before final heat treatment. These latter preforms were insulated and forged using die blocks preheated to 900-1150°C. The forging temperature was 1120-1150°C at a press heat velocity of 25 to 10 cm per minute. A total reduction of approximately 50% was accomplished.

TABLE 1
AF-115 - CHEMICAL ANALYSES; WT. PERCENT

<u>Element</u>	<u>Vacuum Melts</u>		<u>Atomized Heat</u>
C	.155	.164	.155
Mn	.01	.01	<.01
Si	<.01	<.01	.03
P	<.005	<.005	<.005
S	.003	.003	.002
Cr	10.80	11.08	10.20
Ni	Bal.	Bal.	Bal.
Mo	2.86	2.90	2.62
Co	15.04	15.30	14.95
Ti	3.92	3.85	3.90
Al	4.00	3.79	3.85
Cb	1.64	1.75	1.62
W	6.05	6.20	5.62
B	.022	.023	.023
Hf	0	0	2.02
Zr	0	0	.045
O	.0006	.0012	.0044
N	.001	.001	.001

All the billet material was then solution heat treated at 1190°C for 4 hours followed by a fan air cool. The alloy was then aged at 775°C for 16 hours followed by an air cool.

b. AF2-1DA

The AF2-1DA powder was also produced using the argon atomization process. The composition of the heat is given in Table 2. The resulting 100 mesh powder was sealed in a stainless steel can and compacted at 1903°C at 200 MPa for 21 seconds. The compact was then extruded at 1105°C at a reduction ratio of 7.3 to 1. The billet was then superplastically forged at 1105°C at a strain rate of 0.1 cm/cm/min. Superplastic forging provides an energy efficient method of producing a final product with uniform deformation.

The heat treating procedure for AF2-1DA was rather complex which is typical of advanced nickel-base superalloys. The forgings were first solution heat treated at 1210°C for two hours in order to put as much γ' as possible back into solid solution and to allow the grains to grow. The alloy was then stabilized at 1121°C for two hours to precipitate grain boundary γ' , and after an air cool, the forgings were aged at 705°C for 12 hours then at 816°C for 8 hours in order to precipitate and coarsen the fine γ' precipitates.

The major differences in heat treatment, then, between AF-115 and AF2-1DA were that the latter alloy was solution treated at a higher temperature which resulted in a larger grain size, and the AF2-1DA alloy was also stabilized at 1121°C for two hours which allowed the primary γ' to precipitate at the grain boundaries in a well defined network which was absent in the AF-115 microstructure. Although there were some differences in the aging treatments for the two alloys, they had similar γ' precipitate morphologies as will be described in the following section.

TABLE 2
CHEMICAL COMPOSITION - AF2-1DA; WT. PERCENT

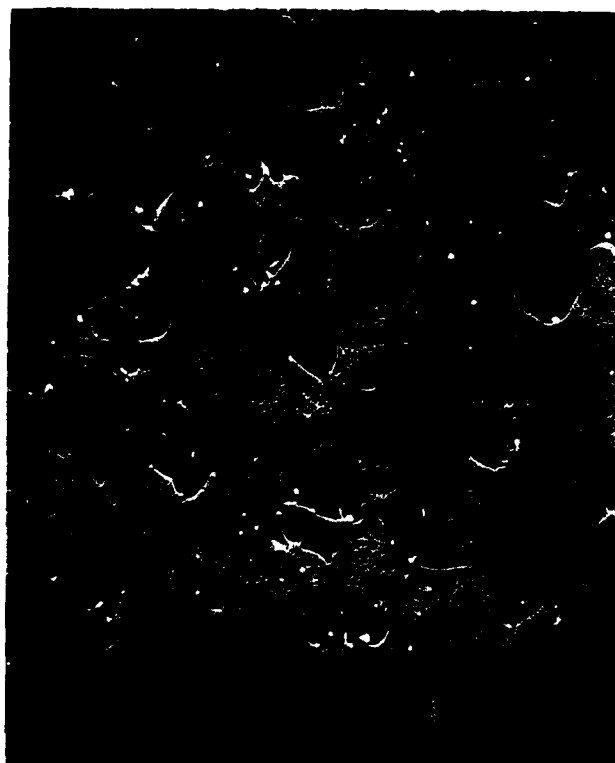
Cr	12.22	Zr	.084
Ti	2.89	Si	<0.1
Co	10.10	Fe	<0.1
W	5.70	B	.016
Al	4.70	C	.31
Mo	3.00	S	.007
Ta	1.90	P	< .002
Mn	<0.1	O ₂	65 PPM

Balance - Nickel

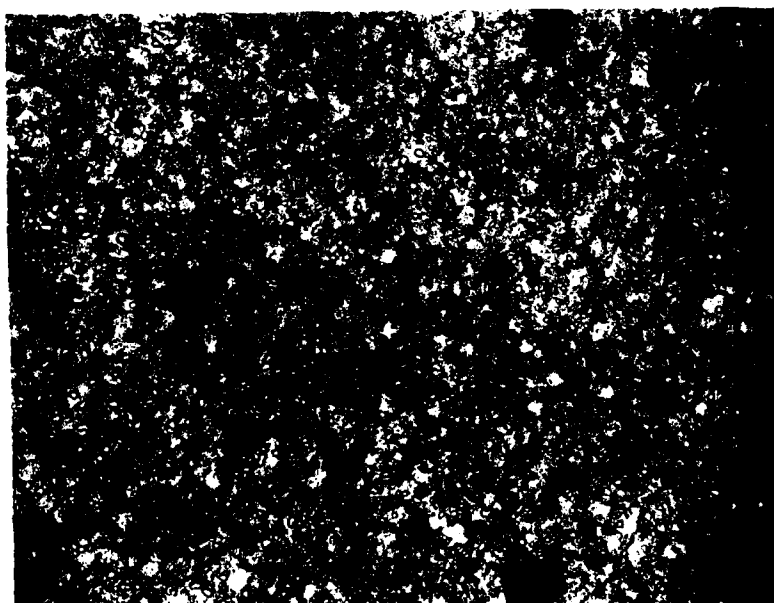
2. MICROSTRUCTURE

a. AF-115

In this investigation, the AF-115 alloy was studied in the HIP and heat treated, as well as the HIP plus forged and heat treated conditions. The recommended processing parameters which had been previously established for these treatments (Reference 93) resulted in very similar microstructures, differing significantly only in final grain size. The AF-115 microstructure was dominated by three distinct sizes of γ' precipitate which are shown in Figures 2b and 4a. The irregular shaped unsolutioned γ' precipitates laid along the grain boundaries and were approximately 3-10 μm along their major axis, and the cooling γ' which were contained within the grains were cuboidal in shape and approximately .25 μ on edge (Figure 4a). The ultra-fine aging γ' were more spherical in shape and had a diameter of .02 - .04 μm (Figure 2b).



(a)



(b)

50 μ m

Figure 4. a) SEM Micrograph of the AF-115 Microstructure Showing the Large Unsolutioned γ' and the Smaller Cooling γ' ; b) Optical Micrograph of Carbides Outlining Prior Powder Particle Boundaries

AF-115 also contained a small density of carbides approximately .50 μm in diameter. The carbides were, in general, uniformly distributed through the grains often lying near the unsolutionized γ' particles. There were observations in isolated areas of carbide particles decorating prior powder particle boundaries (Figure 4b), but this did not appear to be a general feature. Although neither quantitative chemical analysis nor microdiffraction studies were undertaken, the majority of the carbides in AF-115 was believed to be MC type. This was supported by microprobe analysis which indicated that the carbides were rich in MC formers; titanium, columbium, tantalum, and hafnium, and depleted in chromium, a M_{23}C_6 carbide former.

As previously mentioned, the two processing treatments of AF-115 resulted in different grain sizes. The average grain diameter of the as-HIP AF-115 was approximately 30 μm (ASTM #7.0), while the HIP plus forged alloy had an approximate average grain diameter of 19 μm (ASTM #8.5).

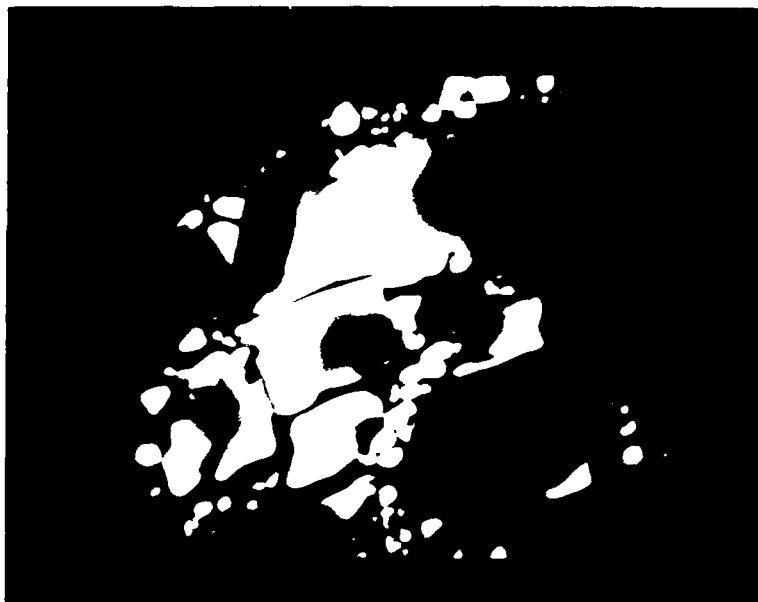
b. AF2-1DA

The AF2-1DA microstructure also had three sizes of γ' precipitates which are shown in Figures 2a, 5a, and 5b. An irregular shaped primary γ' (1-3 μm) decorated the grain boundaries while cuboidal cooling γ' (.25 μm) and aging γ' (.06 - .08 μm) were contained within the grains. As with AF-115, the total volume fraction of γ' was estimated to be greater than 60%. Due to the higher carbon content of this alloy, there were also more carbides in the AF2-1DA microstructure than in AF-115. The carbides were again rich in MC carbide formers, and were evenly dispersed through the microstructure (Figure 5a).

Figure 6a is an optical micrograph of the AF2-1DA structure which illustrates the very coarse grain size (approximately 200 μm diameter) of this alloy. The grains were purposely grown to this size to improve the creep rupture resistance of the alloy. Also pictured within the grains in Figure 6a are annealing twins which were prevalent throughout the microstructure. The twins were examined by thin foil analysis, and



(d)



(e)

1 μ m

Figure 1. (a) Micrograph of the surface of the test specimen showing the typical texture of the surface. (b) Micrograph of the surface of the test specimen showing the typical texture of the surface. (c) Micrograph of the surface of the test specimen showing the typical texture of the surface. (d) Micrograph of the surface of the test specimen showing the typical texture of the surface. (e) Micrograph of the surface of the test specimen showing the typical texture of the surface.



(a)



(b)

Figure 6. a) Optical Micrograph of the AF2-1DA Microstructure;
b) Diffraction Pattern of a Twin in AF2-1DA 110
Zone Axis, $[111]$ Twin Plane

they were found to be of the $\{111\}$ type, as expected for FCC alloys. The diffraction pattern of a typical twin is shown in Figure 4b which illustrates the $(\bar{1}\bar{1}\bar{1})$ nature.

3. DEFECTS

a. AF-115

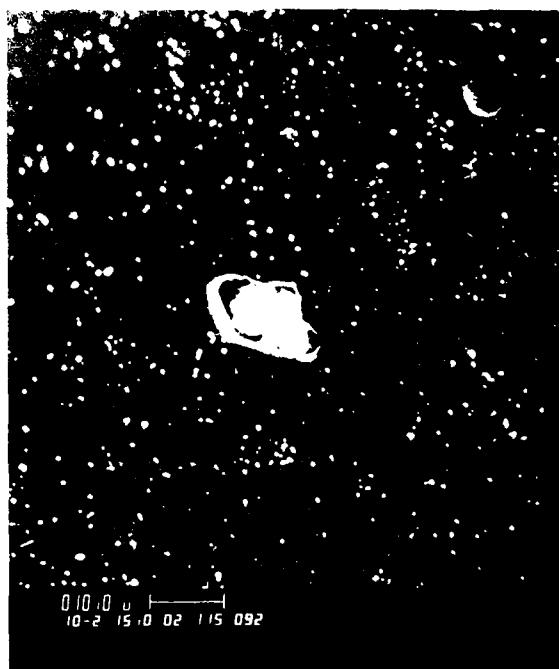
There were three distinct defect types found in the AF-115 alloy; pores, nonmetallic inclusion, and hafnium oxide inclusions. The pores, which were a by-product of the powder production process, were the most populous of the defects. The porosity was a result of argon gas having been adsorbed onto the powder surface or entrapped in hollow particles during the argon atomization phase. The gas then expanded during the solution heat treatment which resulted in the large pores.

The level of porosity, which is considered a function of atomization processing and solutionizing temperature, was quantitatively determined using a thermal induced porosity (TIP) test. This test involves measuring the density of a sample of the billet material before and after the solutionizing heat treatment. The change in density due to the expansion of the gas at high temperature was thus a measure of the porosity level. The heat of AF-115 used in this study had a change in density due to thermal-induced porosity of .42% after solutionizing at 1190°C. While this was probably too high a level to be used for many applications, it did provide an ideal material with which to study the effect of spherical defects. The pores ranged in size from a few microns in diameter to approximately 130 μm in diameter, and the pores were basically spherical in shape (Figure 7a).

The second most prevalent defect in AF-115 was the nonmetallic inclusions; their population was much less than that of the pores. These inclusions were tramp pieces of ceramic equipment liners used in the powder production process (Figure 7b), and they were generally high in concentrations of calcium, silicon, aluminum, and magnesium. The inclusions ranged in size up to 100 μm in length, and their shape varied



(a)



(b)

Figure 7. a) SEM Micrograph of a Pre-existing Argon Pore in AF-115; b) SEM Micrograph of a Nonmetallic Inclusion in AF-115

from spherical to elliptical. The inclusions were often fractured before fatigue testing, and they were usually poorly bonded to the matrix. As a result, ceramic pieces often fell out during metallographic preparation, leaving empty holes. However, at high magnification, the inclusion holes could generally be distinguished from pre-existing argon pores by the fact that they were more irregularly shaped than the relative symmetrical pores. A representative area is presented in Figure 8a which shows the typical population of pores and inclusions in AF-115 at low magnification.

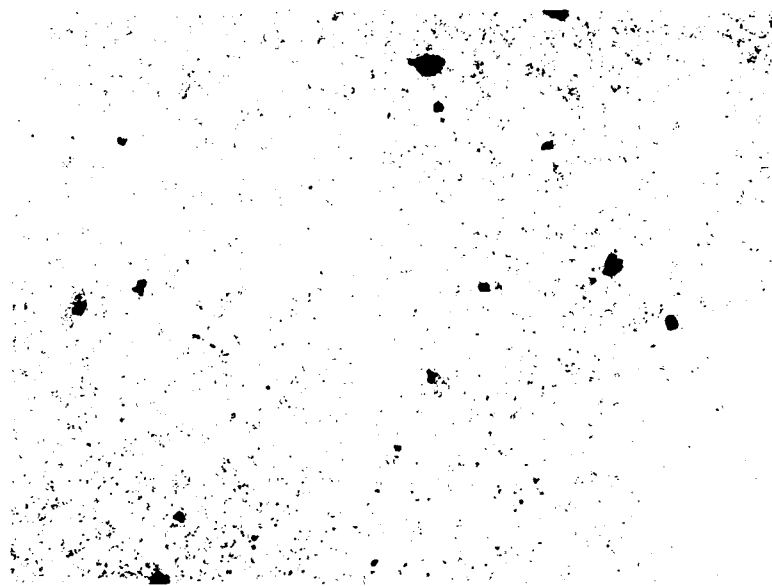
The least populous defects in this heat of AF-115 were the hafnium oxide inclusions (probably HfO_2). These were plate-like and were up to 125 μm in diameter with a thickness of only 5 μm (Figure 8b). They formed in the melt as a result of the high hafnium content which was included as a carbide former. HfO_2 particles were normally bonded more strongly to the matrix than the ceramic inclusions, and could be polished and viewed in cross section without being pulled out of the structure.

b. AF2-1DA

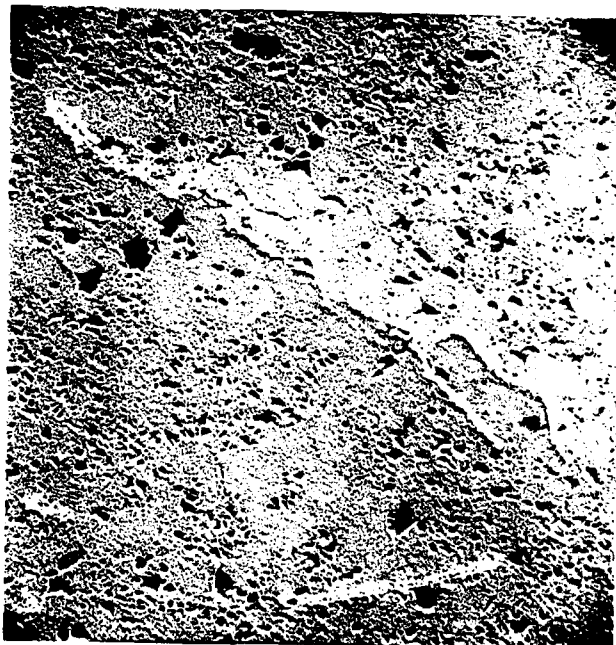
Although the AF2-1DA powder was also made by the argon atomization technique, the processing of this heat of powder was such that there was no significant level of porosity in the forgings. There were also no HfO_2 inclusions in the AF2-1DA billet. The only defects were tramp ceramic inclusions which were similar to those in the AF-115 alloy. Their size ranged up to 100 μm in length, and they often appeared as holes on a metallographic section, again, due to the poor bonding between the inclusion and matrix. A representative micrograph of the defect population in AF2-1DA is presented in Figure 9.

4. SUMMARY

AF-115 and AF2-1DA are high strength P/M nickel-base superalloys with complex microstructures dominated by a high volume fraction of the γ' precipitate. The two heats studied in this investigation contained contrasting populations of defects which covered a range of sizes and shapes. AF-115 contained ceramic inclusions, plate-like HfO_2 inclusions,



(a)



(b)

Figure 8. a) Representative Distribution of Pores and Non-metallic Inclusions in AF-115; b) SEM Micrograph of a Hafnium Oxide Inclusion

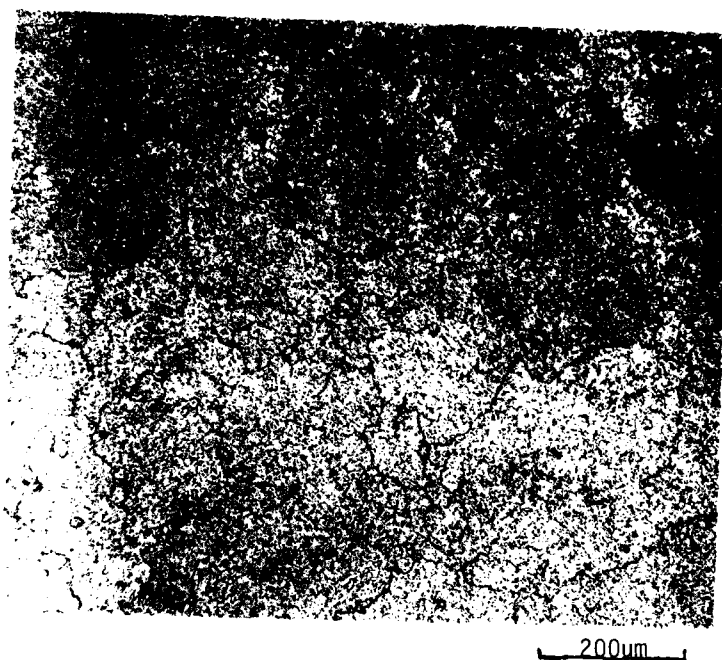


Figure 9. Representative Distribution of Nonmetallic Inclusions
in AF2-1DA

and a large population of spherical pores. AF2-1DA, however, only had elliptical nonmetallic inclusions similar to those in AF-115. The alloys also had microstructures which differed significantly in grain size. This would be expected to result in differences in strength and rupture properties between the two alloys. A finer grain size generally promotes tensile strength, and more coarse grains would usually result in better creep resistance. The contrasting differences in defect population would also be expected to influence mechanical properties, especially fatigue properties, based on the findings reported in the literature review. It is this influence of defect character which is of primary concern in this investigation.

SECTION IV

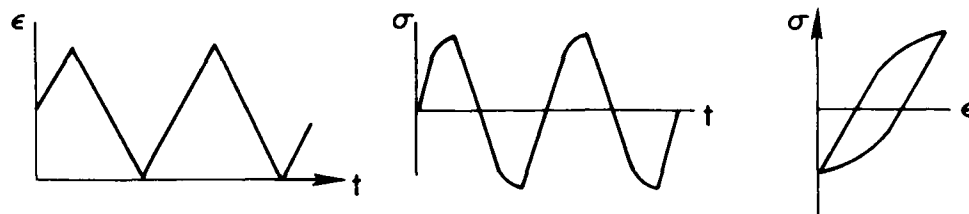
EXPERIMENTAL PROCEDURES

1. FATIGUE TESTING

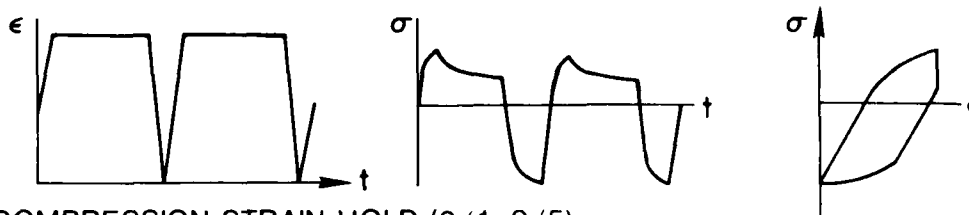
The fatigue test program was designed to investigate the effect of defects on the crack initiation behavior of two P/M superalloys over a range of experimental conditions, and to determine the role of the concurrent time-dependent deformation on the low cycle fatigue behavior of these same alloys. As a result, fatigue tests were performed at three temperatures, at two cyclic frequencies, and with two different waveforms. The test temperatures were 22°C, 640°C, and 760°C. The maximum temperature at which both alloys maintained their high strength was 760°C, and it was thus chosen as the primary test temperature to accentuate the effect of time dependent damage; 649°C, still a relatively high temperature for these alloy systems, was also included to compare time dependent damage rates with the higher temperature data. Finally, room temperature tests were performed to contrast with the elevated temperature results since at low temperature the slip behavior and initiation mechanisms were expected to be different than at 649°C and 760°C due to the lack of significant thermal activation.

Strain-controlled fatigue testing was used predominantly in this test program. Strain control testing is considered to better simulate the cyclic behavior of localized plastic strain concentrations in nominally elastic bodies than does stress control testing. Two general waveforms were included in the testing, continuously cycling and cyclic dwell; these waveforms are illustrated in Figure 10. The continuously cycling tests comprised the major portion of the testing effort, and these included specimens fatigued at two frequencies, 20 cycles per minute and 0.2 cycles per minute (cpm). The 20 cpm frequency both represented the upper limit of the strain-controlled fatigue system and was also rapid enough to consider the damage as being free of any time-dependent deformation (creep). The 0.2 cpm rate was chosen to accentuate the time-dependent deformation at elevated temperature for comparison with the 20 cpm data. The cyclic dwell testing included

CONTINUOUS STRAIN CYCLING (20 cpm, 0.2 cpm)



TENSION STRAIN HOLD (1/0, 5/0)



COMPRESSION STRAIN HOLD (0/1, 0/5)

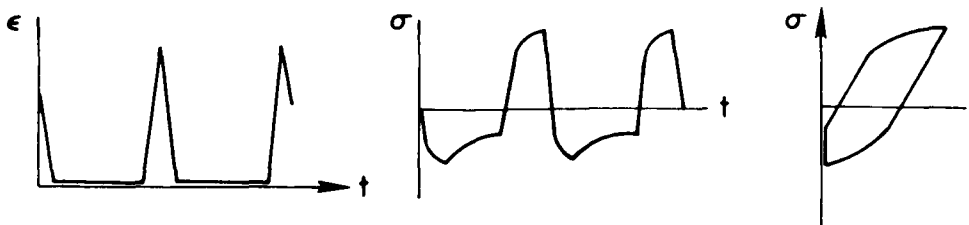


Figure 10. Fatigue Waveforms Used in the Test Program

both one and five minute hold periods in either tension or compression, again, as shown in Figure 10. Note that since the tests were performed in strain control, the maximum strain limit was maintained during a cyclic dwell test and the load was allowed to relax. The magnitude of the load reduction could then be equated to an increase in time dependent strain by dividing by the elastic modulus.

All tests were performed, as mentioned, in total strain control using a servohydraulic closed-loop fatigue system and an axial extensometer. The test specimens used were uniform section smooth bars with a diameter of .250 inches, as shown in Figure 11. Due to the statistical nature of the influence of defects on fatigue behavior, this specimen was chosen over the hourglass type in order to test as great a volume of material as possible. Standard specimen preparation techniques were used including low stress grinding and mechanical polishing. The effect of surface finish on crack initiation will be discussed later.

Specimens were tested at a strain ratio, A , of +1 where

$$A = \frac{\text{Alternating Strain}}{\text{Mean Strain}}$$

A strain ratio of $A = +1$ corresponds to zero to tension to zero strain cycling as illustrated in Figure 10. During the tests, the inelastic strain and the load range were continuously recorded on strip chart recorders. The specimens were run to complete failure, and the number of cycles to failure, N_f , was the fatigue life value reported. Attempts were made to establish a value for cycles to crack initiation, N_i , using the load drop method. This procedure considers that crack initiation occurs when the stress range decreases a certain percentage of the original value, usually 5% or 10%. For these alloys, N_i did not vary appreciably, however, from N_f using this method. This indicated that this method was not sensitive to microcracking in superalloys since initiation was observed in the very early stages of fatigue life for some specimens.

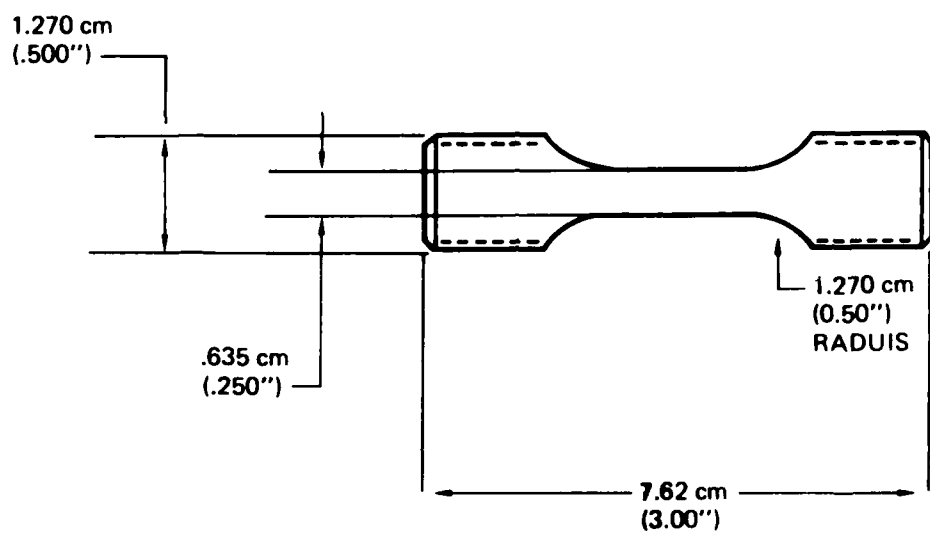


Figure 11. Uniform Section Smooth Bar Fatigue Specimen

2. METALLOGRAPHIC EXAMINATION

After a fatigue specimen had been tested to failure, one of the fracture surfaces was generally retained for SEM examination and the other half of the specimen was nickel-plated, sectioned axially, mounted, and polished for metallographic observation. The SEM fractographic study usually centered on identifying both the location and character of the fatigue origin, and the morphology of the early stage of crack growth. The crack that was identified and shown to be responsible for failure was termed the "dominant" crack.

Observations on the metallographic cross-section were of particular importance in this study. "Secondary cracks", those cracks that initiated independently but were not responsible for failure, were studied using optical microscopy, as well as scanning and transmission electron microscopy since they were small enough to detail their interaction with the microstructure. In many instances, it was necessary to locate and identify a particular crack using the SEM and then characterize the details of the cracking process at a higher magnification using the TEM and two stage carbon-platinum replicas. Using a special numbered grid (Figure 12) the specific crack or feature could be located on the replica inside the TEM. Figure 13 is a schematic of the types of data obtained from both the fractographic and metallographic examinations of the failed specimens.

Thin foils were also cut from the gage section of failed AF2-1DA specimens and prepared for TEM analysis using a jet polisher and solution of 300 ml methanol, 120 ml N-butyl alcohol, and 30 ml perchloric acid. Specimens were polished at -60°C at a potential of 30 volts and a current of 10-12 milliamps. It was found that both the temperature and amperage were critical in this process. The polishing solution was necessarily discarded after two specimens due to unexplained but consistently found contamination. The TEM work was necessarily limited to AF2-1DA due to the extreme difficulty in thinning AF-115 because of its high porosity level. The electron optic instruments used during the course of this study were the JEOL 100C TEM, JEM 200 TEM, and the ETEC Autoscan SEM.

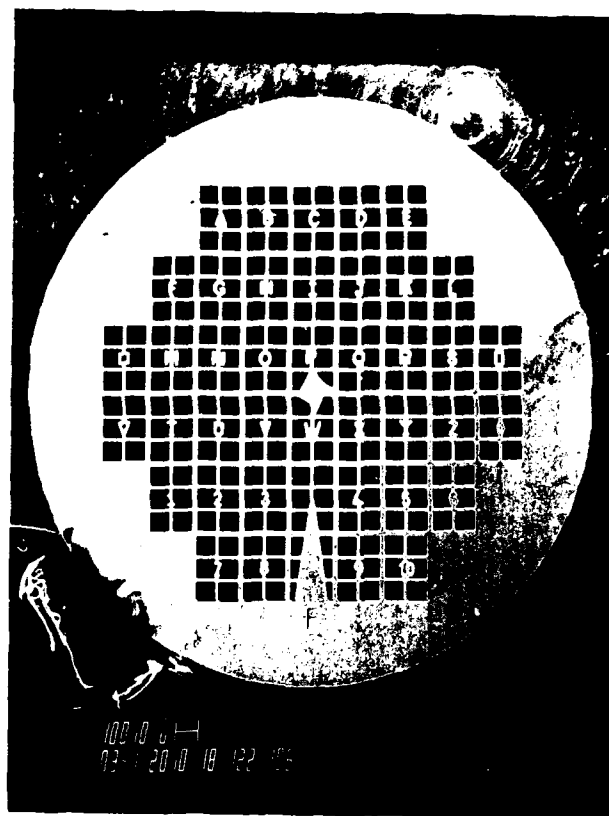
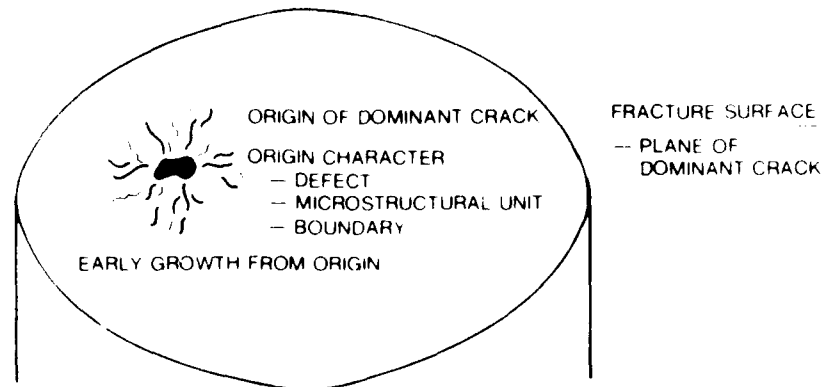


Figure 12. TEM Replica Grid Used to Locate Specific Features While in the Microscope

METALLOGRAPHIC OBSERVATIONS

DOMINANT CRACK



SECONDARY CRACKS

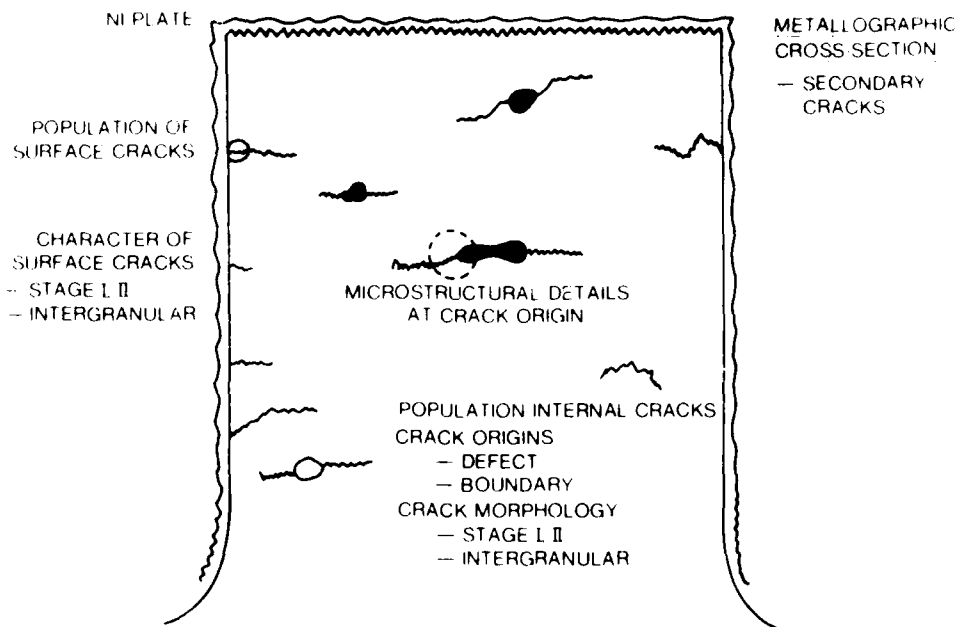


Figure 13. Illustration of the Range of Metallographic Observations Made in Galled Specimens

SECTION V

TEST RESULTS

In this section, the tensile and fatigue results for both alloys will be presented. Tensile data will be described as a function of temperature and strain rate. The effect of temperature, cyclic frequency, and waveform on fatigue life will also be discussed. Alloy performance will be compared and a rationale for this behavior will be presented.

1. TENSILE PROPERTIES

The 760°C tensile properties for AF2-1DA and for the HIP and HIP plus forged conditions of AF-115 are presented in Table 3. In addition, the 0.2 offset yield strength values for these same materials have been obtained from the initial quarter cycle of loading of fatigue tests at room temperature, 649°C, 760°C, and 816°C at cyclic frequencies of 20 and 0.2 cycles per minute (cpm). These data are summarized in Table 4 and all the data are also plotted in Figures 14a, 14b, and 15. Curves have been included to suggest approximate data trends.

Both the HIP and HIP plus forged conditions of AF-115 were comparable in strength. The data in Table 4 and Figures 14a and 14b show that the yield strengths were greatest at room temperature and relatively constant at 649°C and 760°C at both strain rates of .40/min and .004/min. The yield strengths also decreased significantly at 816°C.

The yield strength of AF2-1DA was considerably less than that of AF-115 at all test conditions. Generally, the same behavior pattern existed, though, the room temperature strength was greatest and the strength decreased as the temperature increased. However, the fall-off in strength now began at 760°C and again it was a strong function of strain rate (Figure 15).

These results are particularly important in that the fatigue behavior of superalloys is generally a function of the alloy's yield strength; the

TABLE 3
TENSILE PROPERTIES

<u>Spec.</u>	<u>Temp (°C)</u>	<u>Y.S., MPa (ksi)</u>		<u>UTS MPa (ksi)</u>		<u>R_a (%)</u>	<u>Elong. (%)</u>
AF-115-HIP							
2-19	760	989	(143.5)	1156	(167.7)	8.3	11.6
7-19	760	1013	(146.9)	1196	(173.4)	7.6	12.9
9-20	760	1051	(152.5)	1192	(172.9)	8.9	9.5
9-19	815	934	(135.4)	1010	(146.5)	11.7	11.2
AF-115-HIP + Forge							
5-33	760	1040	(150.9)	1132	(164.2)	8.0	13.1
5-35	760	1041	(151.0)	1164	(168.8)	10.0	12.8
AF2-1DA							
B2-4	760	909	(131.8)	958	(138.9)	-	17.9
B2-5	760	898	(130.3)	964	(139.8)	-	17.5
B1-67	815	871	(126.3)	927	(134.4)	28.8	24.0

TABLE 4
YIELD STRENGTH DATA*

<u>Spec.</u>	<u>Temp (°C)</u>	<u>ε̇ (min)</u>	<u>Y.S., MPa (ksi)</u>	
AF-115-HIP				
2-9	20	~ .40	1098	(159.2)
2-7	649	.004	1009	(146.4)
7-1	760	.40	1003	(145.4)
7-2	760	.40	1013	(146.9)
7-6	760	.004	982	(142.4)
7-8	760	.004	955	(138.5)
4-1	812	.40	963	(139.6)
9-3	812	.004	794	(115.2)
7-13	812	.004	832	(120.6)
AF-115-HIP + Forge				
5-7	760	~ .40	995	(144.3)
5-20	760	.40	1045	(151.6)
5-4	760	.004	955	(138.5)
5-16	760	.004	1009	(146.3)
5-17	815	.40	1020	(147.9)
5-24	815	.40	994	(144.1)
5-21	815	.004	763	(110.6)
5-22	815	.004	688	(99.8)
AF2-1DA				
1-19	20	~ .40	942	(136.6)
1-20	20	.40	945	(137.0)
2-30	649	.40	885	(128.3)
2-12	649	.40	886	(128.5)
2-17	649	.004	899	(130.4)
2-36	649	.004	874	(126.7)
2-8	760	.40	899	(130.4)
2-32	760	.004	845	(122.5)
2-33	760	.004	838	(121.5)
1-1	812	.40	765	(111.0)
2-40	812	.40	772	(112.0)
2-45	812	.004	646	(93.7)
1-5	812	.004	667	(96.7)

*.2% yield stress from first cycle of fatigue tests at 20 cpm and 0.2 cpm.

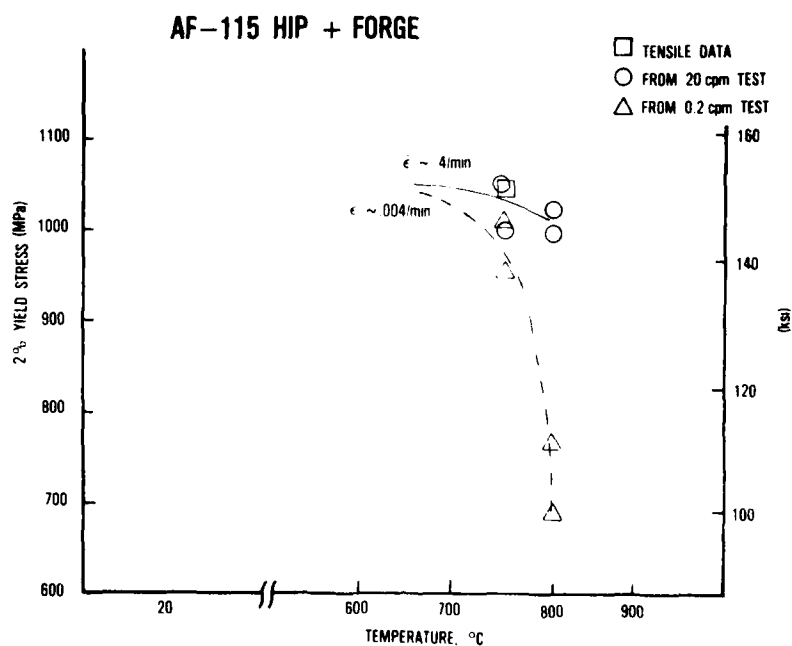
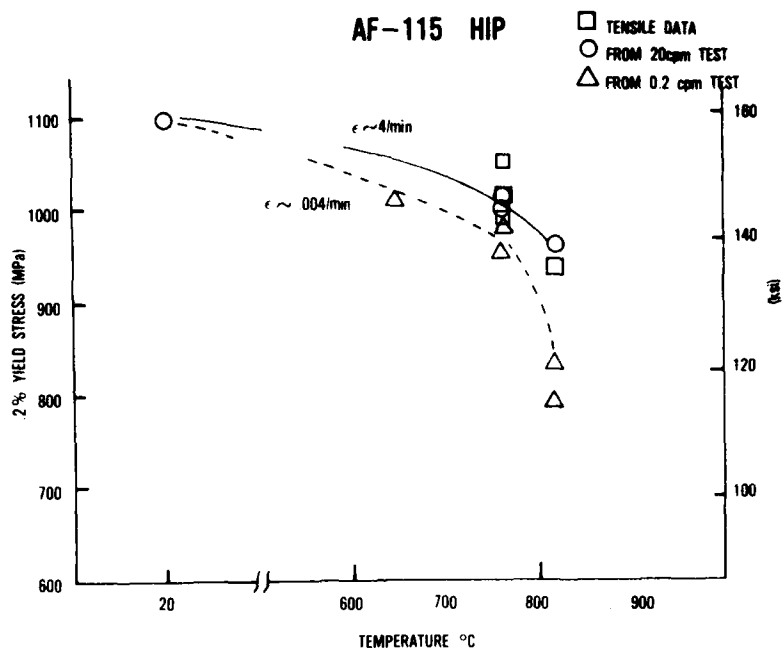


Figure 14. 0.2% Yield Strength vs Temperature for a) AS HIP AF-115,
b) HIP Plus Forged AF-115

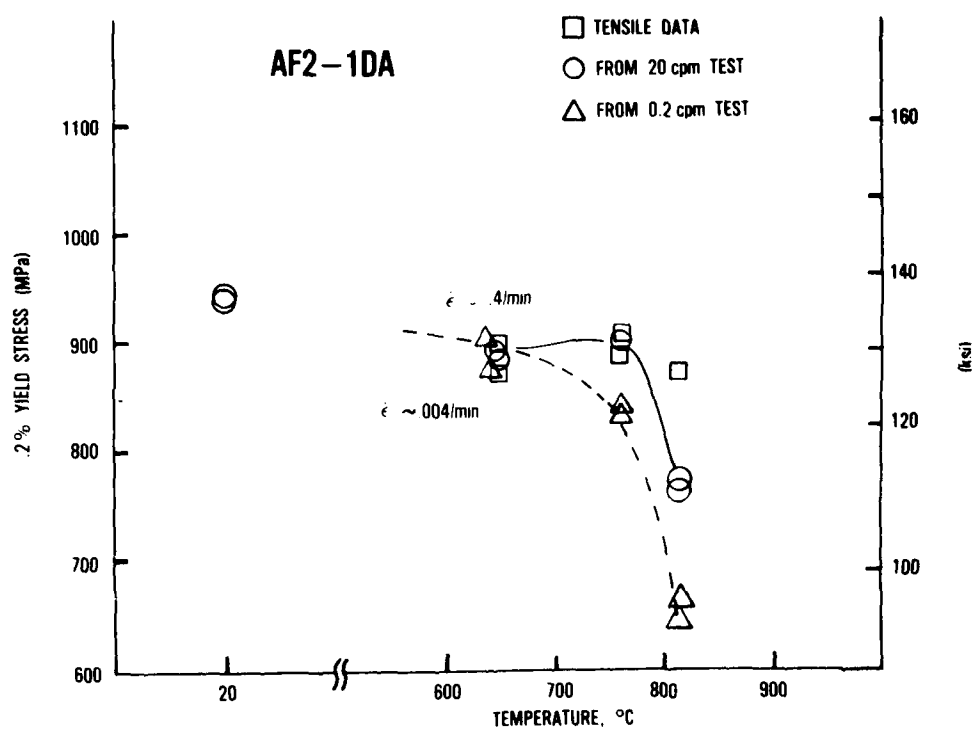


Figure 15. 0.2% Yield Strength vs Temperature for AF2-1DA

greater an alloy's strength, the longer the fatigue lives when the lives are compared as a function of the total strain range or stress range (References 94, 95). This is due to the fact that fatigue initiation is controlled by localized plastic strain, and at a constant total strain range, the greater the yield strength of the alloy the smaller will be the plastic strain component. The tensile results of the two alloys, therefore, suggest that the fatigue performance of AF-115 should be superior to AF2-1DA, and the fatigue lives for both alloys should degrade as the temperature is increased and the frequency decreased.

2. FATIGUE TEST RESULTS

a. AF-115

The continuously cycling fatigue data for AF-115 in the HIP and HIP plus forged conditions are presented in Figures 16 and 17, respectively and a complete summary of all the fatigue testing is also compiled in Appendix B. The data in both cases exhibited a near linear relationship with total (elastic + plastic) strain range, and at high temperature, there was neither a significant effect of temperature nor frequency for the strain ranges tested. Tests at 0.2 cpm, however, were realistically limited to the higher strain ranges (shorter lives) due to limitations on testing time. Again, the included lines suggest data trends.

The room temperature fatigue tests for the as HIP condition of AF-115 (Figure 16) were limited in number. There was a large increase in life compared to the elevated temperature results for the test at $0.9 \Delta \epsilon_t$, but the apparent amount of scatter for the three room temperature tests preclude any conclusions being drawn.

The fatigue behavior of the HIP and HIP plus forged conditions of AF-115 at 760°C are compared in Figure 18. There was no significant difference in life for the two alloy conditions. This result might have been expected since, as discussed, there was only a small difference in microstructure for the two conditions. Due to this similar fatigue behavior, all AF-115 test specimens will be referred to in this investigation as one population unless specifically noted otherwise.

FATIGUE BEHAVIOR - AF-115 HIP

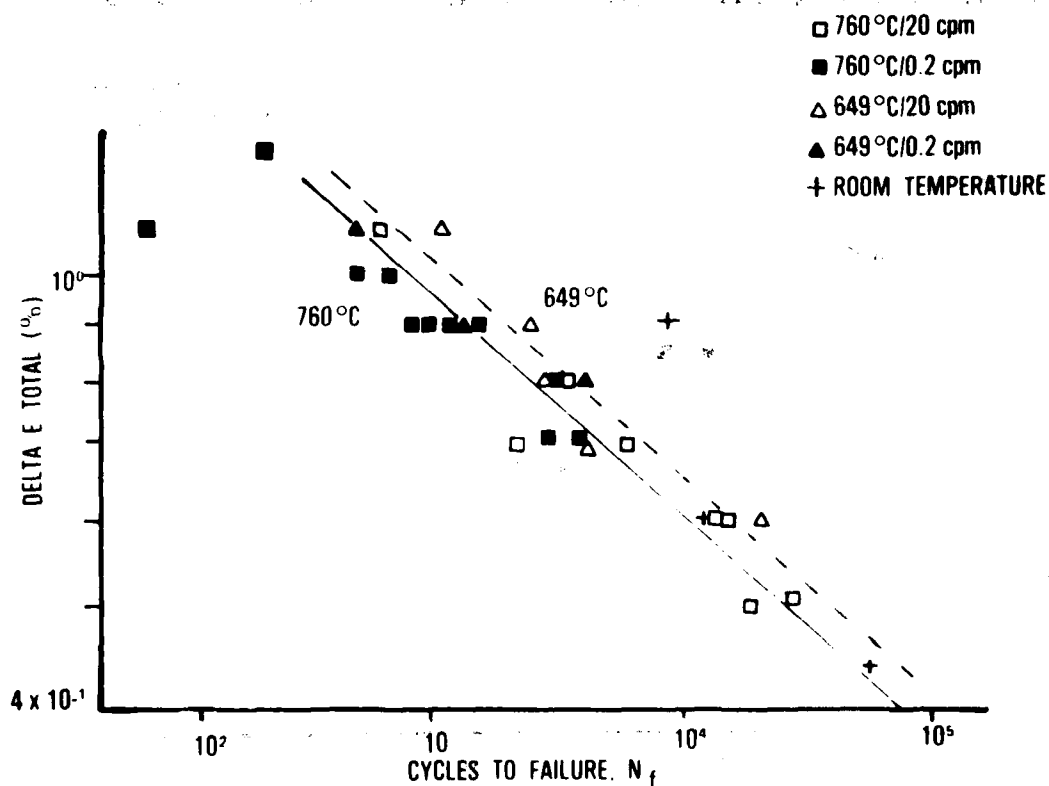


Figure 16. Continuously Cycling Fatigue Data for AF-115, AS-HIP

FATIGUE BEHAVIOR AF - 115 HIP & FORGED

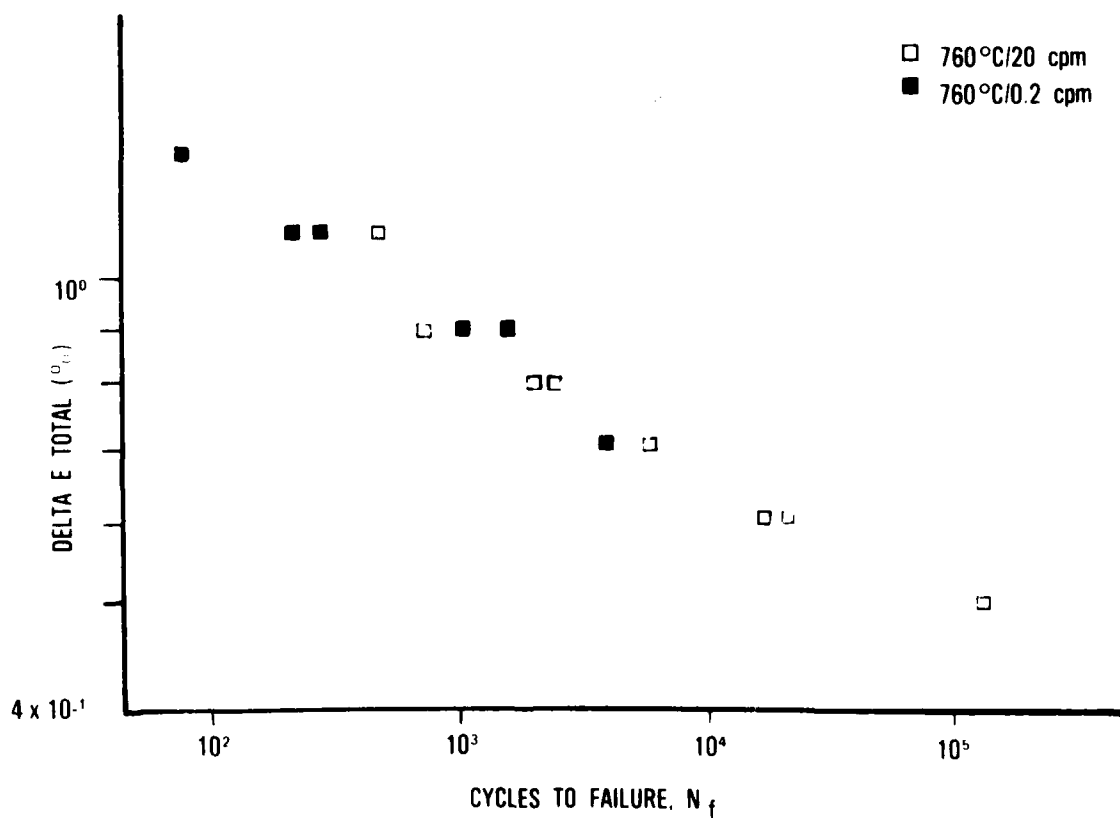


Figure 17. Continuously Cycling Fatigue Data for AF-115, HIP Plus Forged

HIP VS HIP + FORGED CONDITIONS AF-115

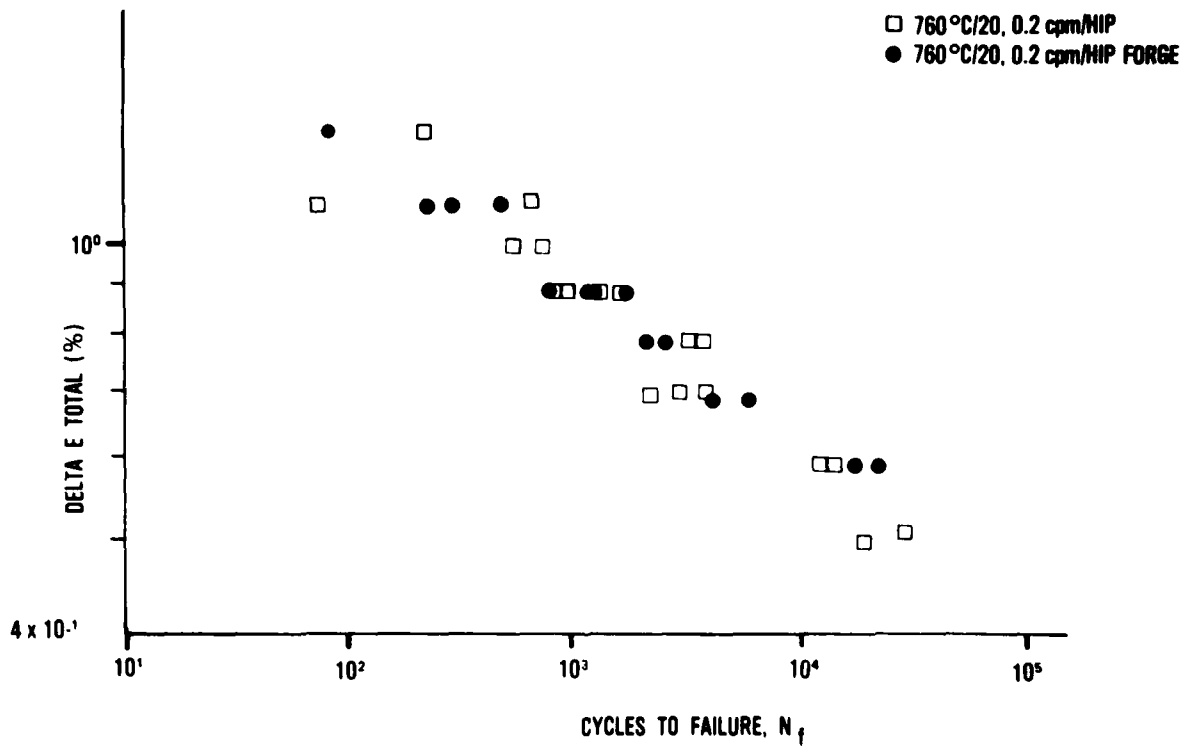


Figure 18. Comparison of the Fatigue Behaviors of the AS-HIP and HIP Plus Forged Conditions of AF-115, 760°C

Both tensile and compressive dwell tests were performed for AF-115 at 760°C. The data are summarized in Figure 19 and included for reference is the line from Figure 16 representing the 760°C continuously cycling data. Figure 19 shows that when tests are compared at the same total strain range, tensile dwell tests had longer fatigue lives than did the compressive dwell tests, and the tensile dwell tests had even longer lives than the continuously cycling tests. The behavior has been studied previously in more detail by Hyzak and Bernstein (Reference 90) for the superalloy, René 95, and will be discussed later.

b. AF2-1DA

The fatigue test results for the AF2-1DA alloy are presented in Figure 20. The data are represented by linear relationships with total strain range but now in two separate regimes. This representation was chosen since it appears to better describe the data than a single straight line and the change in slope can be correlated with a change in initiation mode as will be described in the following section. Figure 20 shows that there was a small reduction in life when the temperature was raised from 649°C to 760°C. As with AF-115, however, there was no frequency effect over the strain ranges tested. The room temperature test results again showed a large increase in life at 0.9% $\Delta\epsilon_t$, but due to the limited data no conclusions could be drawn.

Tensile and compressive strain dwell tests were also performed for AF2-1DA at 760°C and 649°C and the results are presented in Figure 21 along with the line from Figure 20 representing the 760°C continuously cycling data at high strain ranges. At 760°C, the tensile hold tests had longer lives than the compressive hold tests when compared at the same total strain range, in agreement with the AF-115 results. The 649°C dwell tests had nearly equal lives in tension and compression, and the values of life were comparable to those for the continuously cycling tests at the same temperature.

CYCLIC DWELL TESTS – AF – 115

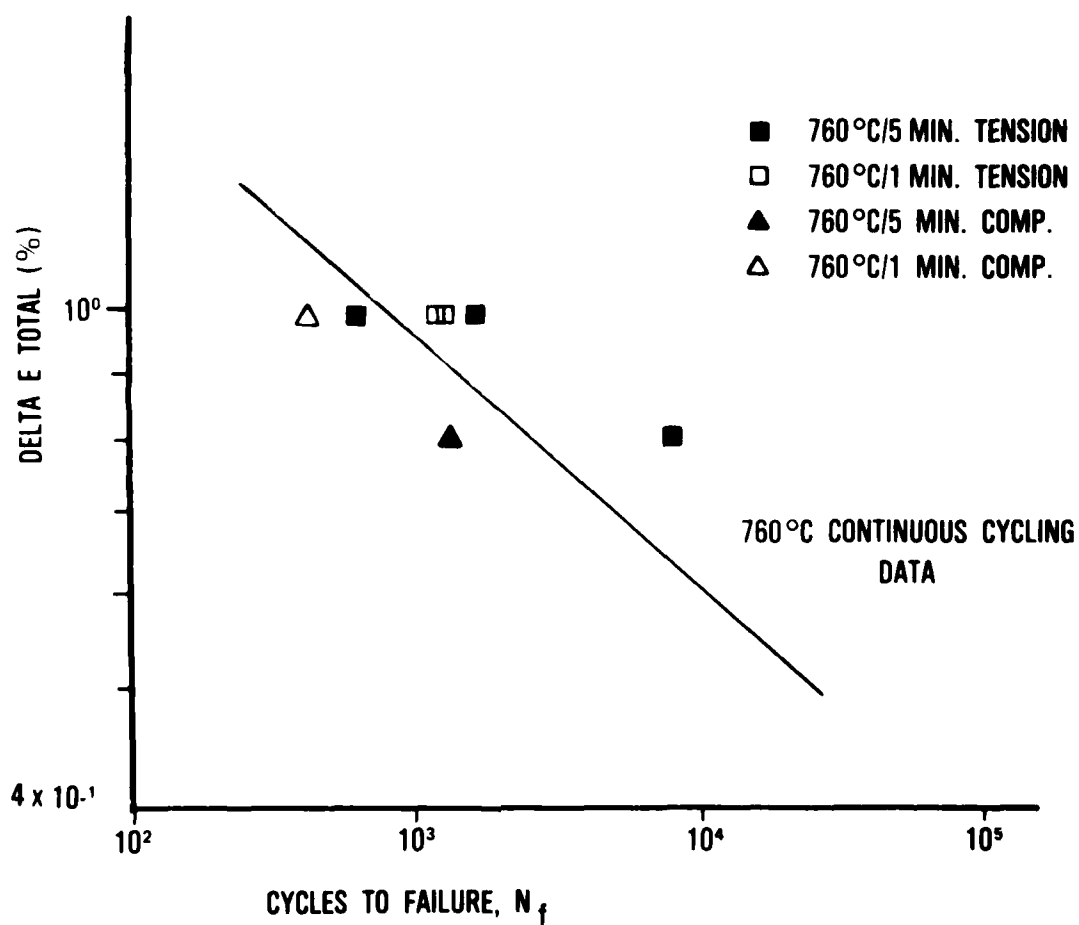


Figure 19. Cyclic Dwell Tests, AF-115, 760°C

FATIGUE BEHAVIOR — AF2-1DA

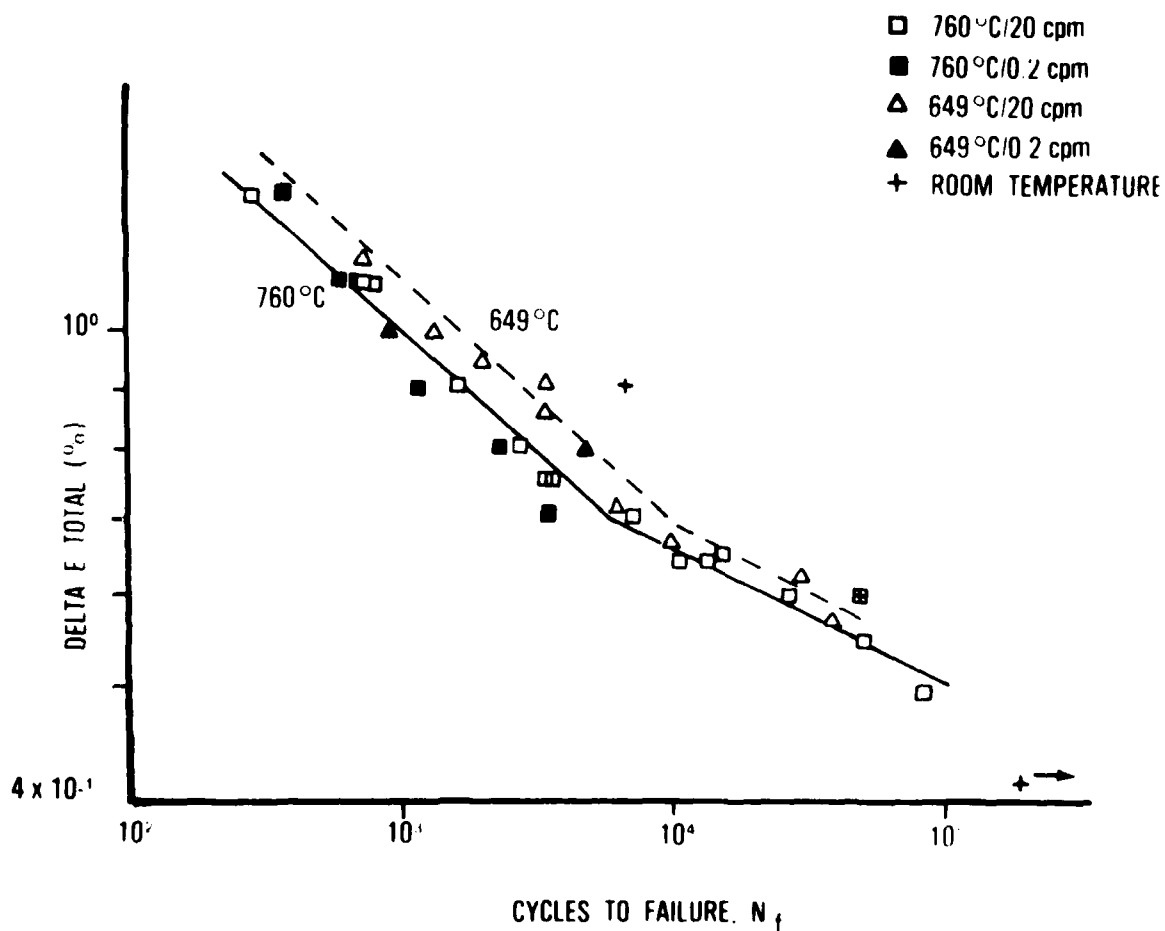


Figure 20. Continuously Cycling Fatigue Data for AF2-1DA

CYCLIC DWELL TESTS — AF2-1DA

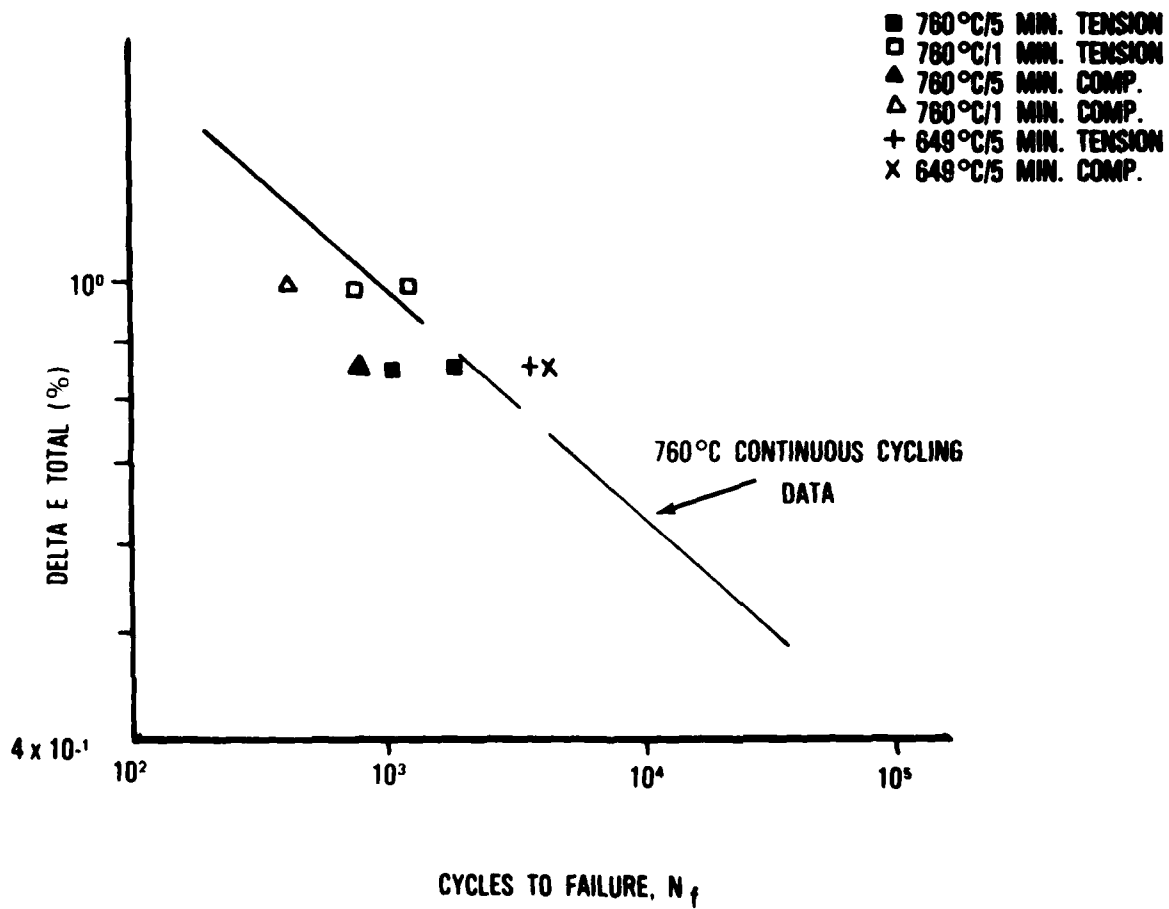


Figure 21. Cyclic Dwell Tests, AF2-1DA, 760°C and 649°C

The 760°C, 20 cpm fatigue data for AF-115 and AF2-IDA are compared in Figure 22. The results show that at high strain ranges the two alloys had comparable fatigue lives, but in the longer life regime, AF2-IDA tests had longer lives.

3. SUMMARY

The results of the continuously cycling fatigue tests have shown that there is a good correlation of the fatigue data with total strain range. This relationship was also noted for Udimet 700 by Wells and Sullivan (Reference 12) who concluded that total strain range should give a better correlation than the plastic strain range for materials that deform and crack heterogeneously. They reasoned that the range of individual slip band displacements which most directly affects the fatigue life is proportional to the total strain range while the plastic strain range represents the integration of slip band displacements throughout the gage length. The data also showed there was only a small effect of test temperature (649°C, 760°C), and essentially no effect of cyclic frequency over the range of conditions tested. Extrapolation of these results for longer life tests (lower strain range, slower frequency), however, is not recommended since time-dependent damage mechanisms (oxidation, creep) will surely have more of an effect as the test time is increased. The room temperature fatigue results were comparable with the elevated temperature data at the lower strain ranges, while they appeared to be superior, i.e., exhibit longer life, at the higher strain ranges.

The incorporation of a dwell period at high temperature significantly affected the fatigue lives of both alloys. When the data were compared at the same total strain ranges, tensile dwell tests had longer fatigue lives than both the compressive dwell tests and the continuously cycling tests. Although this same observation has been made before, this result is unusual in that creep damage would be expected to be more pronounced in the tensile hold tests, and, as a result, the tensile dwell tests would be anticipated to have shorter lives than the compressive dwell tests. This behavior, however is believed to be due to the development of appreciable mean stresses during cyclic dwell tests, as will be discussed in a subsequent section.

AF - 115 VS AF2 - 1DA FATIGUE BEHAVIOR/ 760°C

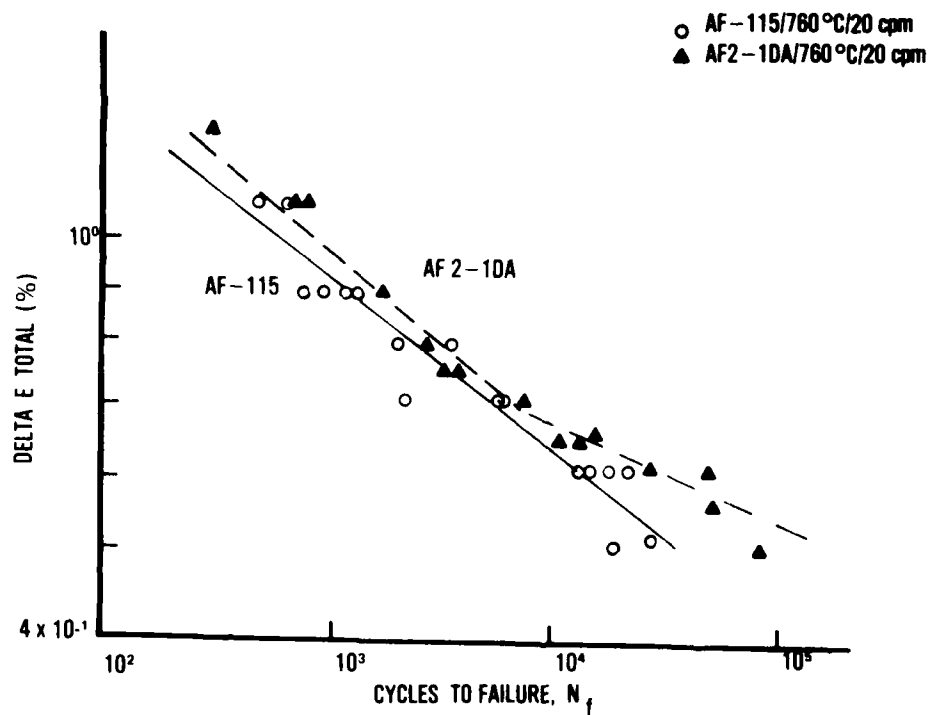


Figure 22. Comparison of the Fatigue Behaviors of AF-115 and AF2-1DA, 760°C and 20 cpm

SECTION VI

CRACK INITIATION MODES - ELEVATED TEMPERATURE
CONTINUOUSLY CYCLING FATIGUE

In this section the process of crack initiation will be described for specimens fatigued at elevated temperature under continuously cycling conditions. SEM observations of both fracture surfaces, and polished and etched metallographic cross-sections of failed specimens will be presented. The mechanisms of nucleation will be described with particular attention to the origins of cracking, as well as to the morphology of the early stages of crack growth. These results will later be correlated with thin foil studies of the deformation behavior.

1. OVERVIEW - FATIGUE ORIGINS

SEM examination of all the AF-115 and AF2-1DA elevated temperature tests showed that for both alloys there was a transition in the nucleation site of the dominant crack from a surface or near surface site to an internal location as the fatigue strain range was reduced. This transition will subsequently be referred to as the surface-subsurface transition (SST). Figure 23 shows a schematic of the fatigue life curves for both alloys with representative examples of the predominant initiation modes in each regime. In brief, at higher strain ranges, AF-115 initiated the dominant crack at a near surface pore and below the SST the mechanism changed to crack nucleation at a subsurface metallic inclusion. For AF2-1DA above the SST, initiation occurred at the surface in a Stage II mode but at lower strain ranges the cracks originate internally also at inclusions.

The location of the fatigue origins are included on the fatigue life curves in Figures 24 and 25 for all specimens tested. For AF2-1DA the SST occurred at $0.64 \Delta \epsilon_t$, and for AF-115 the transition was between 0.70 and $0.60 \Delta \epsilon_t$. Thus there was a similar behavior associated with these two alloys although they had very different defect populations. It was also discovered that other high strength P/M superalloys exhibited a

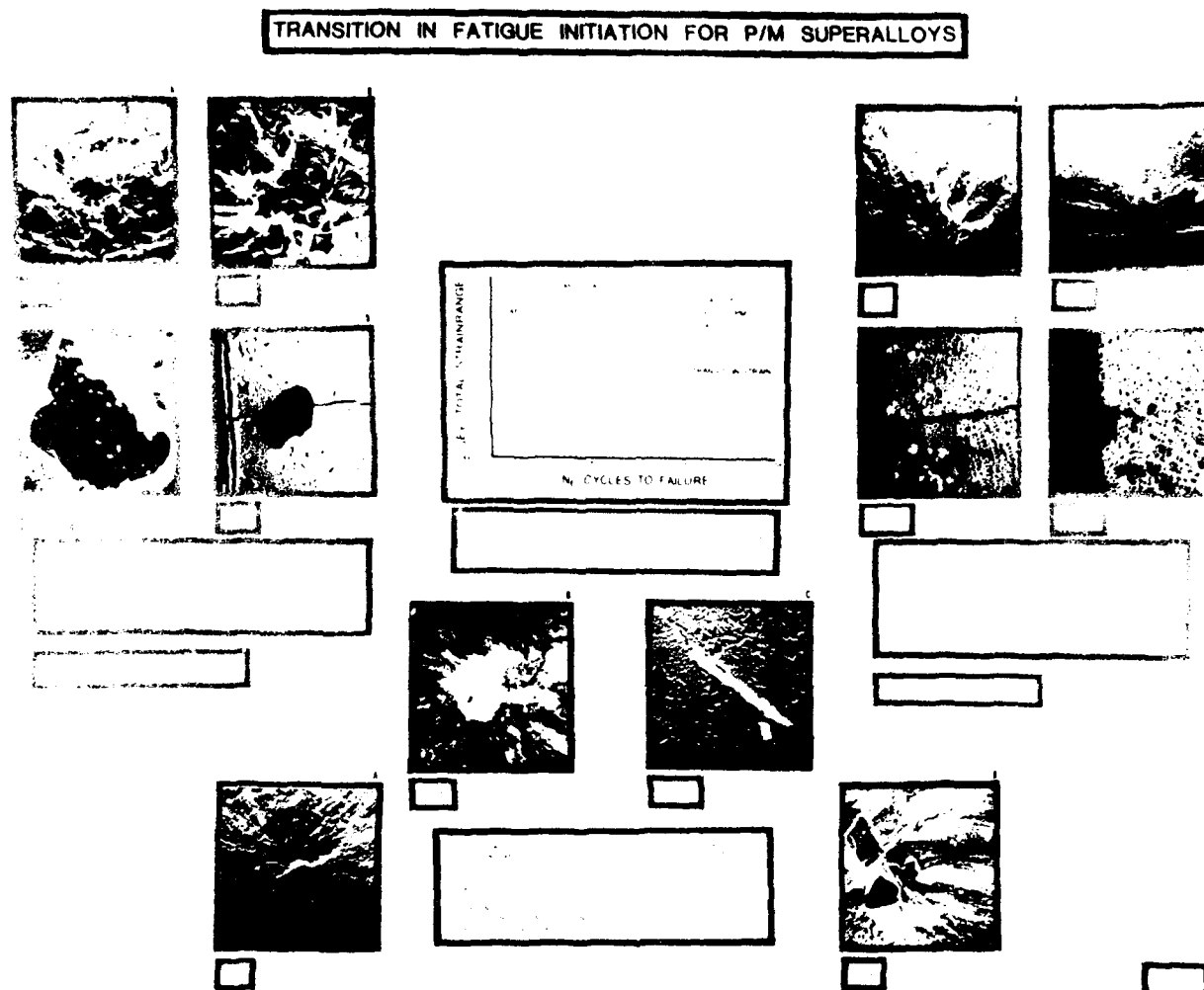


Figure 23. Summary of the Surface-Subsurface Transition (SST) in the Site of the Dominant Fatigue Origins at Elevated Temperatures

similar transition in the site of fatigue initiation (Reference 96). It was, therefore, concluded that the SST is a general phenomenon at least for the high strength P/M nickel-base superalloys.

In this section, the crack initiation processes will be described in detail. First the mechanisms of surface initiation for both alloys above the SST will be presented, followed by a description of subsurface initiation at the lower strain ranges.

2. SURFACE INITIATION - HIGH STRAIN RANGE

a. AF2-1DA

In this temperature and strain range regime, there were three surface crack initiation mechanisms that were observed, depending on cyclic frequency and temperature (649°C or 760°C); there were transgranular initiation on a plane normal to the tensile axis, transgranular initiation at an angle approximately 45° to the tensile axis, and intergranular cracking. The most prevalent mode of initiation and early growth, however, was transgranular initiation normal to the tensile direction (References 1, 6). On the fracture surface, these sites were usually flat and featureless as shown in Figures 26a and 26b for different specimens. In each case, the shape of the crack and the morphology of the tear lines indicated that the crack originated at the specimen's surface, although there was generally no obvious microstructural feature or defect that could be associated with the origin (Figure 27a). The microscopic resolution was limited, however, in the area of the origin due to oxidation and rubbing of the fracture surfaces during fatigue cycling (Figure 27b). Features on the order of carbides, large γ' precipitates, and small inclusions ($\approx 1\mu\text{m}$) could easily go unnoticed under these conditions. In limited cases, however, larger defects were identified at the crack origin (Figure 28). The surrounding area of early crack growth had the same appearance as did the fracture surfaces for specimens where no defect could be identified indicating that in both cases there was a similar cracking process.

AF-115 FATIGUE ORIGINS/ELEVATED TEMP

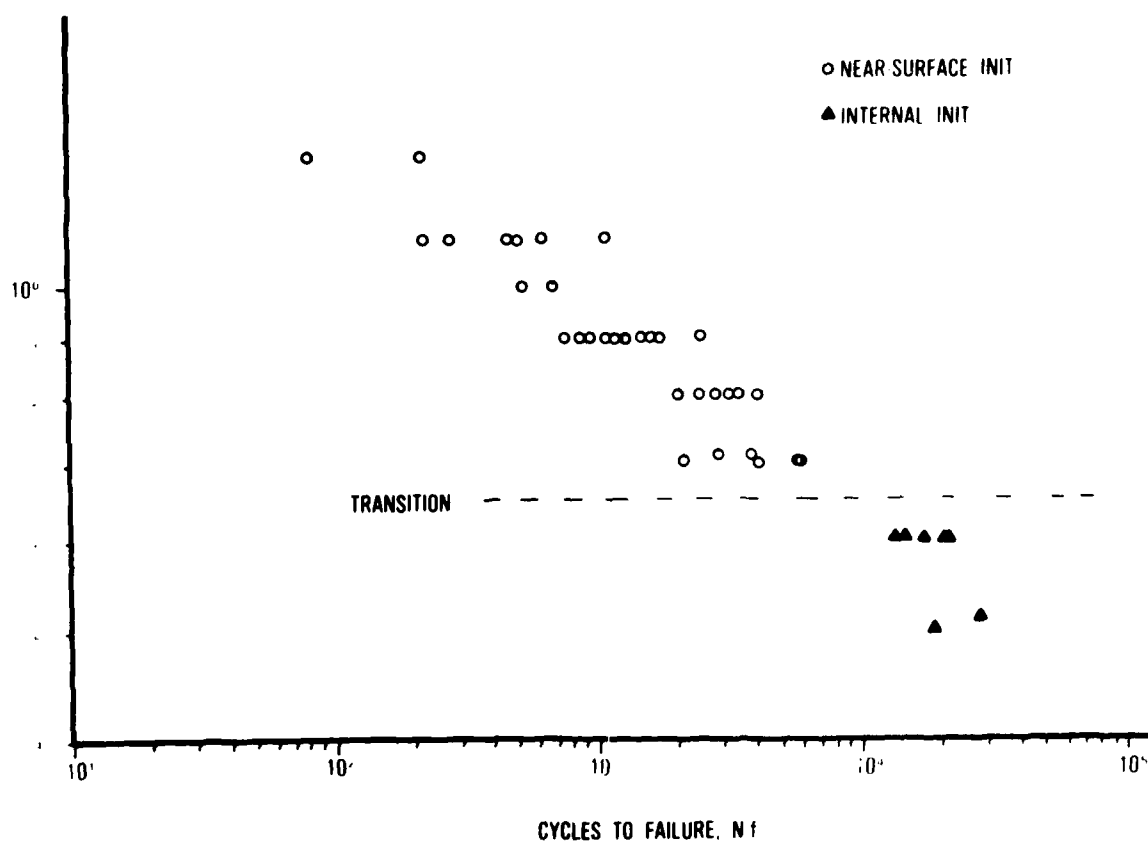


Figure 24. Location of the Dominant Fatigue Origins for the Elevated Temperature AF-115 Tests

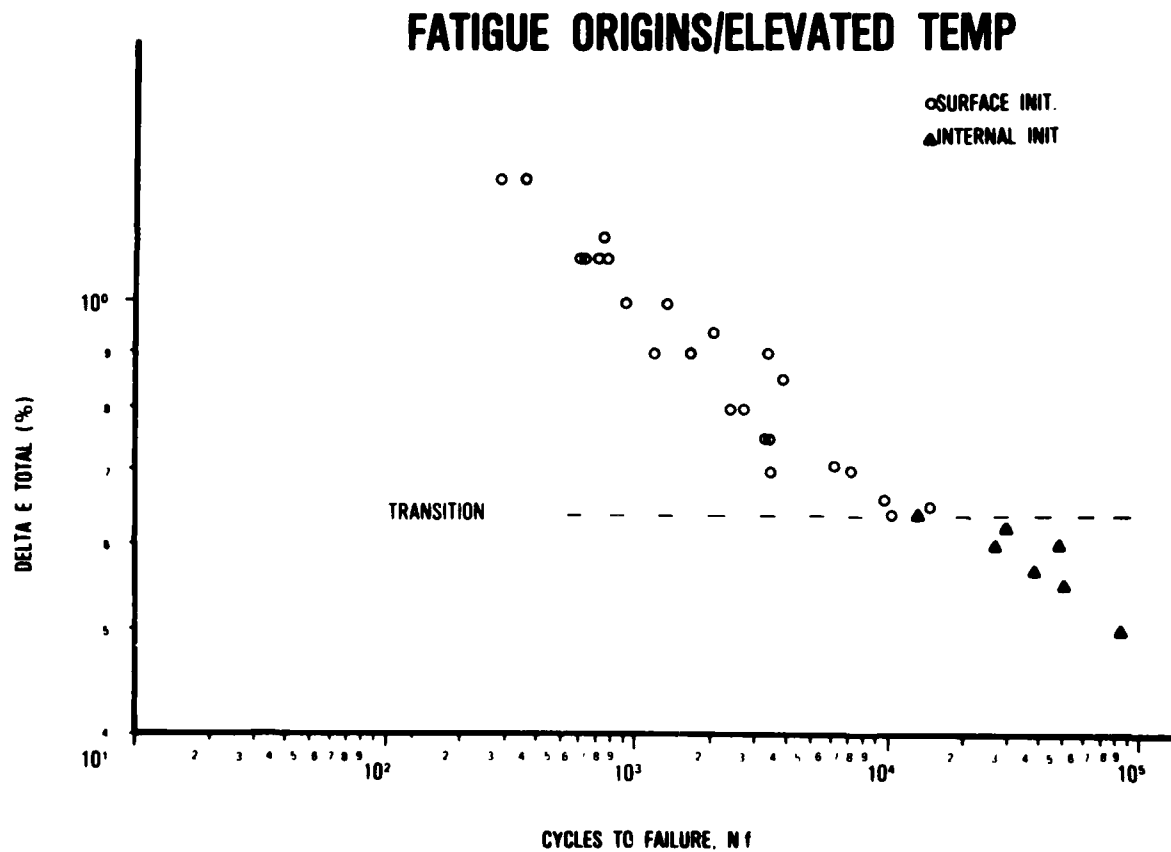


Figure 25. Location of the Dominant Fatigue Origins for the Elevated Temperature AF2-1DA tests

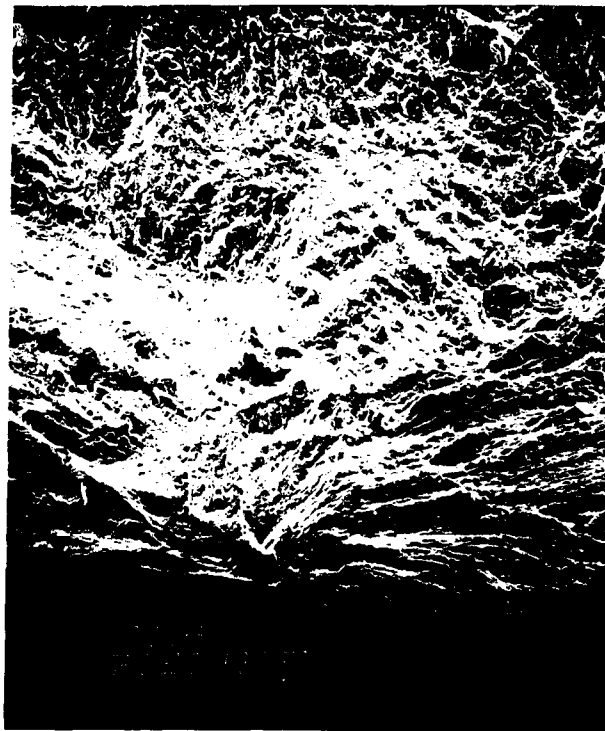


Figure 26. SEM Micrographs of Typical Stage II Surface Crack Initiation Sites on AF2-1DA Fracture Surfaces



(a)



(b)

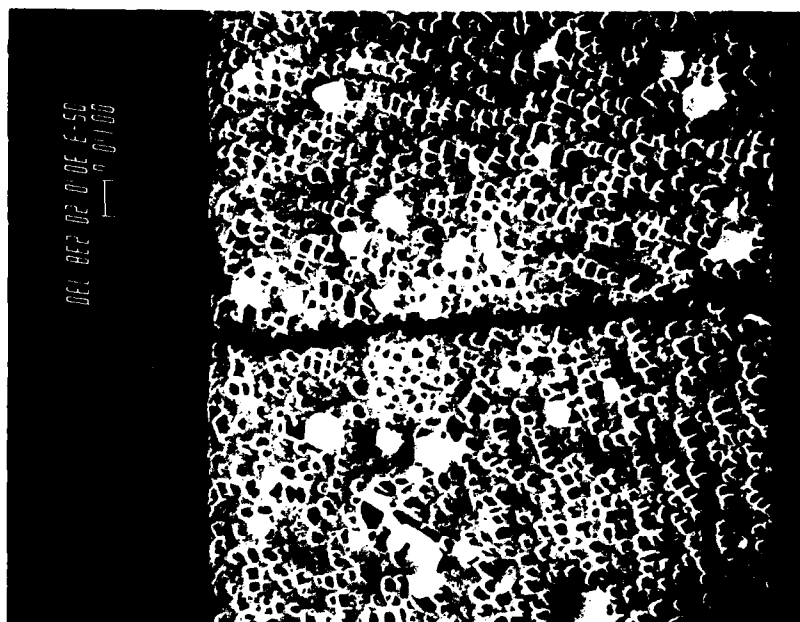
Figure 27. a) High Magnification Micrograph of a Stage II Fatigue Origin on an AF2-1DA Fracture Surface; b) Distorted Fracture Surface Near a Stage II Crack Origin, 760°C



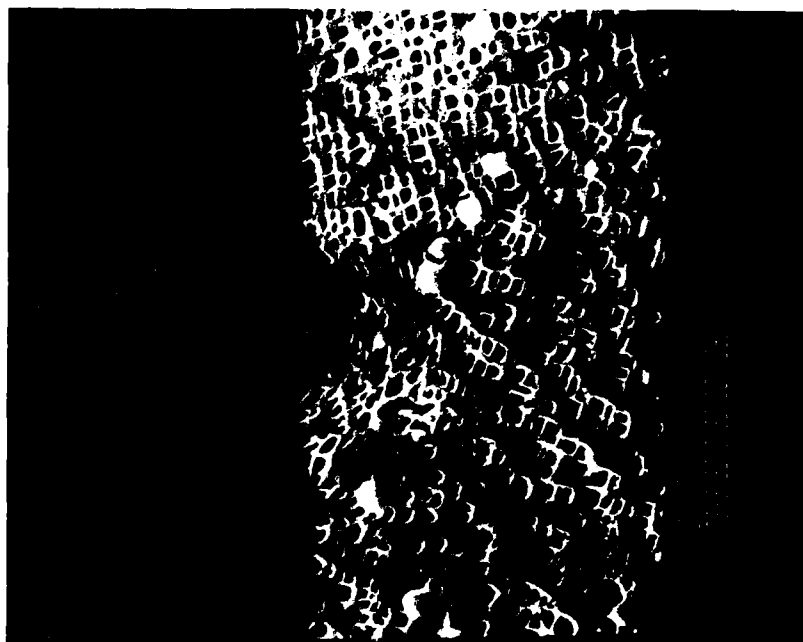
Figure 28. Defect Cavity at the Origin of a Stage II Fatigue Crack in AF2-1DA

Examination of the metallographic cross-sections of failed specimens, as illustrated in Figure 13, revealed the profile of these surface initiated cracks in AF2-1DA (Figure 29a); in this example, the crack appeared to grow transgranularly normal to the tensile direction. Serial sectioning through the cross-section of a selected specimen at increments of approximately .0005 of an inch revealed additional information. Of the 18 cracks that were examined during the study, four had crack origins at small nonmetallic inclusions ($< 1 \mu\text{m}$ diameter) lying near the specimen's surface (Figure 29b), two had origins near suspect carbides (Figure 30a), and two had no identifiable points of origin even though they were sectioned completely through their cross section. The remainder of the cracks were not sectioned through their entire cross-section so no conclusion could be made concerning their origins. The serial sectioning also showed that the cracks intersected the plane of observation at the same latitude after each polishing step. This confirmed that these cracks were normal to the tensile axis and were, therefore, Stage II cracks. In addition, no surface offsets were associated with these cracks indicating that cracking in these cases did not occur by a surface shearing mechanism. As has been noted, Gell and Leverant (Reference 1), and Wells (Reference 6) have observed Stage II crack initiation in other superalloys at elevated temperature.

In addition to the dominant cracks, there were many secondary cracks that were initiated in these specimens, especially at the higher strain ranges ($> 0.90\% \Delta\epsilon_f$). Extensive observations of metallographic sections have shown that although dominant cracks originated only at the surface in the high strain range regime, a large number of secondary cracks nucleated internally as well as at the surface, and subsurface cracks usually initiated at large nonmetallic inclusions (Figure 30b). The observations also indicated that the number and the length of the secondary cracks, both on the surface and internally, decreased as the fatigue strain range decreased. This observation is in agreement with the findings of other investigators for a range of alloy including steels (Reference 97) aluminum (References 97, 98), and pure copper (Reference 99). These investigators found that at high strain ranges, crack initiation occurred at many sites at a small fraction of the



(a)

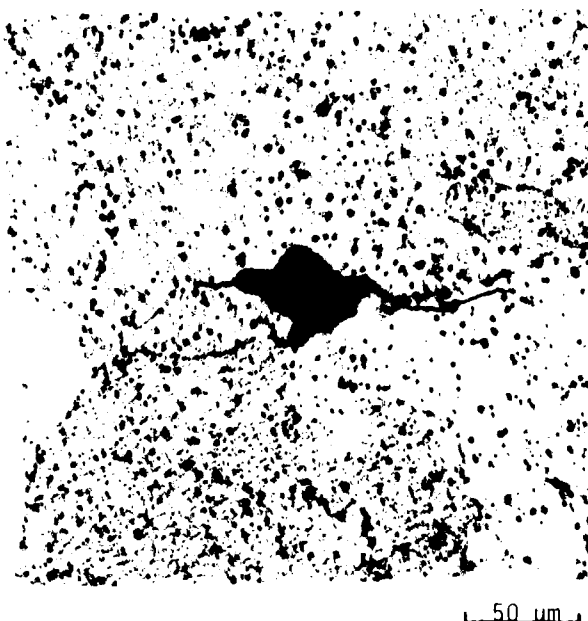


(b)

Figure 29. Polished and Etched Cross-Section of a Failed AF2-1DA Specimen. a) Surface Crack Propagating Normal to the Tensile Axis; b) Crack Initiating at a Small Surface Inclusion



(a)

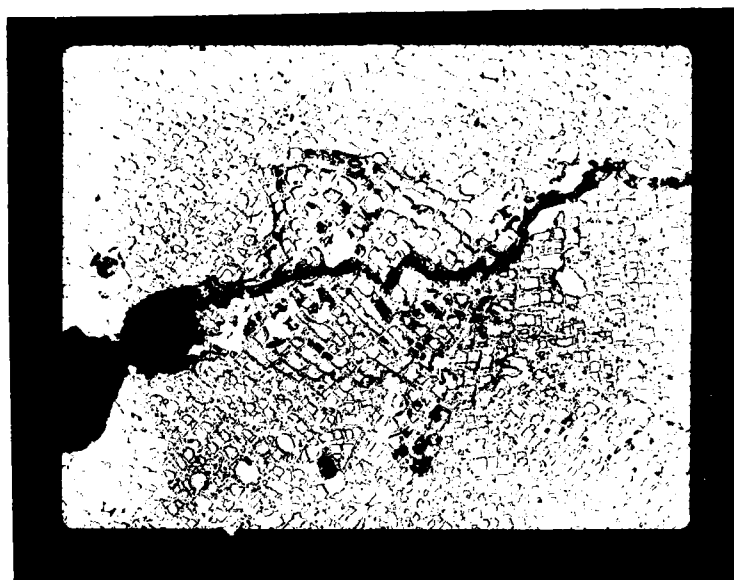


(b)

Figure 30. a) Surface Crack Possibly Having Originated at an MC Carbide in AF2-1DA; b) Subsurface Cracking at an Inclusion in AF2-1DA After Testing at a High Strain Range

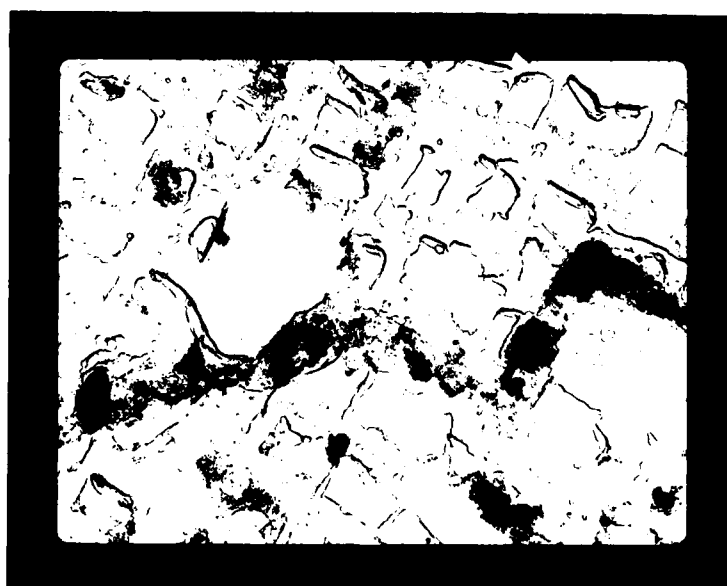
total fatigue life (< 10%) and the percentage of the fatigue life spent in crack nucleation increased as the cyclic strain range decreased. As a result, crack propagation was found to control most of the life in this high strain regime.

As was noted earlier, Stage II crack initiation is not usually observed for most alloys; cracking generally begins in Stage I mode and then changes to Stage II propagation. For this reason, the mechanism of Stage II initiation has not been addressed in the literature. There has been some research published, however, on the general mechanism of Stage II crack propagation, most notably by Laird (Reference 7) and Neumann (References 8, 100). The mechanism of Stage II growth was shown by Neumann to consist of alternating slip on local slip planes at the crack tip in copper single crystals and Fe 3% Si, and Laird has proposed a model for Stage II propagation referred to as the plastic blunting mechanism. This latter model accounts for several features of Stage II growth including striation formation. To try to understand the mechanism of Stage II initiation in nickel-base superalloys, however, the path of Stage II cracks in AF2-1DA were studied using TEM replica techniques. Observations of the crack path morphology were made on internally initiation cracks to reduce the obliteration of microstructural features due to surface oxidation. Already shown in Figure 30b was a Stage II crack originating from an inclusion in a specimen fatigued at $1.1\% \Delta \epsilon_t$. Figure 31a is a view of the same inclusion and crack on a two stage carbon-platinum replica examined in the TEM. At higher magnification, Figure 31b shows that the crack propagated in the γ matrix avoiding the large γ' particles, often making extreme changes in direction in order to do this. Although the details are somewhat inconclusive, it also appears that the crack preferred to travel along the γ - γ' interface rather than strictly within the γ . Similar behavior was also observed for another crack emanating from an inclusion, as shown in Figure 32a. The TEM replica image of the crack path, Figure 32b, shows the crack traveling around the precipitates, as well as around the MC carbide.



(a)

10 μm



(b)

1 μm

Figure 31. TEM Image of Two Stage Carbon-Platinum Replica Showing
a) A Crack Initiating at an Inclusion; b) At Higher
Magnification, the Crack Avoiding Large ' Precipitates

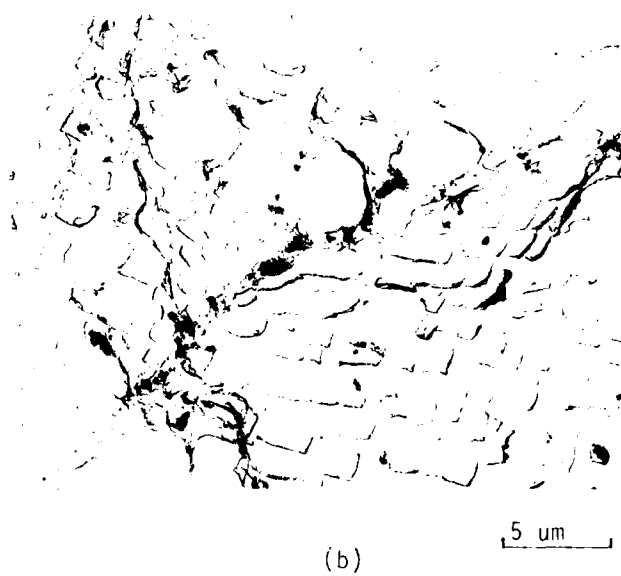
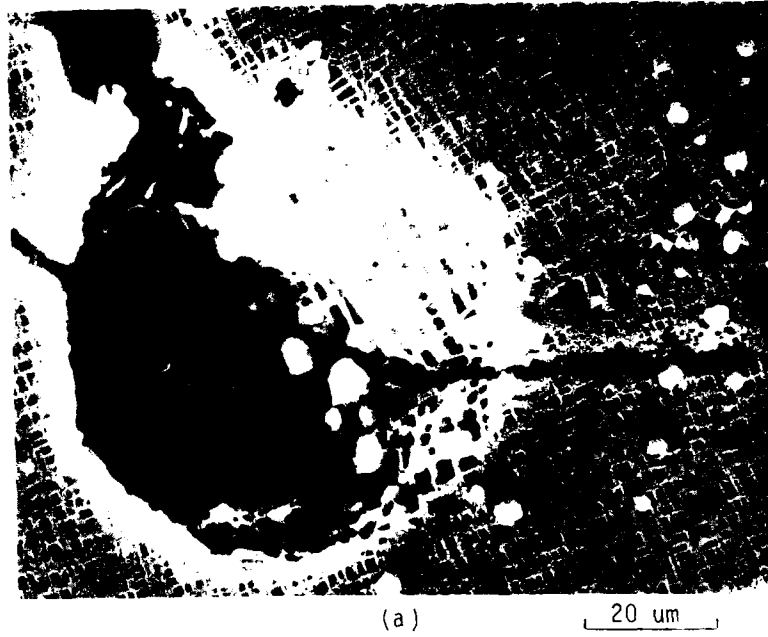


Figure 32. a) SEM Micrograph of a Cracked Inclusion Cavity;
b) TEM Replica Showing the Crack Path

There was also some evidence that cracks behave in a similar fashion on or near the surface. Figures 33a and 33b show two different areas on the surface of a polished and etched specimen which had been fatigued to failure. Approximately .0005 of an inch had been polished from the surface to remove the oxide. The surface cracks again avoid shearing the larger γ' precipitates in both areas, and in Figure 33b the preference for the crack to follow the γ - γ' interface was better defined. It also appeared that the carbide in Figure 33a may have been the site of initiation since it was the largest surface discontinuity in the vicinity of the crack.

Information concerning Stage II initiation was difficult to obtain directly from the fracture surfaces. In the area of crack nucleation, invariably very near the specimen's surface, the features were distorted by heavy oxidation and surface rubbing (Figure 27b). However, in isolated areas 30-40 μm from the specimen's edge, which is still in the Stage II early propagation area, there were some interesting observations made. Figure 34 shows a portion of this area at high magnification in which small dimples could be resolved on the fracture surface. It was concluded that these features were γ' precipitates because they had the same size, shape, and preferred arrangement as did the cooling γ' particles in the microstructure. Since these features were smooth and symmetrically shaped, the observations further supported the premise that Stage II cracks travel around the γ' precipitates as opposed to fracturing or shearing them.

In summary, dominant Stage II cracks invariably initiated at the specimen's surface and grew normal to the tensile stress axis. The data indicated that the cracks avoided shearing the larger γ' precipitates and that they preferred to travel along the γ - γ' interfaces.

As stated previously, two other mechanisms of surface crack initiation were observed, transgranular cracking at a near 45° angle to the tensile axis and intergranular nucleation. The smooth relatively featureless

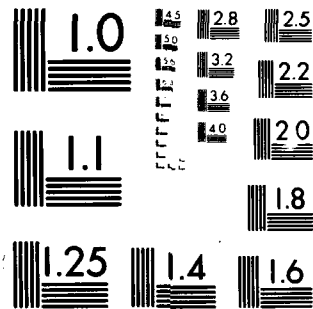
AD-A093 509

AIR FORCE WRIGHT AERONAUTICAL LABS WRIGHT-PATTERSON AFB OH F/6 11/6
THE EFFECT OF DEFECTS ON THE FATIGUE INITIATION PROCESS IN TWO --ETC(U)
SEP 80 J M HYZAK
AFWL-TR-80-4063
NL

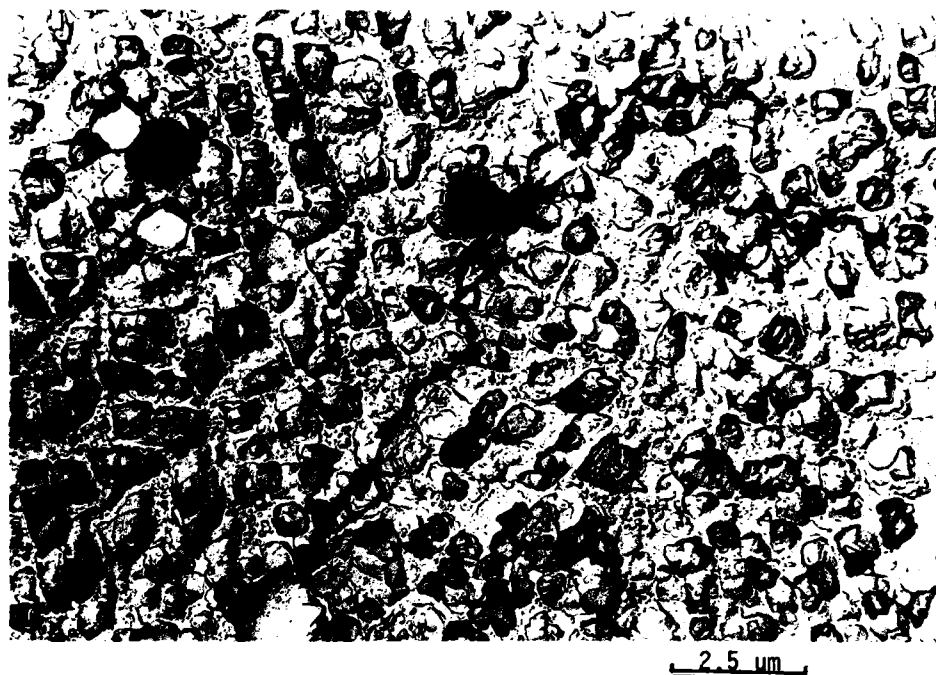
UNCLASSIFIED

NL

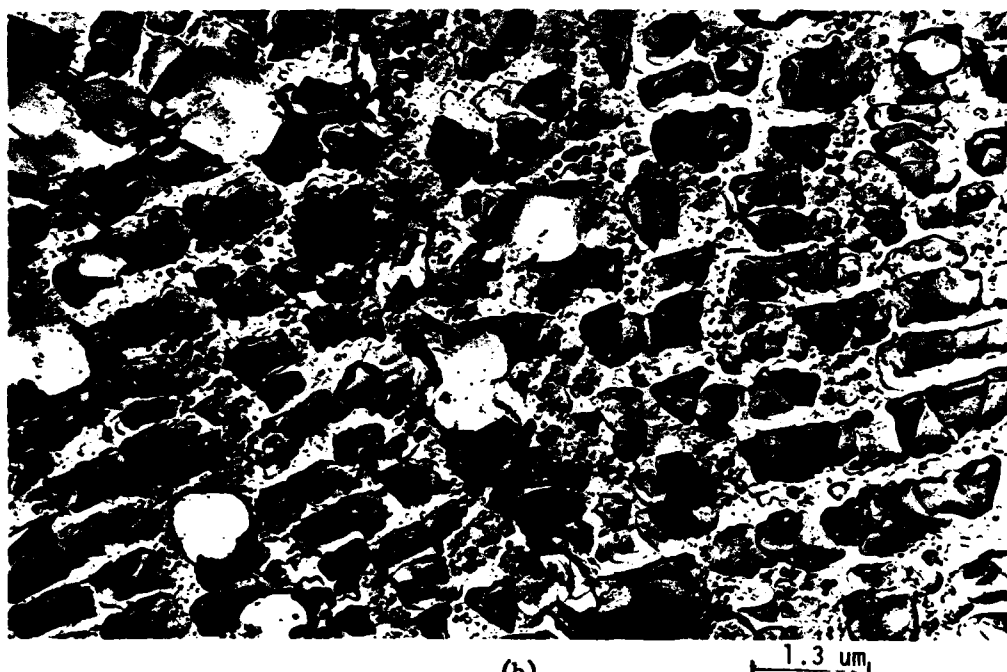
2:3
AGA
(29350)



MICROCOPY RESOLUTION TEST CHART
NATIONAL BUREAU OF STANDARDS-1963-A



(a)



(b)

Figure 33. TEM Replica Images of Surface Cracks in AF2-1DA



Figure 34. SEM Micrograph of the Stage II Crack Propagation Region on a Fracture Surface Showing Intact Cuboidal γ' Precipitates

facets associated with the former mechanism (Figure 35) were found on the same fracture surfaces as Stage II initiation at all strain ranges in this regime. In only one case, at a strain range just above the surface-subsurface transition strain, did a specimen fail from a crystallographic crack (45°) where there was no Stage II cracks on the fracture surface. Examination of metallographic sections showed that in several instances these crystallographic cracks were associated with annealing twin boundaries (Figure 36a). The twins were identified by the change in γ' orientation at the twin boundary and by the change in etching character. Figure 36b also shows slip lines with offsets in the γ' parallel to a cracked twin boundary; both the slip planes and twinning planes in FCC have been established to be of the $\{111\}$ type (Reference 20). Similar observations have also been made by Organ and Gell (Reference 14) for Mar-M200; they attributed cracking to the localization of deformation at the twin-matrix interface.

Intergranular initiation occurred at 760°C as the frequency was changed from 20 cpm to 0.2 cpm. Although it was not determined whether the intergranular cracking was a result of cavitation or environmental attack, the change from Stage II initiation at 760°C at a frequency of 20 cpm to intergranular initiation at 760°C and 0.2 cpm was both temperature and frequency dependent since intergranular cracking was not observed at 649°C at the lower frequency. Figure 37 shows a typical cross-sectional view of intergranular crack initiation from the specimen's surface. Cracking occurred on grain boundaries perpendicular to the tensile stress axis, and the crack propagated in a Stage II mode as the boundary turned away from the normal direction. As shown in Figure 20, the change in initiation mode did not significantly affect the total fatigue life as compared to the 760°C , 20 cpm data. This was probably due to the fact that in this high strain range regime, crack initiation comprised only a small fraction of the total fatigue life. This point will be addressed in more detail in a later section.

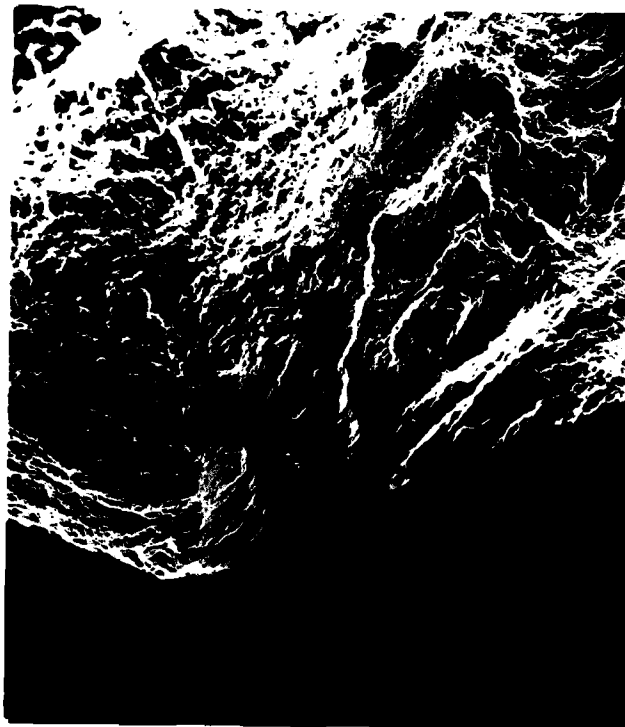


Figure 35. SEM Micrograph of a Stage I Initiation Facet on the Fracture Surface of an AF2-1DA Specimen



(a)



(b)

Figure 36. a) Surface Crack Along a Twin Boundary in AF2-1DA;
b) Slip Lines Parallel to the Twin Boundary



Figure 37. Intergranular Surface Initiation in AF2-1DA at 760°C and 0.2 cpm

b. AF-115

For AF-115 at elevated temperature and in the high strain range regime, the dominant fatigue cracks initiated at surface or near surface defects, generally pre-existing argon pores. The AF-115 alloy, as previously described, had a greater defect population than AF2-1DA which included a large density of argon pores on the order of 50-100 μm in diameter. Figure 38a shows a typical initiation site for this alloy with the pre-existing pore at the fatigue origin. The pores that were the origins of the dominant cracks in AF-115 were invariably located 10-20 μm below the specimen's surface, and the diameter of these same pores ranged from 30 μm to 130 μm with the majority being between 70 and 100 μm . At higher magnification (Figure 38b), the granular internal topography of the pore was better defined, as were the details of the Stage II crack which propagated from the pore. These results, therefore, indicate that defects did affect the crack initiation process of AF-115, and the lower than expected fatigue lives for AF-115 as described in Section V may indeed be due to its high defect population.

Examination of the metallographic sections of failed specimens showed that although the dominant cracks initiated near the surface, secondary cracking occurred both near the surface and internally at pores and inclusions. As with the AF2-1DA alloy, the number and size of these secondary cracks decreased as the strain range was decreased. The detailed morphology of typical pore initiated cracks is shown in cross-sectional view in Figure 39a. Cracks initiated along the equator of the pore, usually at the edges of the granular features; the crack then propagated into the matrix normal to the tensile axis. At the lower strain ranges in this regime, 0.7 - 0.85% $\Delta\epsilon_t$ cracks were observed at the bottom of the pores without growth into the matrix as shown in Figure 39b. This indicates that there may be a threshold growth requirement. That is, there may be some minimum stress or strain required for significant crack advance; fatiguing below this limit would then result in no detectable crack propagation. This supposition is analogous to the threshold stress intensity, ΔK_{TH} , required for crack propagation in linear elastic materials (Reference 101).

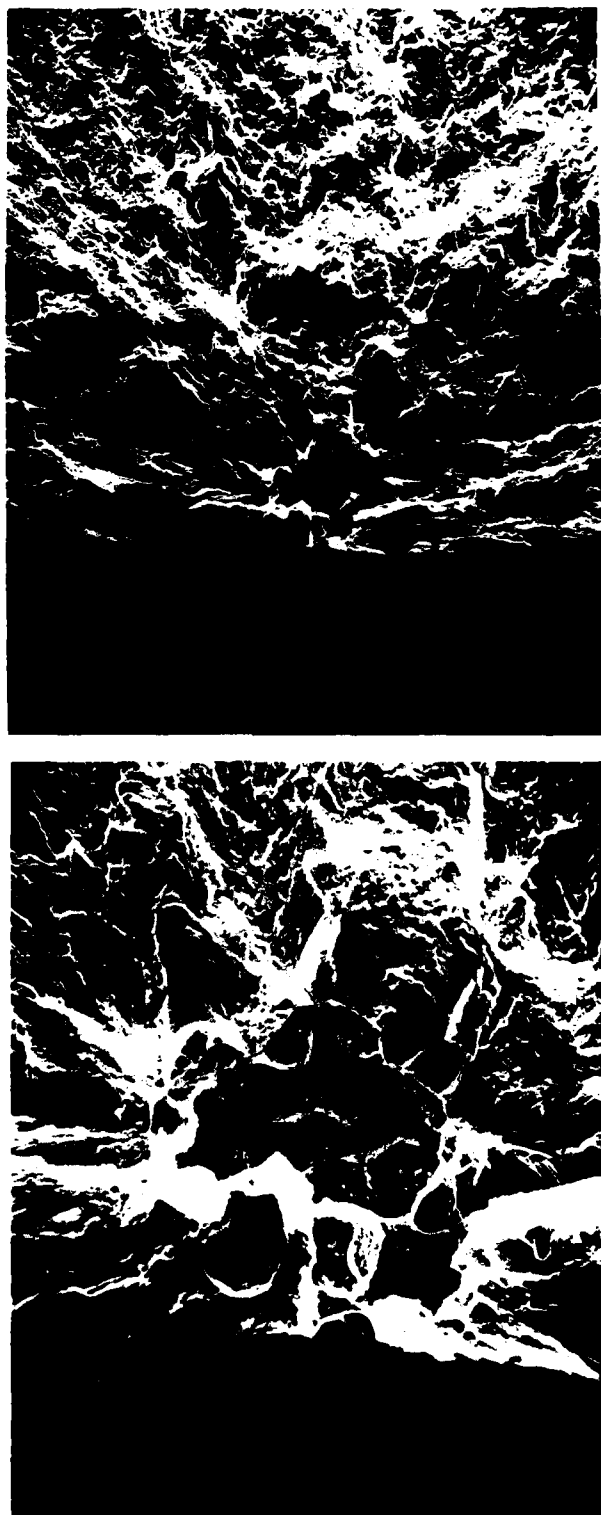
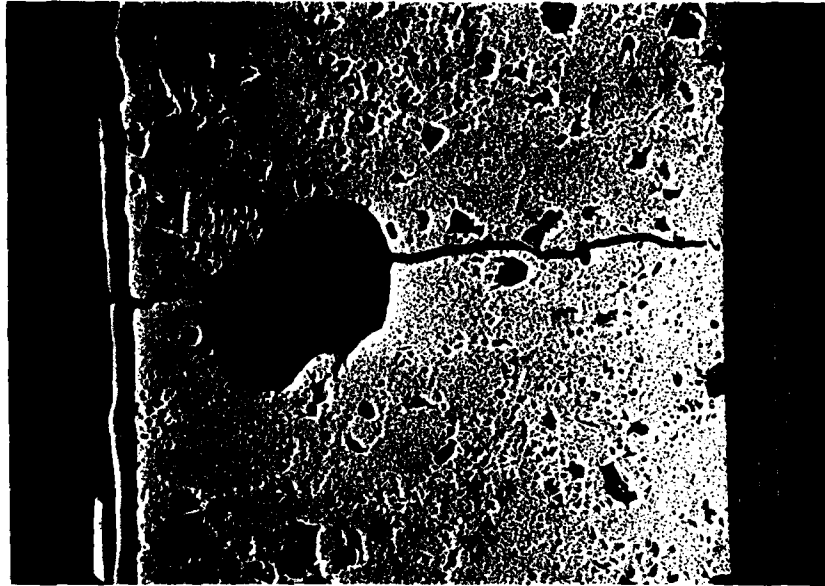
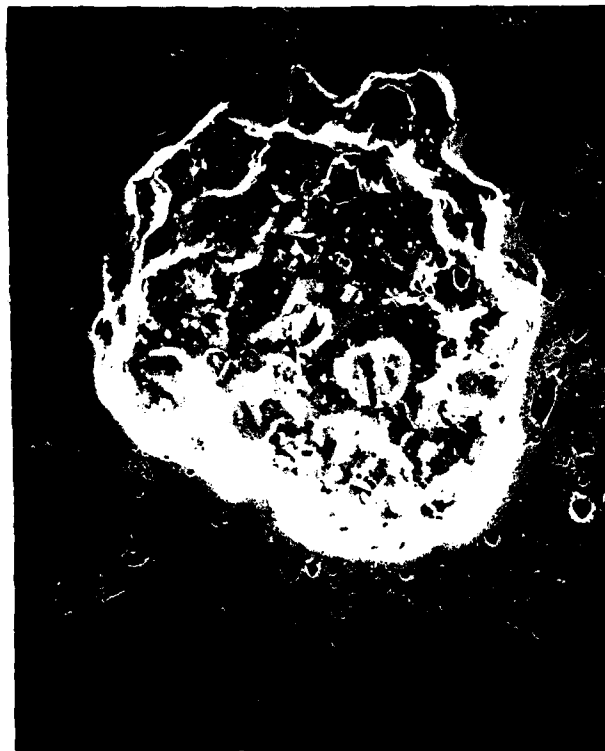


Figure 38. Crack Initiation at AF-115 at a Near-Surface Pore



(a)



(b)

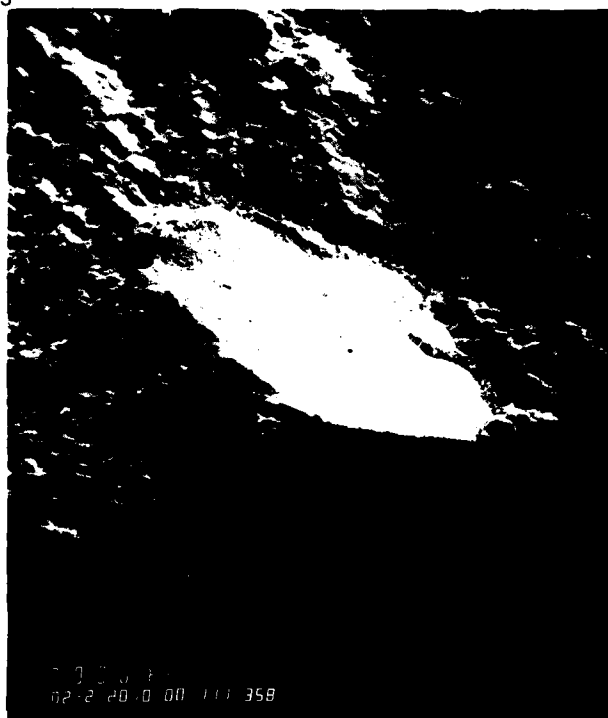
Figure 39. a) Stage II Crack Initiated at a Near-Surface Pore;
b) Crack Initiation Along the Equator of a Pore

Initiation of the dominant crack at near surface pre-existing pores occurred in over 90% of the cases for AF-115 fatigued above the SST. There was, however, one case of initiation at a surface hafnium oxide inclusion, (Figure 40a), and two cases of specimens that failed due to surface initiation at nonmetallic inclusions (Figure 40b). Those specimens whose origins were at nonmetallic inclusions had fatigue lives comparable to the mean; specimen 2-3 whose dominant crack initiated at the HfO_2 inclusion had a fatigue life significantly less than the mean. One conclusion from these observations is that the defect's location, near the specimen's surface, was seemingly more important than the nature of the defect in causing initiation.

There was no intergranular initiation observed for AF-115 at either temperature (649, 760°C) or frequency (20, 0.2 cpm). This result indicates one of two things; either that the grain boundary strength of AF-115 is superior to that of AF2-1DA, or the large number of defects, particularly pores, in AF-115 nucleated cracks before intergranular initiation occurred. Although it has not been thoroughly demonstrated, the latter was probably the case since there was a considerable number of grain boundary cracks in the companion tensile dwell tests for this alloy. These results will be described in Section IX.

c. Summary - Surface Initiation

At elevated temperature and at strain ranges above approximately $0.64\% \Delta \epsilon_t$, fatigue initiation occurred at or near the specimen's surface, usually at the most populous defect for both alloys. For AF2-1DA, which had a relatively small P/M defect population, those origins large enough to identify were shown to be small nonmetallic inclusions approximately $1 \mu\text{m}$ in diameter. For AF-115, which contained a large population of P/M defects, particularly pores, initiation occurred very near the specimen's surface at a pore or other large defect ($100 \mu\text{m}$ diameter). It also appears that the influence of the large defect population on the crack initiation behavior of AF-115 was responsible for that alloy's lower than expected fatigue lives. This important point will be addressed in more detail later.



(a)



(b)

Figure 40. Crack Initiation in AF-115 Originating at a Near-Surface Defect. a) Hafnium Oxide Inclusion; b) Nonmetallic Inclusion

Although the dominant cracks that caused failure for both alloys were initiated at the surface or at the near surface defects in all cases, many secondary cracks also nucleated at internal defects. The number and size of both the surface and internal cracks decreased with total strain range supporting the premise that as crack initiation is dependent on the magnitude of the localized strain.

3. SUBSURFACE INITIATION - LOW STRAIN RANGE

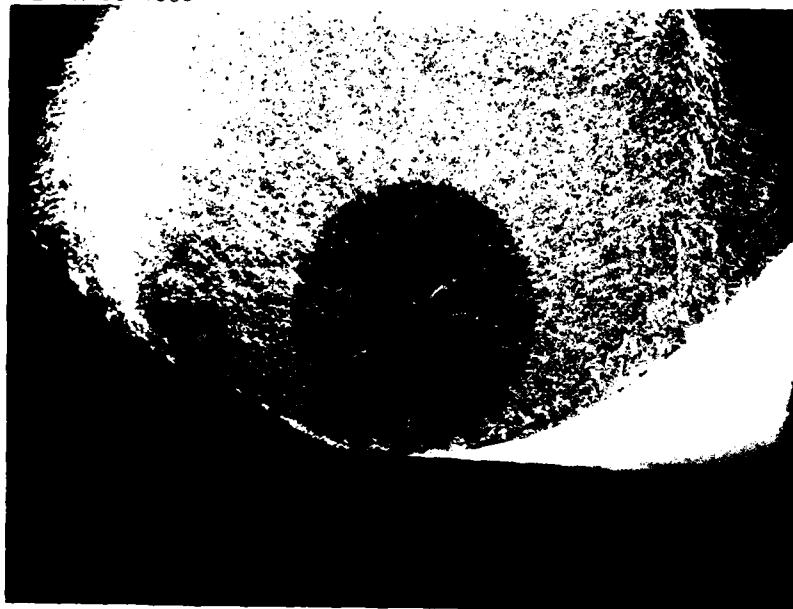
At lower strain ranges, below approximately $0.65\% \Delta\epsilon_t$, the location of initiation of the dominant crack moved from the surface to a subsurface site. The origins also changed from the more populous defects such as pores, carbides, and micron size inclusion to the larger less numerous inclusions. The details of the initiation process for each alloy will now be described.

a. AF2-1DA

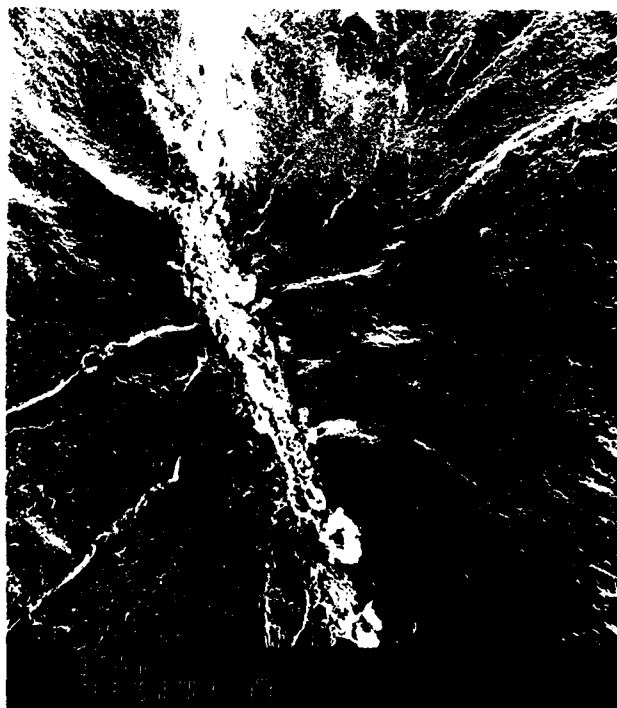
For AF2-1DA in the lower strain range regime, the initiation site of the dominant fatigue cracks were at large nonmetallic inclusions located in the interior of the specimen. Figure 41a is a low magnification micrograph showing the origin of a fatigue failure well below the specimen's surface. This origin was identified to be a stringer type inclusion rich in Al, Mg, and Zr (Figure 41b). The mechanism of initiation from such an inclusion was generally observed to be Stage I cracking along slip bands originating at the defect, followed by crack propagation in Stage II mode after growth of about one grain diameter. An example of this mode of cracking is shown in Figure 42a which is a SEM micrograph of another internal initiation. At higher magnification (Figure 42b), the Stage I facet which resulted from the initial stage of crack nucleation can readily be seen at the defect's edge surrounded by fracture area typical of Stage II propagation.

To better document the process of Stage I initiation at the tip of an inclusion, a crack originating from an internal defect was located on a polished and etched cross-section of a failed specimen and examined (Figure 43). TEM replica studies clearly showed slip traces parallel to

AFWAL-TR-80-4063

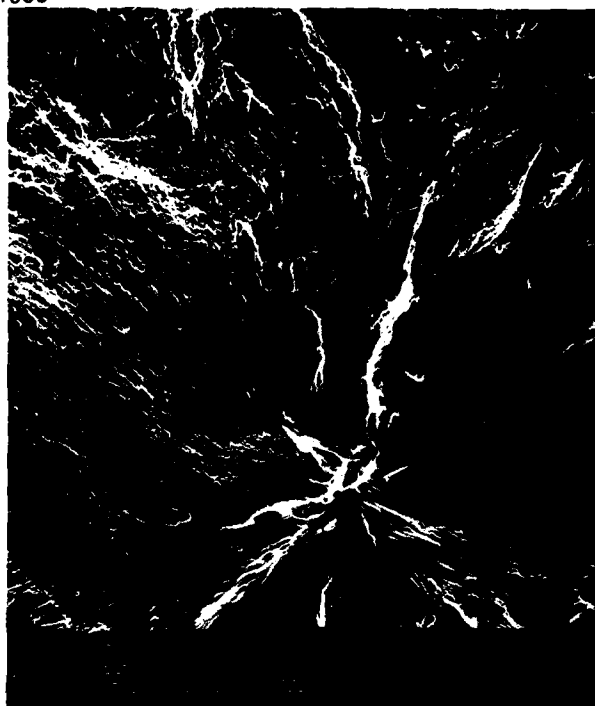


(a) 20x



(b)

Figure 41. a) Subsurface Crack Initiation as Observed on the Fracture Surface of a AF2-1DA Specimen; b) Higher Magnification of the Crack Origin, a Nonmetallic Inclusion



(a)



(b)

Figure 42. a) Internal Crack Initiation at an Inclusion Cavity in AF2-10A; b) A Stage I Facet at the Defect's Edge



Figure 43. Fatigue Crack Originating at an Internal Cavity in Stage I Mode (Shown by Arrow)

the crack at the inclusion's edge as shown in Figure 44a. At higher magnification, cutting of the γ' precipitates in these bands was also evident (Figure 44b) demonstrating that indeed the crack first formed along crystallographic shear bands.

Examination of the metallographic sections of six nickel-plated specimens fatigued at strain ranges less than 0.65%, revealed that there were no surface connected cracks of any size that could be resolved in the SEM at 1000X. Even favorably positioned defects near the surface did not initiate cracks as shown in Figure 45. This was particularly significant because surface cracks controlled the dominant fatigue process in the higher strain range regime. Also very few internal cracks were observed at inclusions other than the dominant crack that led to failure. These observations support the results presented for the high strain range tests further demonstrating that the number of both surface and internal secondary cracks decreased with cyclic strain range. The importance of this observation will become more apparent when the mechanisms responsible for the surface-subsurface transition are discussed in Section XI.

b. AF-115

Below the initiation transition, the dominant fatigue cracks in AF-115 were initiated at subsurface hafnium oxide inclusions. Figure 46a shows the location on the fracture surface of one such internal origin, and at higher magnification, a backscattered SEM image indicated a high concentration of a heavy element at the origin (the light area in Figure 46b). Subsequent analysis using energy dispersive x-ray confirmed the presence of hafnium, and the bluish glow of the inclusion under the electron beam indicated that the particle was also an oxide. These HfO_2 inclusions were plate-like particles with a large diameter to thickness ratio, and the inclusions responsible for failure were typically 100 μm in diameter and 2-5 μm thick.

Examination of the metallographic sections of failed specimens has shown other HfO_2 inclusions with secondary cracks radiating from them.



(a)

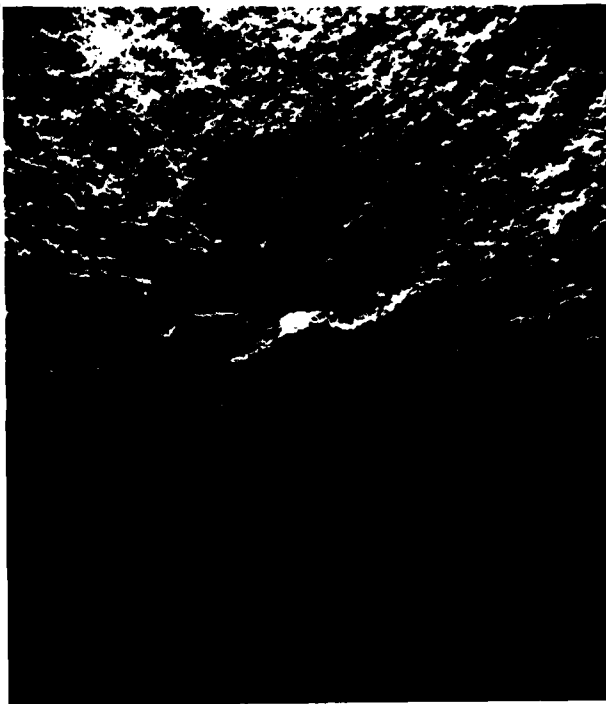


(b)

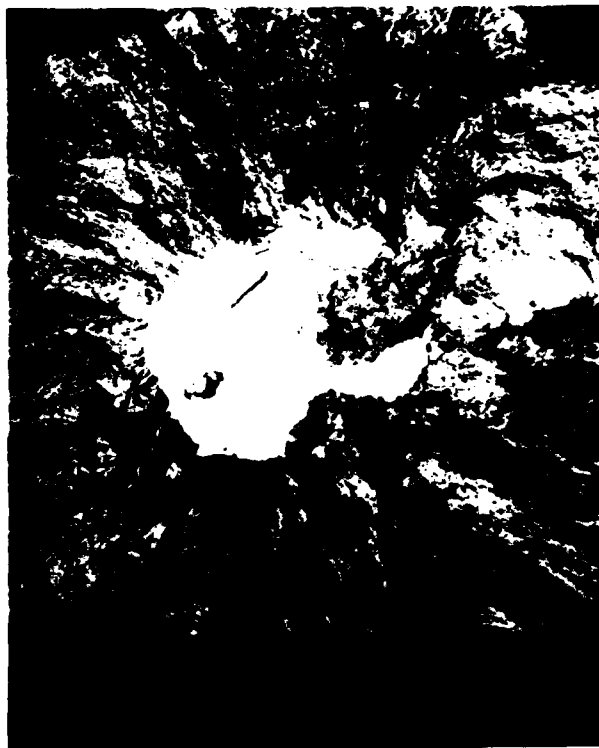
Figure 44. a) TEM Replica Image of the Stage I Initiation Region Shown in Figure 43; b) Higher Magnification of the Planar Slip Bands Originating at the Defect



Figure 45. Near-Surface Elongated Cavity Devoid of Crack Initiation



(a)



(b)

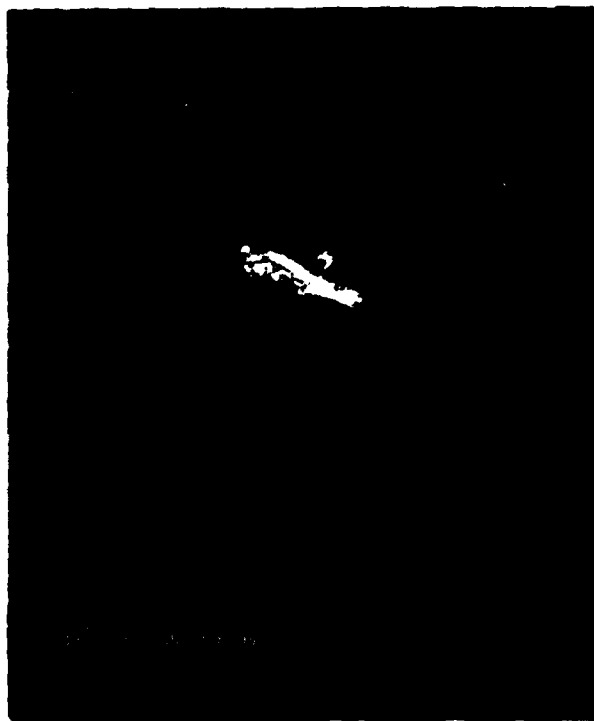
Figure 46. a) Subsurface Initiation Site on the Fracture Surface of an AF-115 Specimen; b) SEM Back-Scattered Electron Image of the Fatigue Origin

The mode of crack initiation in these cases appeared to be inclusion-matrix decohesion, which is shown in Figure 47a, and Stage II cracks were observed to propagate normal to the stress axis from the tips of the HfO_2 inclusions, as pictured in Figure 47b. These cracks were apparently sharp enough, as a result of the particle-matrix decohesion process, to immediately grow in a Stage II mode without initial Stage I nucleation; Stage II propagation has been related to a presence of a higher stress intensity at the crack tip than for Stage I cracking (Reference 6). Detailed examination of the area adjacent to the cracked HfO_2 inclusions has also shown no evidence of intense slip band cracking or γ' shearing. This again indicates that the Stage II cracking process is very localized as compared to the Stage I process in which intense slip bands radiate across many precipitates, and which sometimes extend a full grain diameter. It may also indicate that the Stage II process is generally confined to the matrix phase.

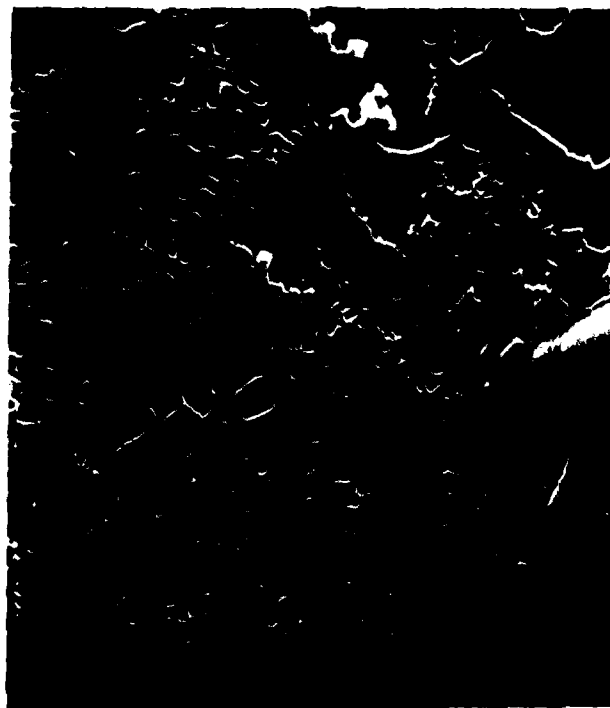
As with AF2-1DA, there were typically no surface or near surface secondary cracks in this strain range regime and very few internal cracks. Although there were both metallic hafnium oxide and nonmetallic inclusions in AF-115, the HfO_2 particles dominated the initiation process apparently due to their more acute shape. The topic of strain concentration as a function of defect shape is an important consideration in this study, and it will be treated in more detail in the Discussion Section.

c. Summary - Subsurface Initiation

At strain ranges below approximately $0.65\% \Delta\epsilon_t$, both alloys failed from cracks initiated in the specimen's interior. For AF2-1DA, the dominant cracks initiated at nonmetallic inclusions, whereas for AF-115, which contained both hafnium oxide and nonmetallic inclusions, the dominant crack always originated at the more acutely shaped hafnium oxide type of inclusions. No cracks from the surface or from near surface pores were observed in this regime; the only secondary cracks noted were initiated internally at inclusions. This observation is particularly significant since surface initiation controlled the fatigue process in the high strain range regime.



(a)



(b)

Figure 47. a) Crack Initiation as the Result of Inclusion-Matrix Decohesion; b) Stage II Propagation from a HfO_2 Inclusion

SECTION VII

LOW DEFECT AF-115

In order to better understand the effect of defect population of fatigue behavior, several LCF tests were performed with specimens from a heat of AF-115 which had a significantly lower defect density than the primary AF-115 heat used in this study. In this section, the results of the fatigue tests and the details of the fractographic examination of these low defect specimens will be presented. These results will then be contrasted with the behavior of the primary AF-115 material.

1. MATERIALS CHARACTERIZATION

The chemistry of the low defect heat of AF-115, subsequently referred to as AF-115-LD, differed from the primary AF-115 powder in that the carbon and hafnium contents were reduced to 0.043% and 0.85%, respectively. In addition, the processing for AF-115-LD was altered to include a lower solutionizing temperature (1182°C). These changes resulted in a compact of AF-115-LD powder with a low porosity level (TIP 0.16%) and no large HfO inclusions, defects which have been shown to be particularly detrimental to the fatigue behavior of the primary AF-115. The AF-115-LD billet did, however, contain approximately the same number of tramp nonmetallic inclusions as the primary AF-115 material. Since the microstructure and the 760°C yield strength (1069 MPa) of the AF-115-LD material were comparable to the primary heat, differences in fatigue properties could be attributed directly to the differences in the respective defect populations.

2. FATIGUE BEHAVIOR

Uniform section fatigue specimens were tested at 760°C, at 20 cpm, at a strain ratio of +1, and at total axial strain ranges of 1.1%, 0.9%, 0.7%, and 0.55%. The results of the fatigue tests are compared in Figure 48 with the data for the primary AF-115 alloy. The data show a significant difference in fatigue properties between the two heats of AF-115; the lives of the AF-115-LD heat were 2-5 times greater than for the baseline alloy.

AF - 115 HIGH DEFECT VS AF - 115 LOW DEFECT

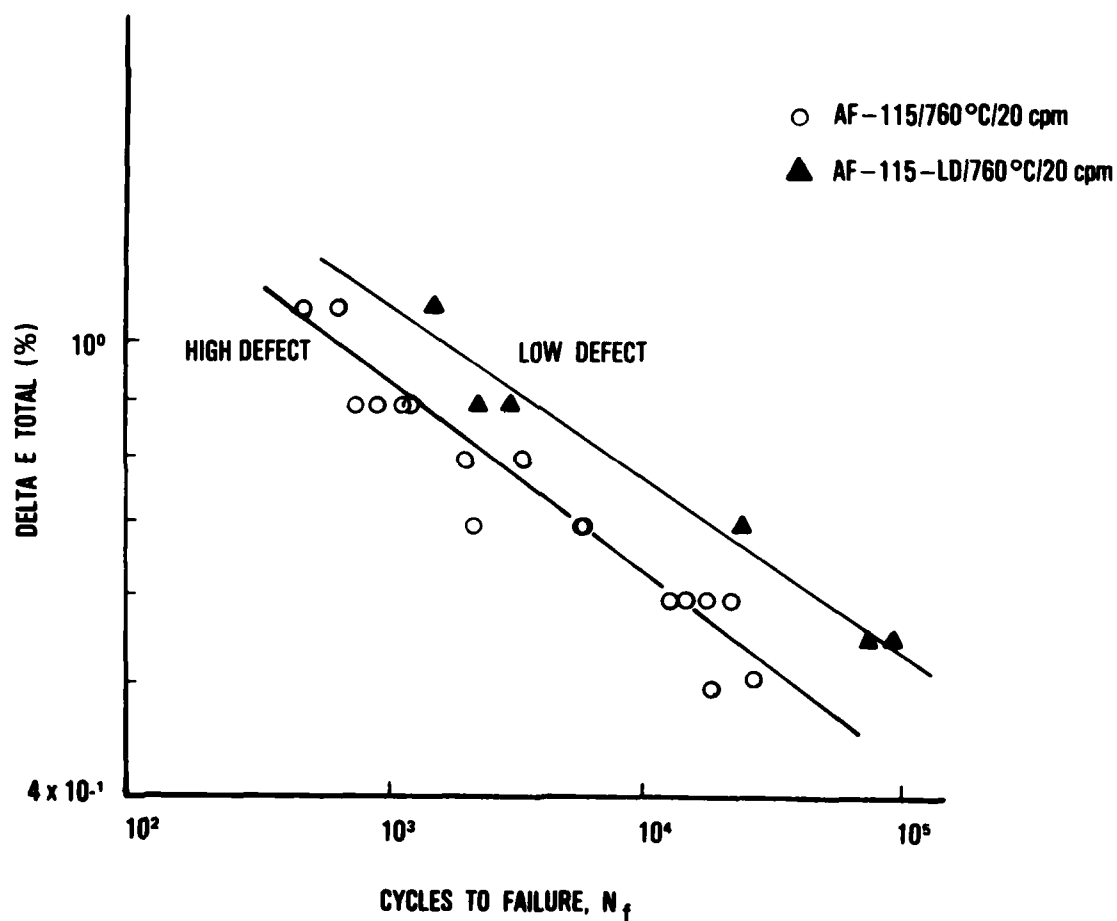
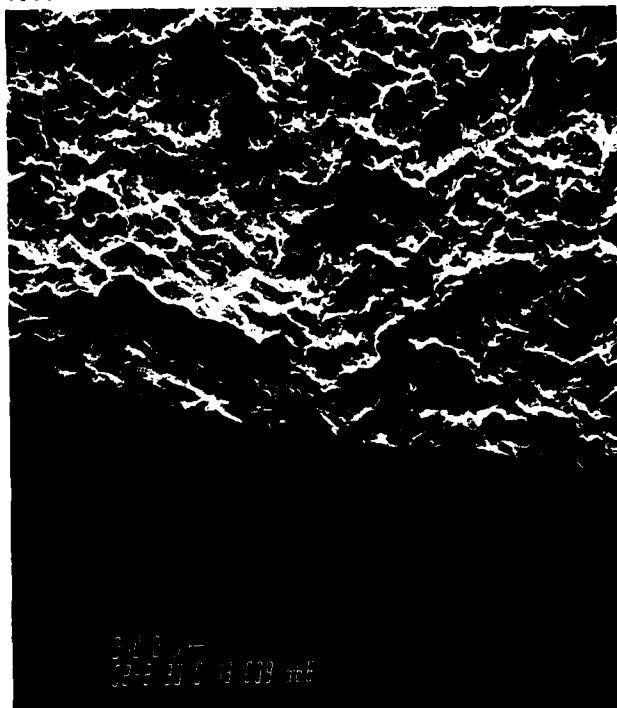


Figure 48. Fatigue Behavior of Low Defect AF-115 Compared to the Primary Heat of AF-115

The crack initiation sites of the AF-115-LD specimens were also examined in detail. The dominant crack for the specimens fatigued at either 1.1% or 0.9% total strain ranges initiated at the specimen surface in what appeared to be a Stage II mode (Figure 49a). Examination at higher magnification failed to reveal any Stage I faceting or obvious microstructural defect at the origin. At 0.7 and 0.55% $\Delta\epsilon_t$, the specimens failed from internally initiated cracks nucleated at nonmetallic inclusions (Figure 49b). Stage I facets, similar to those described for AF2-1DA internal initiation in the low strain range regime, were found near the defect at the crack origin.

The results of the fractographic examination of the low defect fatigue specimens have demonstrated that there was also a SST for this heat of material; for AF-115-LD, the SST occurred between 0.9% and 0.7% $\Delta\epsilon_t$, while the transition for the primary heat of AF-115 was between 0.7% and 0.6% $\Delta\epsilon_t$. From these limited results, it appears that the strain range corresponding to the SST varies with defect population. This possibility will be further considered in Section XII.

The tests have also shown that changing the defect population can significantly affect the fatigue life. At high strain ranges there was an increase in fatigue life attributed to a change in initiation mode from pore-related nucleation for the primary heat of AF-115 to Stage II surface initiation for AF-115-LD. Below the SST, there was an added increase in life due to the change from initiation at an acute HfO_2 inclusion to cracking at a more rounded nonmetallic inclusion. It was also interesting to note that the alloys with similar defect populations, AF-115-LD and AF2-1DA, initiated fatigue cracks in similar fashion. Recall that AF-115-LD and AF2-1DA were both characterized by a low porosity content, no plate-like HfO_2 inclusions, and an equivalent density of tramp ceramic inclusions, and they both exhibited Stage II surface initiation at high strain ranges and Stage I internal initiation from a nonmetallic inclusion at low strain ranges.



(a)



(b)

Figure 49. a) Stage II Surface Crack Initiation in AF-115-LD:
b) Surface Crack Initiation at an Inclusion Cavity

The fact that cracks initiated in a Stage I mode from nonmetallic inclusions (AF2-1DA, AF-115-LD) and cracking from a more acute HfO_2 inclusions occurred in Stage II mode (AF-115) is also important. The transition from Stage I to Stage II growth has previously been attributed to achieving a critical stress intensity at the crack tip (Reference 6). In light of this, the results here indicate that the stress (or strain) intensity at the tip of a debonded HfO_2 inclusion was greater than that at the tip of a nonmetallic inclusion since in the former case cracking proceeds directly by a Stage II mode. These types of comparisons will be developed in the Discussion Section to help explain the existence of a SST, as well as the differences in fatigue life for the different alloys.

SECTION VIII

INITIATION MECHANISMS - SPECIAL TESTS

The results for three different heats of superalloy powders have shown that a SST exists for crack initiation at elevated temperature. To help explain the mechanism responsible for this behavior, several additional fatigue tests were performed. Selected factors were investigated which were hypothesized to be critical in the nucleation event; these parameters included the environment, surface residual stress, and the value of the maximum tensile stress during fatigue which was partly determined by the strain ratio, A , of the test. An additional test was performed to determine if the SST also existed for specimens tested at low cyclic frequency since all the 0.2 cpm tests in this study had been limited to strain ranges above the transition strain range ($0.7\% \Delta \epsilon_t$). Finally, one further experiment was carried out to determine if crack initiation occurs at a small fraction of the total fatigue life in superalloys, as reported for other materials (References 2, 97, 98, 99).

1. ENVIRONMENTAL TESTS

It was considered possible that the presence of a tenacious oxide layer on the surface of the fatigue specimens at high temperature might have been the cause of the transition in initiation mode. For example, the oxide could have been responsible for hardening the surface against strain localization and crack formation at the low strain ranges where the oxide would not crack, while above the transition where cycling was in the plastic range, the oxide could have cracked thereby enhancing surface initiation.

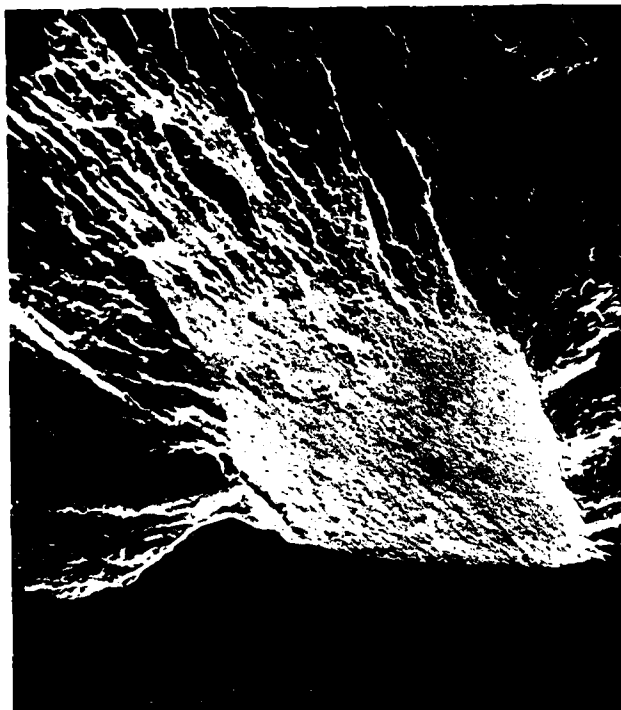
An alternate explanation, based on the work of Gell and Leverant (Reference 26), suggested that at low strain ranges surface oxidation filled small surface cracks and prevented crack closure during the compressive fatigue half cycle. This would have impeded crack tip resharpening and stalled crack growth. At higher strain ranges, however, the magnitude of the strain displacement would have overcome this problem.

Although we found no evidence of microcracks on the surface of low strain range tests, this theory was pursued since it is possible that a small population of microcracks might have been present and yet have gone undetected.

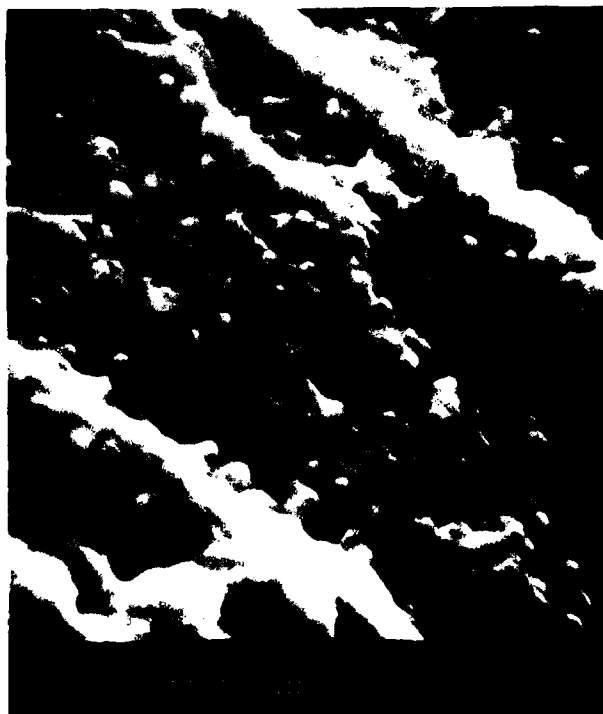
Four high temperature (760°C) fatigue tests were performed in an ultra-high vacuum (10^{-8} Torr) in order to determine if oxidation significantly affected the initiation process for these superalloys. Tests were run at one strain range above and at one strain range below the SST strain range for each alloy. Due to equipment malfunctions, however, only two of the four tests were considered valid, the low strain range AF-115 test and the high strain range AF2-1DA test. The results for these tests will now be described.

The low strain range AF-115 test fatigued in vacuum failed from a crack that was initiated well below the specimen's surface at an origin identified as a hafnium oxide inclusion. This, of course, was the same mode of initiation that was observed for those specimens tested in an air atmosphere at the low strain ranges, and the characteristics of the fracture surfaces did not differ appreciably from those described in Section VI for the baseline tests. Unfortunately, additional tests could not be performed to further substantiate this result, but based on this test it does appear that the SST was not controlled by the effect of oxidation on the initiation process.

The high strain range AF2-1DA test in vacuum was fatigued just above the SST strain range. This specimen failed from a single crack which originated at the specimen's surface in Stage I fashion as shown in Figure 50a. Again, this type of initiation, at the specimen's surface, was consistent with the results of the high temperature tests fatigued in air. From these vacuum results, it is thus considered likely that the oxidation does not solely control the SST. This point will, however, be reviewed in more detail in Section XII.



(a)



(b)

Figure 50. a) Stage I Surface Crack Initiation in the AF2-1DA High Vacuum Test above the SST; b) SEM Micrograph of the Stage II Early Crack Propagation Region

It was not as clear, however, whether oxidation affected the type of surface cracking in AF2-1DA. As mentioned previously, the vacuum test failed from a Stage I initiated crack, yet the observations presented in Section VI showed that cracking in AF2-1DA occurred most often in Stage II mode at the surface, and that Stage I cracking was observed less frequently. This single observation of Stage I surface cracking in vacuum may have no significance other than to suggest that both Stage I and Stage II cracking can also occur in vacuum, or more importantly this observation may indicate that Stage II initiation cannot occur without surface oxidation. This question can only be answered by additional testing, but if the latter possibility is substantiated, this would provide additional valuable information to explain why cracks initiate in a Stage II mode in this alloy and not in other alloys.

For this same reason, to understand the Stage II initiation mode at elevated temperature, SEM observations were made on the fracture surface of the failed AF2-1DA specimen in the region of early Stage II crack growth. The area studied was in the region where the original Stage I crack changed to a Stage II mode. It was hoped that because there was no surface oxide present, the features associated with Stage II growth would be better defined than they were on the fracture surfaces of those specimens tested in air. Figure 50b is a high magnification micrograph of the Stage II region. As in Figure 34 which has been previously described, there were dimples on the fracture surface of similar size and shape as the cooling γ' in the microstructure. This evidence further supports the contention that Stage II crack propagation occurs mainly in the matrix phase and does not involve shearing or fracturing the γ' precipitates. The possible implications of this will be addressed in Section XII.

2. RESIDUAL STRESS

It has been reported in the literature that a compressive residual stress on the surface of a fatigue specimen can retard surface crack initiation (Reference 102). It was therefore hypothesized that residual

machining stresses on the surfaces of the AF-115 and AF2-1DA fatigue specimens might have been responsible for hardening the surface against crack initiation, thus leading to internal initiation at lower strain ranges. This effect would most probably have occurred at the lower strain ranges because fatigue in this region is basically elastic and residual stresses are more likely to be maintained under these conditions. As a result of this concern, the effect of residual machining stresses on fatigue initiation were investigated.

Residual stress measurements were performed on selected specimens using x-ray techniques (Reference 125). The calculations were made based on the changes in the alloy's lattice parameter spacing at the specimen's surface which were determined from the shifts in the x-ray reflections using Bragg's Law. The measurements were all made in accordance with recommended practice (Reference 103).

In the machined and mechanically polished condition, the surface condition used for all fatigue specimens, there was a surface compressive residual stress ranging from 82 MPa to 524 MPa for the six random specimens tested. Incremental electropolishing steps showed that the compressive residual stresses disappeared at a depth of .0038 cm below the surface. To determine then if these stresses controlled the initiation process, three specimens, two AF2-1DA and one AF-115, were electropolished to remove a minimum of .0190 cm from the diameter to insure complete elimination of the residual stress profile, and these specimens were then fatigue tested.

The AF2-1DA specimens were fatigued at 760°C at total strain ranges of 1.1% and 0.55%. The dominant crack for the high strain range test initiated at the specimen's surface in Stage II mode as would be predicted from the baseline results (Section VI). The low strain range test failed from an internally initiated crack nucleated at an MgO inclusion which was also consistent with previous results of the baseline tests. Finally, the AF-115 specimen was tested at 760°C and 1.0% $\Delta\epsilon_t$, and the dominant crack initiated in Stage II mode from a near surface

argon pore in the same manner as described in Section VI. Thus, all three tests failed in the same manner as would be expected from the previous baseline results. The existence of the SST, therefore, does not appear to be explainable in terms of residual stresses.

3. STRAIN RATIO

As has been described, all fatigue tests were performed in strain control at a strain ratio, A , of $+1$. As a result, the hysteresis loops for all tests had a large tensile mean stress at the beginning of each test, as illustrated in Figure 51a. For the high strain range tests, above the SST, however, the hysteresis loops quickly adjusted during the early stages of the test (shake down), so that there was a relatively small mean stress during most of the fatigue life as shown in Figure 51b. For example, a test at a total strain range of 1.1% had a positive mean stress of approximately 9.0 MPa. For tests at lower strain ranges, however, there was less cyclic plastic strain to relax the mean stress, and the high mean stress was maintained during the test as demonstrated in Figure 51c, so that a test at $0.5\% \Delta \epsilon_t$ had a mean tensile stress near 415 MPa. This high mean stress for the low strain range tests resulted in correspondingly high maximum tensile stresses. It was therefore conjectured that this variation in behavior between the high and low strain range tests could be responsible for the surface-subsurface transition.

To test this, one AF-115 specimen was fatigued using a fully reversed strain cycle ($A = \infty$) at 760° and a strain range of 0.55%. The hysteresis behavior for this cycle is shown schematically in Figure 51d. The specimen maintained a 2.7 MPa mean stress during the test and failed in approximately 28.6×10^4 cycles. Fractographic examination showed that the dominant crack initiated at a HfO inclusion in the interior of the specimen, the same initiation mode as for $A = +1$ test at this strain range. This results indicated that the strain ratio, A , does not control the initiation mechanism.

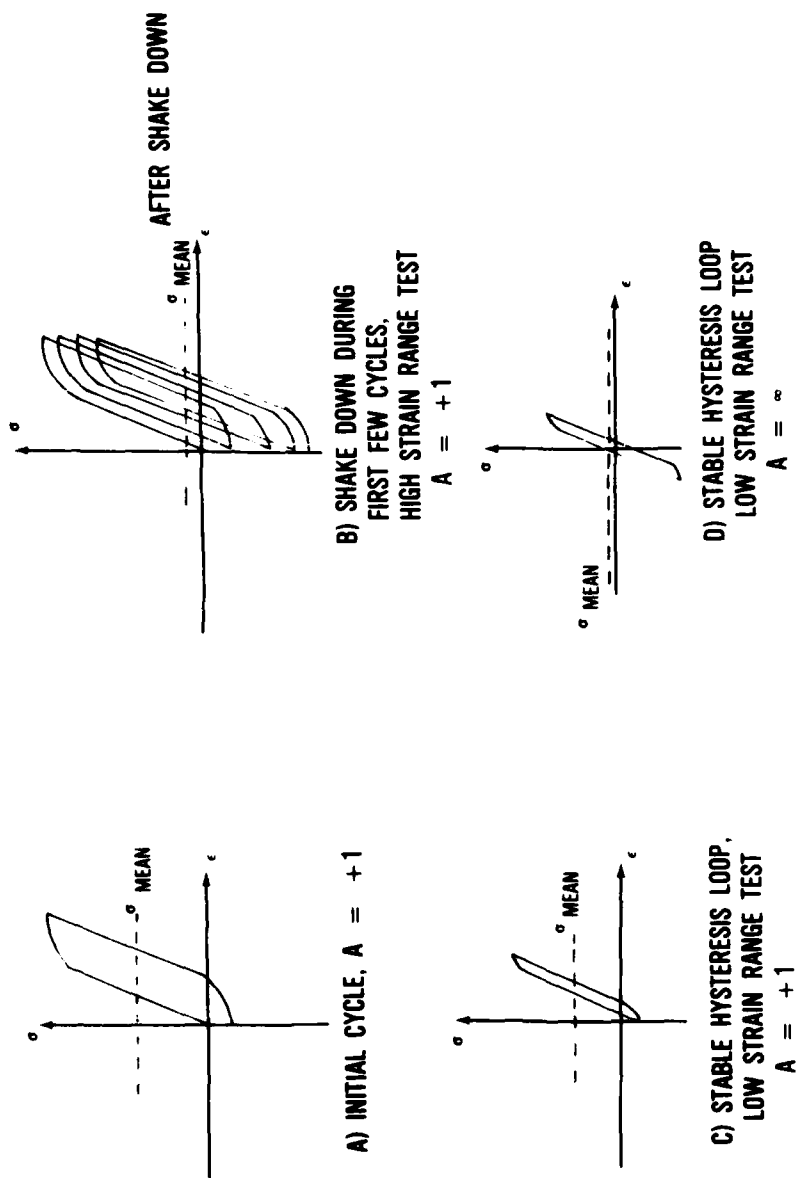


Figure 51. Fatigue Hysteresis Loops. a) Initial Cycle, $A = +1$; b) High Strain Range Stable Loop, $A = +1$; c) Low Strain Range Stable Loop, $A = +1$; d) Low Strain Range Stable Loop, $A = \infty$

This result should not be interpreted, however, to mean that stress ratio does not have an affect on total fatigue life. Since the maximum tensile stress changes with stress ratio, the crack propagation portion of the fatigue life will vary with A-ratio. The dependence of crack propagation rates on the value of maximum tensile stress will be discussed in more detail in a following section.

4. LOW FREQUENCY TESTS

For both AF-115 and AF2-1DA, continuously cycling tests at the lower frequency of 0.2 cpm were only performed at total strain ranges of 0.70% and greater due to constraints on test duration. This lower bound, however, was still above the SST strain range for the 20 cpm frequency tests. One AF-115 specimen was, therefore, fatigued at $0.6\% \Delta\epsilon_t$, at a frequency of 1 cpm, to see if a change in frequency would alter the initiation site. This test failed in 31,500 cycles from a crack initiated at a subsurface hafnium oxide inclusion. This mode of failure would be expected from the results of the baseline tests, and it was therefore, consistent with the SST behavior established for the 20 cpm frequency

Even at the 1 cpm frequency, however, there was not much of a difference in the inelastic behavior of the test as compared to the 20 cpm results. Therefore, extrapolation of this result to even lower strain ranges or lower frequencies, would seem unwise. Environmental interactions and time dependent deformation will certainly increase for longer test durations, and therefore, these factors may alter the initiation process at lower strain ranges and frequencies. Long term tests are recommended to examine this possibility.

5. CRACK INITIATION LIFE

As previously stated, crack initiation has been shown to occur in many materials at a small fraction of their fatigue lives (Reference 2). For example, cracks have been detected in pure copper at as low as 5 percent of the total life (Reference 99). The percentage of life spent in crack initiation has also been shown to increase as the cyclic strain

range was decreased for a variety of alloys (Reference 2). Since the percentages of fatigue life spent in crack initiation and crack propagation are critical in the overall analysis of fatigue behavior, an experiment was performed to see if the nickel-base superalloys under investigation follow these same patterns.

An AF2-1DA test specimen was fatigued at 760° at a total strain range of 1.0% for 70 cycles, which was approximately 10% of the expected fatigue life to failure. The specimen was then inspected optically after it had been very lightly polished to remove the surface oxide layer. Under the light microscope, many cracks were evident on the specimen's surface; a representative area is shown in Figure 52. As can be seen, some of the cracks have a surface length of greater than 150 μm . This observation, therefore, confirmed that crack initiation occurs at a small fraction of the total fatigue life in the higher strain range regime for these superalloys.

A similar experiment was not carried out at the lower strain ranges since in this regime cracks initiated internally, and, therefore, would be much more difficult to detect. As a result, it was not directly demonstrated that the fraction of the fatigue life spent in crack initiation was greater below the SST than above. However, based on our observations and those of others (References 2, 97, 98, 99) that the frequency of secondary cracking decreased dramatically as the strain range decreased, it is considered likely that the percentage of life spent in crack initiation increased as the cyclic strain range decreased.

In summary, then, from the large amount of data in the literature and from observations of AF-115 and AF2-1DA it was concluded that crack initiation in these nickel-base superalloys occurred at a small fraction of its life at high strain ranges, and that the percentage of life spent in crack initiation increased as the total strain range decreased.

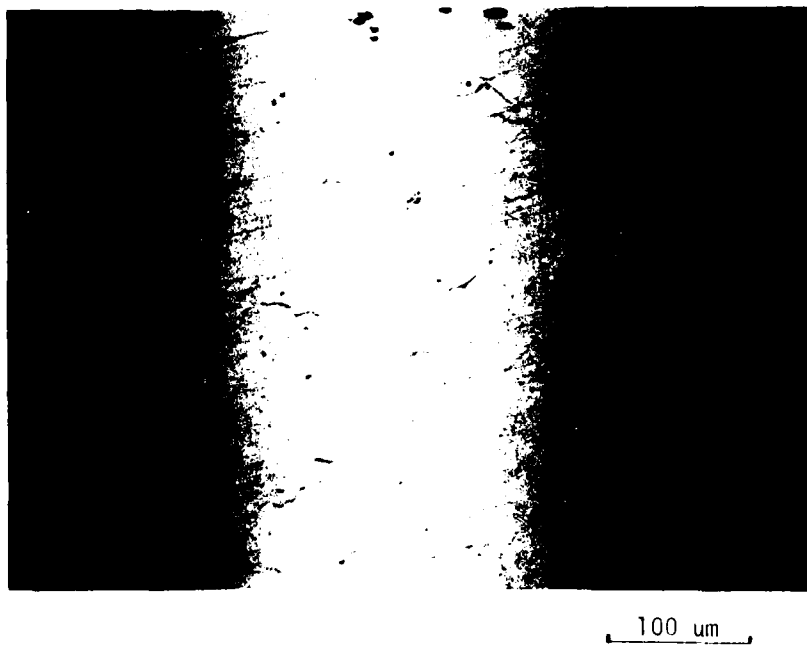


Figure 52. Cracks on the Surface of an AF2-1DA Specimen
Fatigue to 10% of It's Expected Life

6. SUMMARY

The results of these special tests have shown that the SST was not controlled by surface residual stresses or the fatigue stress ratio, A . The limited number of high vacuum tests also suggested that the SST was not solely the result of oxidation effects. There was, however, some indication that the environment may affect the mode of crack initiation at high strain ranges for AF2-IDA; Stage I surface initiation was observed rather than the Stage II initiation predominant in the high temperature air atmosphere tests. It was also concluded that crack initiation occurred at a small fraction of the fatigue life at high strain ranges, and that the percentage of life spent in crack initiation increased as the total strain range decreased.

SECTION IX

ELEVATED TEMPERATURE - CYCLIC DWELL TESTS

The results of the cyclic dwell tests presented in Section V showed that the compressive dwell tests lasted fewer cycles than did the tensile dwell tests when the two were compared at the same total strain range. The results of the fractographic examination, which will be described in this section, have shown, however, that the tensile dwell specimens sustained considerable creep-fatigue damage while the compressive dwell tests failed in the same manner as the "creep-free" continuously cycling tests previously described in Section VI. The reason for this unexpected behavior is believed to be that the tensile and compressive dwell specimens developed significantly different mean stresses during the respective tests, and although the tensile dwell tests suffered the more detrimental creep-fatigue cracking, the rate of fatigue damage accumulation in the compressive dwell tests was considerably greater due to a higher mean stress. In this section, then, the metallographic observations of the cyclic dwell specimens will be presented followed by a review of the cyclic behavior of both the tensile and compressive dwell tests.

1. AF-115 TENSILE DWELL TESTS

For the AF-115 alloy, there was a major difference between the initiation mechanism for the continuously cycling tests and tests with a tensile dwell. When a tensile dwell was incorporated in the fatigue cycle, it was found that the process was controlled by the nucleation and growth of intergranular cracks from surface and subsurface locations. Figure 53 shows an example of an AF-115 specimen fatigued under a tensile dwell cycle. Cracks have initiated at the surface, or in some cases at near surface pores, while other cracks have initiated internally well below the specimen's surface. Observations of metallographic sections have shown that cracks initiated internally in two ways; some cracks originated at defects and propagated both transgranularly and intergranularly through the structure, while other cracks nucleated by a creep cavitation process along grain boundaries normal to the tensile stress axis. Figure 54a shows an example of internal cracking

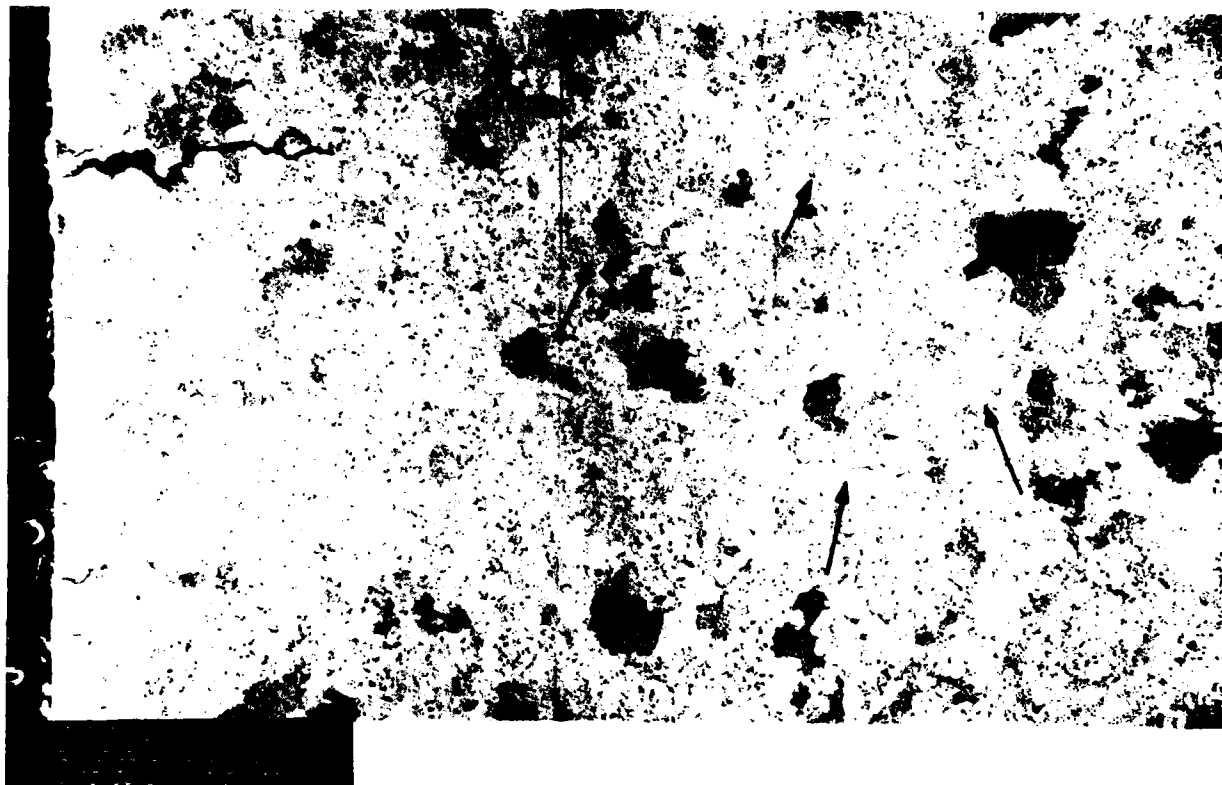
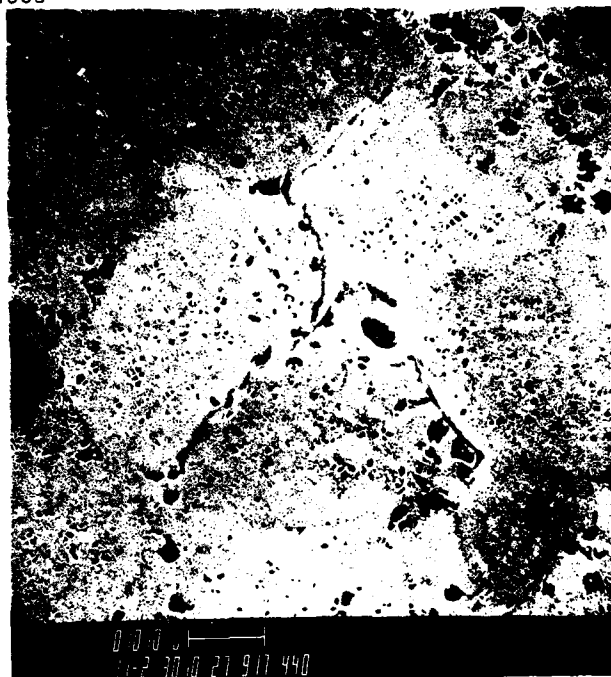
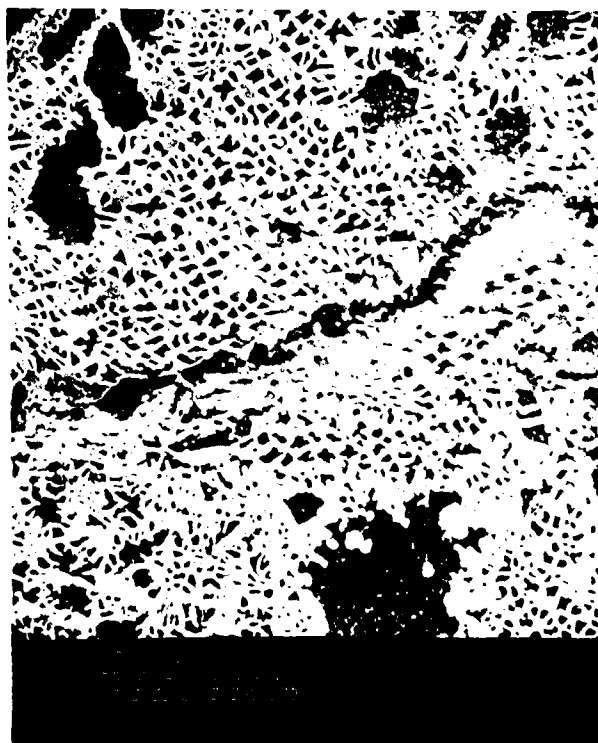


Figure 53. Surface and Internal Cracking in a Tensile Dwell Specimen, Arrows Indicate Some of the Internal Cracks



(a)



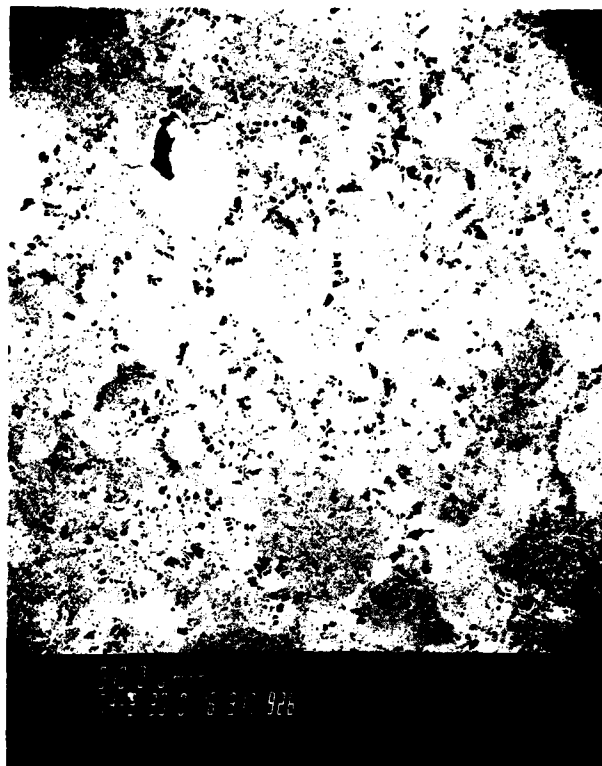
(b)

Figure 54. a) Intergranular Crack Initiation from an Internal Defect; b) Grain Boundary Cavitation Cracking, Arrow Indicates the Tensile Axis

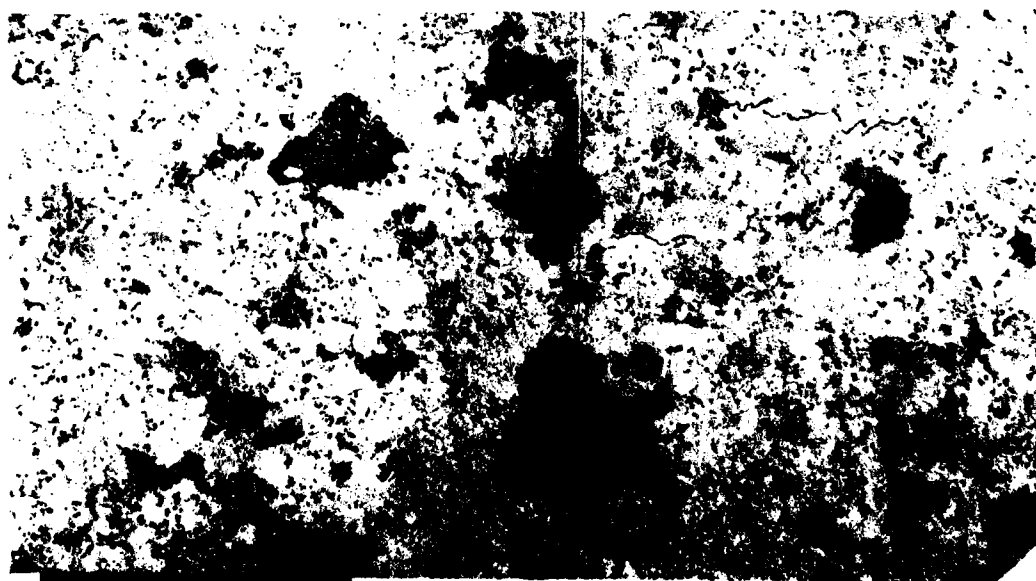
at a P/M defect. In this case the defect was located near a grain boundary triple-point and the cracks grew out along the grain boundaries. In Figure 54b, cavitation initiation along a grain boundary normal to the tensile direction is shown. It is apparent from this micrograph that cavities were nucleated at the particle-matrix interfaces of grain boundary γ' precipitates.

For AF-115 at the higher strain range tested with a dwell cycle ($1.0\% \Delta \epsilon_t$), the internal cracks nucleated almost exclusively at existing defects as shown in Figure 55a, while at the lower strain range ($0.80\% \Delta \epsilon_t$), internal cracks initiated both at defects and by cavitation along grain boundaries (Figure 55b). This observation indicates that at a constant temperature (760°C), there was a threshold exposure time required to nucleate cavitation cracks at grain boundaries. Apparently, the test at the higher strain range failed before the cavitation process was developed enough to cause cracking.

The initiation of internal cracks was also reflected on the fracture surfaces of failed AF-115 tensile dwell specimens. The fracture surfaces of tensile dwell specimens were much more tortuous in appearance than those of specimens tested with no tensile dwell, and there were also a large number of defects evident on the fracture surfaces. These defects in many cases were identified as the origins of internal crack initiation by the morphology of the cracking around them. Figure 56a shows an example of such an internal defect of the fracture surface, with what appeared to be a region of slow crack growth radiating from it. The tortuosity of the fracture surface was, therefore, considered to be the result of the link-up of these internally initiated cracks. In Figure 56b, as many as five internal crack origins similar to the one pictured in Figure 56a can be seen on the fracture surface. These results suggest that the final failure process involved the growth and coalescence of internal cracks with a dominant surface crack. The proposed failure process of microcrack growth and link-up is further supported by the cross-sectional view in Figure 57; the dominant crack is shown growing from the specimen's surface and it would be expected to link-up with

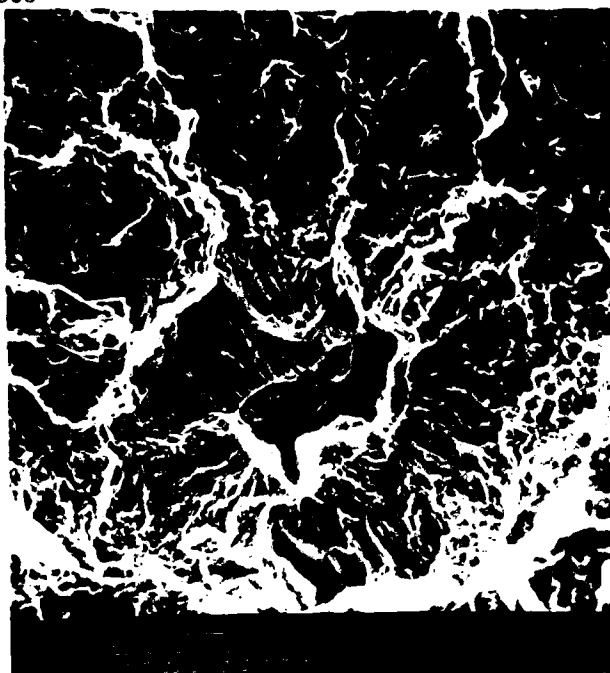


(a)

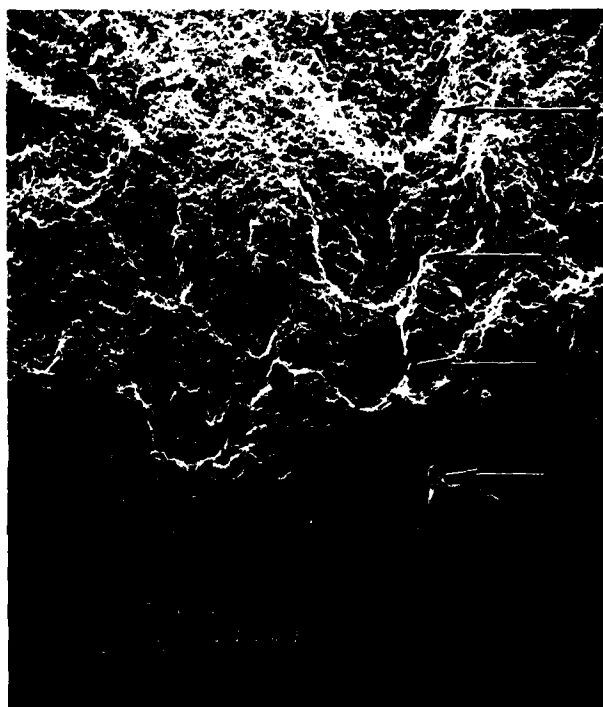


(b)

Figure 55. a) Internal Cracking at Defects in a Cyclic Dwell Specimen Fatigued at $1.0\% \Delta\epsilon_t$; b) Internal Crack Nucleation at Defects and Along Grain Boundaries in a Tensile Dwell Specimen Fatigued at $0.80\% \Delta\epsilon_t$



(a)



(b)

Figure 56. a) An Internal Crack Originating at a Pore on the Fracture Surface of a Failed AF-115 Tensile Dwell Test; b) Fracture Surface of an AF-115 Tensile Dwell Test with Many Internal Crack Nucleation Sites at Defects



Figure 57. Cross-Sectional View of the Microcarc Link-Up Process in Tensile Dwell Tests

the neighboring cracks as local failure criteria are reached. The result of this process would be an irregular fracture plane and therefore a tortuous fracture surface.

It was also observed that the growth of internally initiated cracks appeared to be accelerated by the influence of the stress field associated with the major surface crack. Figure 58a shows the growth of an oxide filled crack from the surface and the presence of several as yet unconnected internal cracks which are free of oxide (Figure 58b). The size and number of microcracks in the vicinity of the major surface crack is much greater than in other areas of the same specimen.

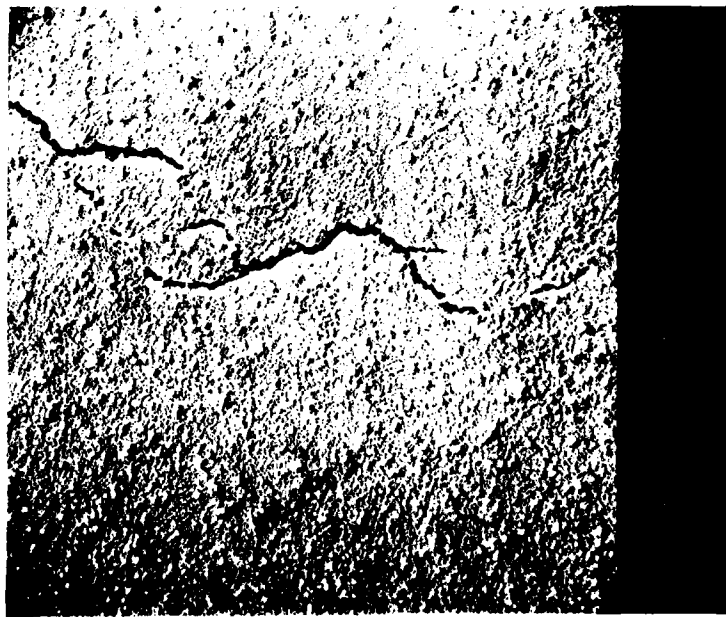
In summary, there was extensive creep-fatigue damage in the AF-115 tensile dwell tests which were characterized by internal crack initiation and link-up. The compressive dwell test showed no evidence of creep damage, and failed in the same manner as the continuously cycling tests.

2. AF2-1DA TENSILE DWELL TESTS

The Process of creep-fatigue interaction for a tensile dwell test was much the same for AF2-1DA as for AF-115. The most significant difference was that cracks from defects did not seem to dominate the process as much in AF2-1DA, even at the higher strain range. This, of course, might have been expected due to the lower defect population of AF2-1DA. Figure 59 shows the existence of extensive grain boundary cracking in AF2-1DA along with the nucleation of a crack at an inclusion. Figure 59 also illustrates the strong dependence of grain boundary cracking on the orientation of the boundary. Crack developed along boundaries normal to the stress axis and either stopped or proceeded transgranularly when the boundary changed direction. Cracking in the grain boundaries was also a cavitation process in AF2-1DA, as shown in Figure 60a and 60b. Cavities formed at the particle-matrix interface of grain boundary γ' precipitates and cracks developed through void growth and coalescence.



(a)



(b)

Figure 58. a) Multiple Crack Initiation Ahead of a Major Surface Crack; b) Microcrack in this Cluster Apparently Free of Surface Oxide



Figure 59. Internal Grain Boundary Cracking in an AF2-IDA Tensile Dwell Test, Tensile Axis (T.A.) as Shown

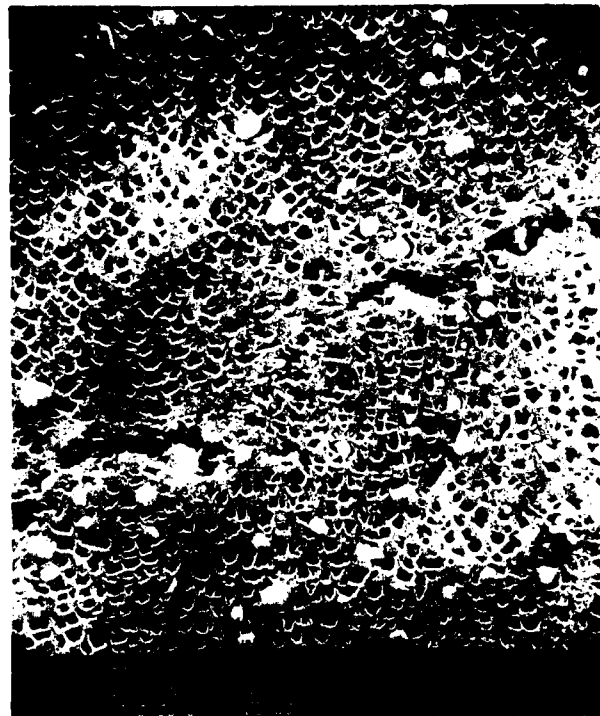
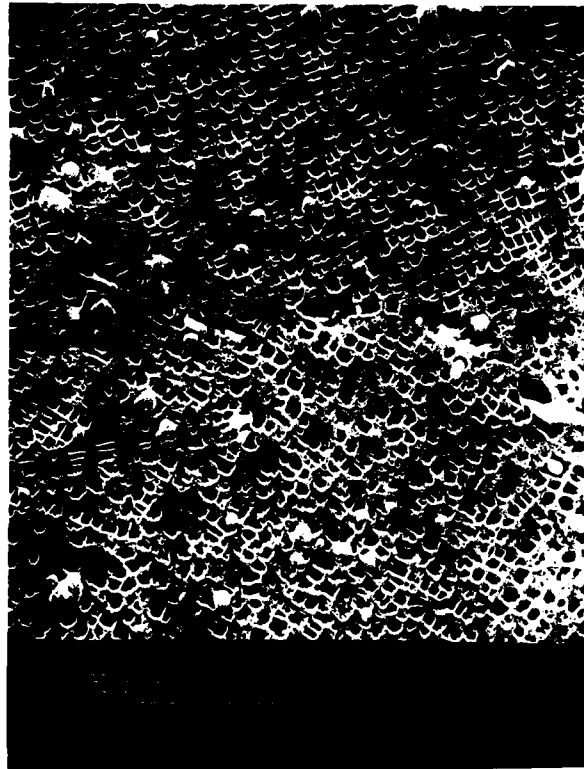


Figure 60. Grain Boundary Cavitation Cracking in an AF2-1DA Tensile Dwell Test

As expected, the fracture surfaces also reflected the rough topography associated with the link-up of internal cracked regions. Figure 61 shows at low magnification the fracture surface of a tensile dwell test, with the intergranular areas pointed out. At higher magnification (Figures 62a and 62b), these areas were more readily identifiable; the intergranular crack morphology and the plastic tear lines radiating from the region indicated that the cracked area had been internally initiated.

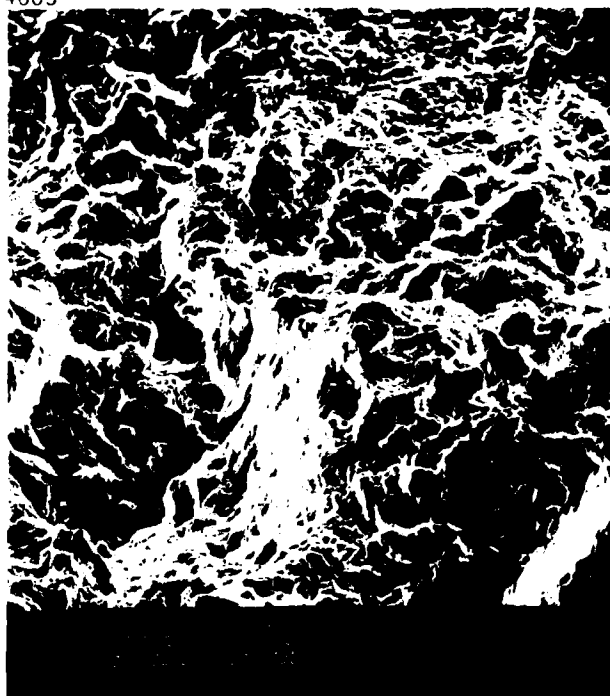
As with the AF-115 alloy, then, the fractographic examination of the AF2-1DA tensile dwell tests has shown that there was an extensive accumulation of creep-fatigue damage in the interior of the specimens. The observations also indicated that the failure process in these specimens was controlled by the link-up of internal cracks with a major surface crack.

Despite the large amount of creep-fatigue damage in the tensile dwell specimens, these tests lasted longer than the compressive dwell tests at the same total strain range. This behavior has previously been studied by Hyzak and Bernstein (Reference 80) for the superalloy, René 95, and it was concluded that the differences in life were due to the large mean stresses that develop during cyclic dwell testing of nickel-base superalloys. During a strain-controlled dwell cycle fatigue test, a specimen can develop a significant mean stress in the opposite direction of the hold cycle. That is, a tensile hold cycle can lead to a compressive mean stress and a compressive hold test to a large tensile mean stress. This behavior is shown graphically in Figure 63 for tests at equal total strain range. The tensile hold loop is displaced in the compressive direction, while the opposite is true for the compressive hold loop. The actual data are available in Appendix B.

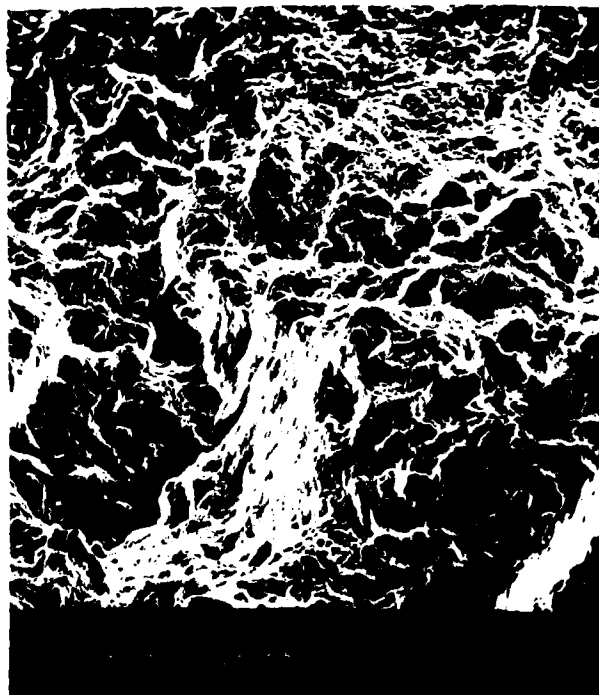
The effect of the mean stress and resultant high maximum tensile stress is to control the rate of fatigue damage, particularly crack propagation. Thus, a compressive dwell test would fail sooner than a tensile dwell test since it has a larger mean stress, and therefore, a



Figure 61. Fracture Surface of an AF2-1DA Tensile Dwell Test with Regions of Internal Crack Initiation



(a)



(b)

Figure 62. Intergranular Internal Initiation Sites on a Tensile Dwell Fracture Surface

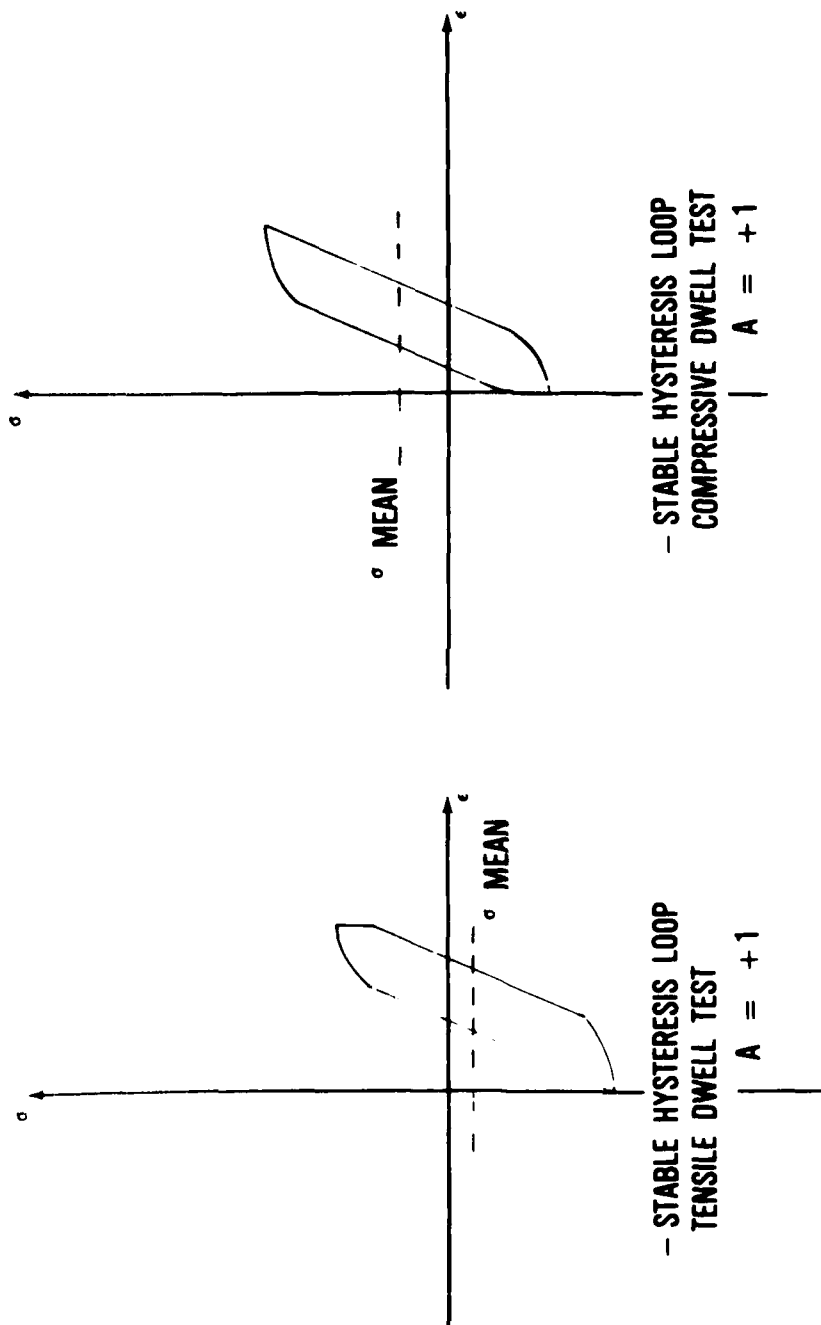


Figure 63. Schematic Illustration of the Stress Biases in Stable Hysteresis Loops of a) Tensile and b) Compressive Dwelling Tests

AFWAL-TR-80-4063

greater driving force for fatigue damage. This theory will be further developed in Section XII, and an alternative way of analyzing the data which better describes the creep effect will be presented.

SECTION X

INITIATION MODES - ROOM TEMPERATURE TESTS

To contrast with the results obtained at elevated temperature, several fatigue tests were performed at room temperature. A change in initiation mode was observed for all tests as compared to the high temperature results and there was no longer a transition from surface to subsurface initiation over the strain ranges tested. These observations will be amplified in this section.

1. AF2-1DA

AF2-1DA specimens were tested at room temperature at total strain ranges of 0.9%, 0.6%, and 0.4%. For the first two tests, initiation occurred by surface cracking along intense planar slip bands at approximately 45° to the tensile axis. The test at 0.4% $\Delta\epsilon_t$ was terminated at 5×10^6 cycles without failure. At that time there was no detectable cracking on the specimen's surface.

Figure 64 shows a central region of the polished and etched cross-section of the failed AF2-1DA specimen tested at 0.9% $\Delta\epsilon_t$; evidence of intense planar slip was in all grains through the specimen. Within the surface grains, parallel cracks formed along the slip bands in Stage I mode as shown in Figure 65a, and a SEM micrograph (Figure 65b) shows the cracking along the slip planes pictured in the previous micrograph (Figure 65a). At higher magnification, other surface-initiated cracks with slip offsets due to the shear mode of cracking are shown in Figure 66a. TEM replica studies also showed cutting of the γ' precipitates in these slip bands (Figure 66b) which would indicate a shear type of initiation mechanism.

Evidence of Stage I initiation was also present on the fracture surfaces of the 0.9, $\Delta\epsilon_t$ test. Figure 67a shows the crystallographic facets at the origin of the dominant crack and in fact at higher magnification SEM observations of these facets revealed the presence of

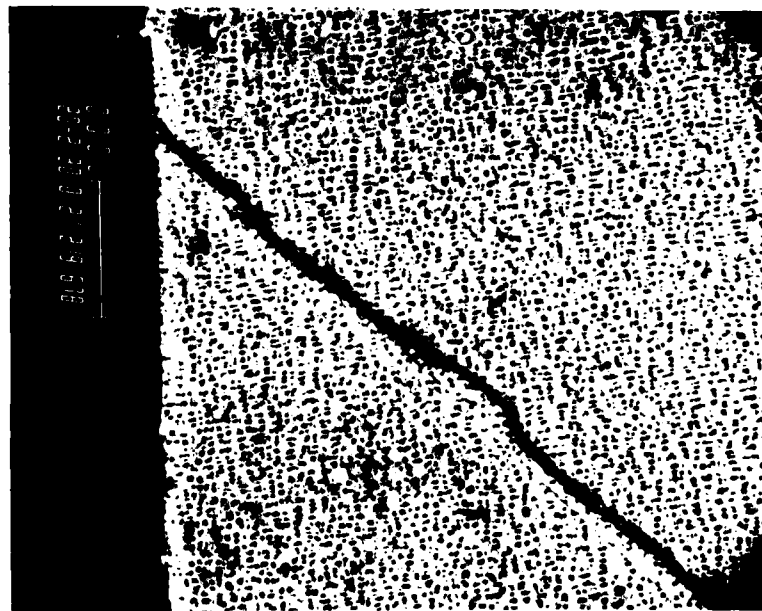


100 μ m

Figure 64. Optical Micrograph Showing the Intense Planar Slip in the Central Portion of a Room Temperature Fatigue Specimen



(a)

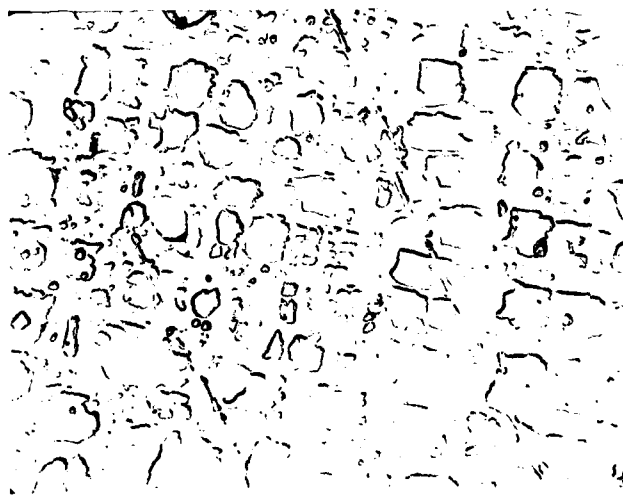


(b)

Figure 65. a) Optical Micrograph of Stage I Surface Cracking;
b) SEM Micrograph of the Middle Crack in the
Figure Above



(a)



(b)

1 μ m

Figure 66. Surface-Offset Associated with Stage I Surface Cracking; b) TEM Replica Image of γ' Shearing in a Planar Slip Band



(a)



(b)

Figure 67. a) Stage I Crystallographic Facets at the Origin of Crack Initiation for a Room Temperature Test;
b) A High Magnification SEM Image of the Stage I Facet Showing Striation Formation

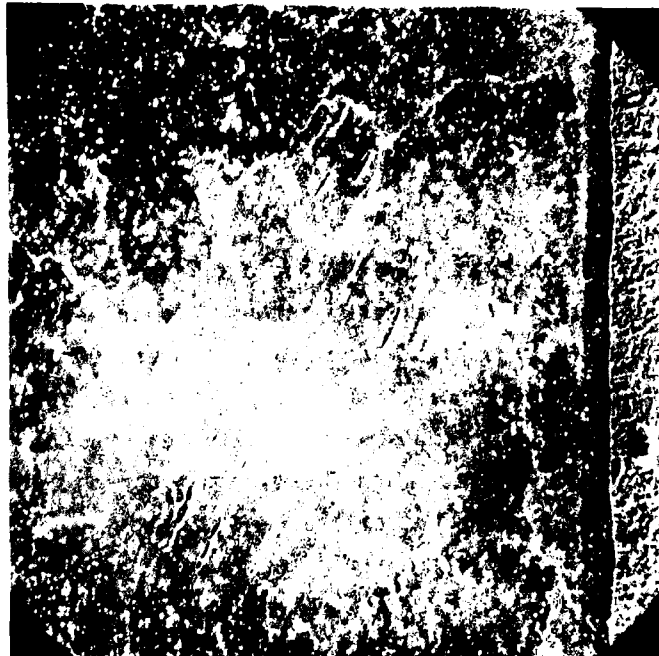
striations (Figure 67b) which suggests that the mechanism of early propagation may be some variant of the plastic blunting process (Reference 2).

The specimen fatigued at $0.6\% \Delta\epsilon_t$ had a similar Stage I facets on the fracture surfaces. The degree of intense planar deformation observed on the metallurgical sections was, however, considerably reduced. Slip traces were not observed throughout the specimen cross-section, but were confined to a few surface or near surface grains, as shown in Figure 68a. A higher magnification micrograph of the area in Figure 68a shows the development of cracks along planar slip bands, apparently in a more favorably oriented near-surface grain (Figure 68b). The number of Stage I surface cracks decreased as the strain range was reduced. Only one crack was observed in the plane of the cross-section for the $0.6\% \Delta\epsilon_t$ test, but for the $0.9\% \Delta\epsilon_t$ test there were over fifteen such cracks. These results are similar to previous elevated temperature observations which indicated that crack initiation consumed a smaller fraction of the total fatigue life as the strain range was increased.

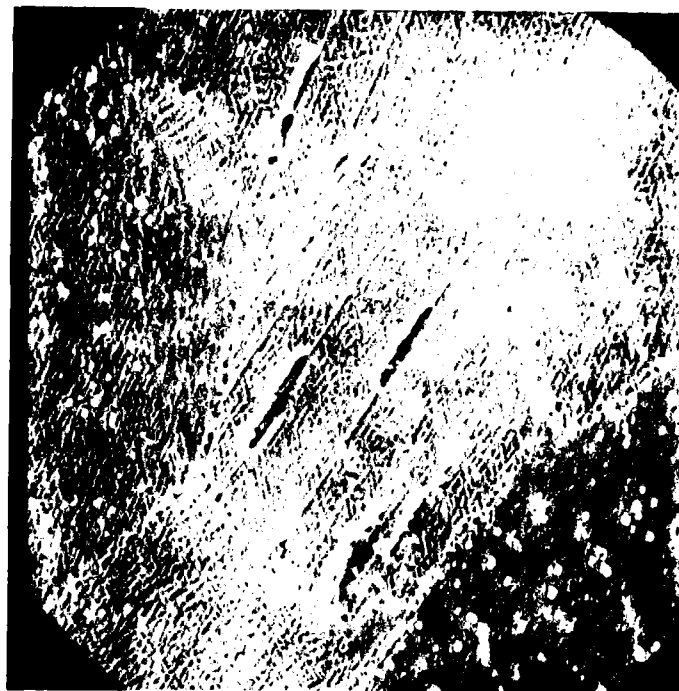
2. AF-115

Three fatigue tests were also performed for AF-115 at room temperature; the cyclic strain ranges were 0.9%, 0.6%, and 0.44% $\Delta\epsilon_t$. In all cases the dominant fatigue cracks were initiated along the planar slip band adjacent to a near-surface pore. On the fracture surface, intense crystallographic cracking was evident around those pores which were the fatigue origins (Figure 69a), and at higher magnification, the Stage I planes appeared similar to cleavage facets with no obvious striations (Figure 69b).

Observations of metallographic sections revealed the details of the Stage I initiation process. Figure 70a shows a near-surface pore with cracks emanating along planes of maximum shear strain at an angle of approximately 45° to the tensile axis. TEM replica examination of this pore showed intense slip traces parallel to the main crack (Figure 70b) as evidenced by cutting the γ' precipitates (Figure 71).



(a) 100 μm



(b) 10 μm

Figure 68. a) Intense Slip Planes in Selected Near-Surface Grains at a Total Strain Range of 0.60 ;
b) Cracking Along Slip Planes in One Grain Pictured in Figure 68a

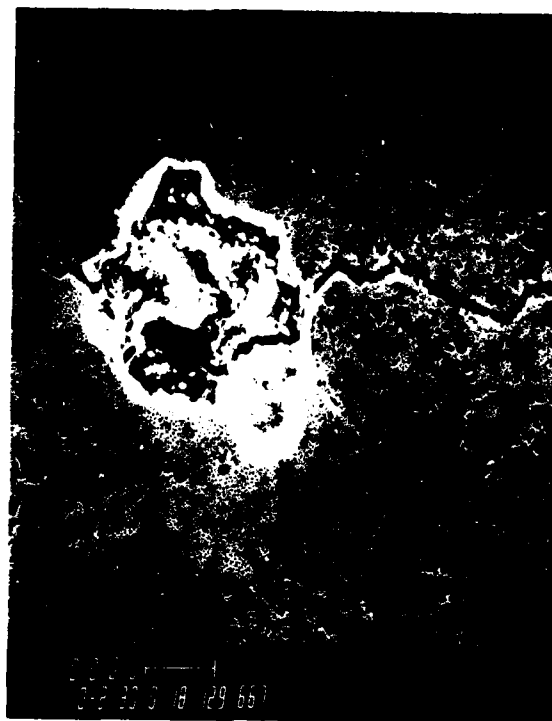


(a)



(b)

Figure 69. a) Stage I Cracking Originating at a Near-Surface Pore in AF-115; b) A High Magnification SEM Image of the Stage I Facet Morphology



(a)



(b)

1.5 um

Figure 70. a) Cross-Sectional View of a Stage I Crack Originating at a Near-Surface Pore in AF-115; b) TEM Replica Image of the Cracked Region Between the Pore and the Surface Edge in the Above Figure Showing Planar Shear Bands Parallel to the Stage I Crack



Figure 71. Shearing of the γ' in Planar Slip Bands Shown in Figure 70b, TEM Replica

In summary, at room temperature, fatigue cracks in both alloys initiated in Stage I mode along intense planar slip bands; this was a different mechanism than observed at elevated temperature in which cracks initiated in Stage II mode, normal to the tensile direction. Cracks nucleated near the specimen's surface for AF2-1DA and at near surface pores in AF-115 in all cases, and there was no transition to subsurface initiation observed down to a fatigue strain range of 0.44% $\Delta\epsilon_t$. The differences in initiation mechanism between room and elevated temperature will be addressed in detail in Section XII, along with the observation that slip appears to occur preferentially at or near the specimens surface. The influence of slip behavior in these two temperature regimes on crack initiation will, however, be discussed first in the following section.

SECTION XI

TEM THIN FOIL ANALYSIS

The main findings of the crack initiation characterization have been that there was a surface to subsurface transition in initiation site at elevated temperature for both AF-115 and AF2-1DA and there was also a significant difference in initiation mode between room and high temperature. These observations have been drawn predominantly from SEM observations. To further detail these findings, the slip behavior of AF2-1DA was examined using TEM thin foil analysis of specimens that had been fatigued at different strain ranges in each temperature regime. The TEM work was necessarily limited to AF2-1DA due to the extreme difficulty in thinning the highly porous AF-115 alloy.

1. ELEVATED TEMPERATURE

In the unfatigued condition, the AF2-1DA microstructure had a very low dislocation density as might be expected since the alloy was solution-annealed after the superplastic forging operation (Figure 72a). The deformation was also homogeneously distributed throughout the microstructure. Included in Figure 72b is another example of the AF2-1DA microstructure; partially evident is the high density of fine aging γ' precipitates between the cuboidal cooling γ' .

For samples fatigued at a total strain range of 0.60% at 760°C, the general dislocation density was still low and homogeneously distributed, as shown in Figure 73a. There was, however, some tendency in a few areas for dislocations to concentrate in localized bands. Figure 73b shows one example of this in which a band of dislocations appear to shear the γ' precipitates along $\{111\}$ traces. In another area, a large density of dislocations was observed lying along $\{111\}$ planes near an MC carbide, whose associated strain concentration was apparently responsible for the localized concentration of deformation (Figure 74a), and at higher magnification it was apparent that the dislocations generated at the carbide avoided the large cuboidal γ' (Figure 74b). Regarding the



(a)

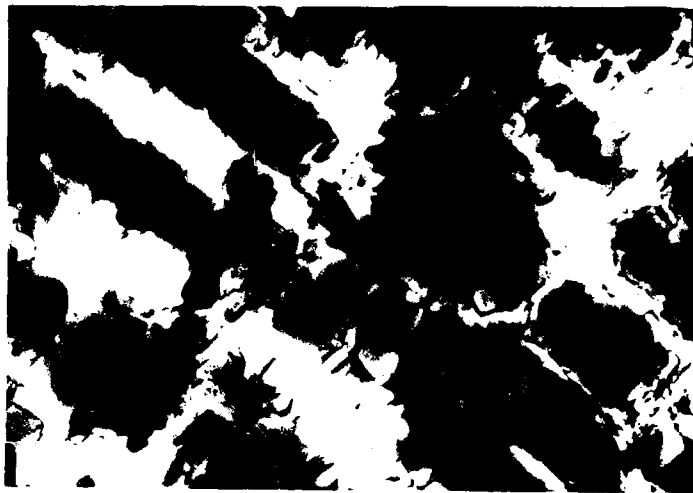
1 μm



(b)

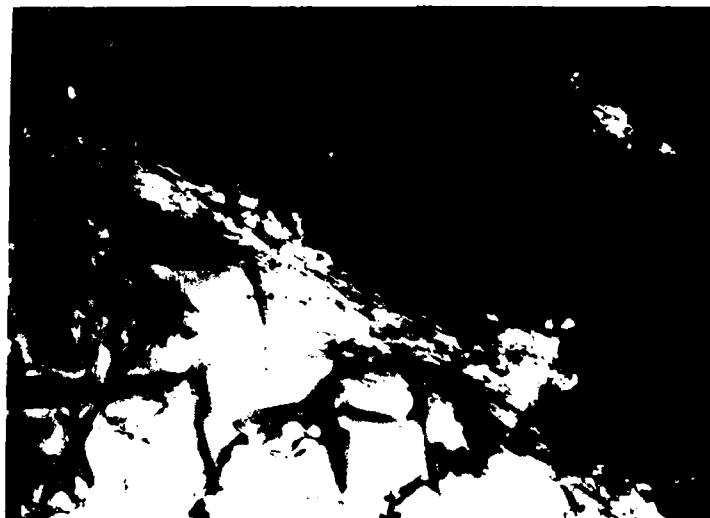
1 μm

Figure 72. a) Dislocation Density of As-Received AF2-1DA;
b) Cracked, ' Precipitates in As-Received AF2-1DA



(a)

1 μm



(b)

1 μm

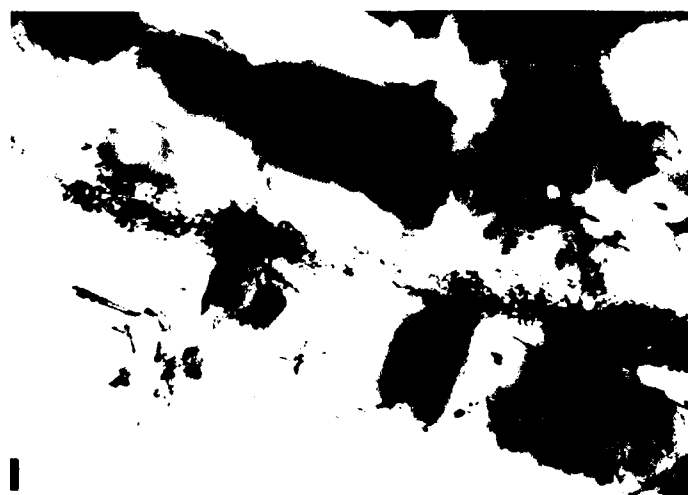
Figure 73. a) Dislocation Density of 0.60 $\times 10^8 \text{ cm}^{-2}$ Test at 760°C
b) Array of Dislocations Along the Trace of the (111) Plane, [110] Z.A.



(a)

1 μ m

$g[111]$



(b)

1 μ m

$g[111]$

$(111)_t$

Figure 74. a) Band of Dislocations Originating at a Carbide, $[110]$ Z.A.; b) Higher Magnification of the Above Showing the Dislocations Preferentially Located in the γ Phase $[110]$ Z.A.

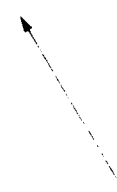
former observation, the difference in concentration of plastic strain at defects of varying geometry will play a key role in the analysis of the surface subsurface transition as presented in Section XII.

At an increased strain range of 0.9%, the dislocation density varied throughout the foil, in some areas the density was high (Figure 75a), while in others it was not very much greater than at 0.6% (Figure 75b). While there was more evidence of dislocations in the γ' precipitates than at 0.6% $\Delta\epsilon_t$, the deformation was still generally characterized as homogeneous and wavy. Figure 76a is a dark field micrograph using a [100] superlattice reflection; the dislocations in the γ' are now more clearly shown shearing the particle. In another area, and at higher magnification, the dislocations could be resolved cutting across the precipitate parallel to the trace of a {111} plane (Figure 76b). In isolated regions, however, more heterogeneous dislocation bands were also observed, as shown in Figure 77a in which the dislocations fell along the trace of a {111} plane. Pictured in Figure 77b is another example of dislocation banding; in this case the dislocations seem to avoid the larger cooling γ' particles as previously noted for Figure 76. These dislocation bands did not usually extend more than 3-4 microns in length before they dissipated into more diffused arrays, and they did not result in any observed slip offsets or cracking in the γ' precipitates.

Finally, for the specimen fatigued at 1.3% $\Delta\epsilon_t$, the deformation was also wavy, but there was a noticeable tendency for the deformation to be more concentrated in the γ phase leaving the blocky cooling γ' now with a lower dislocation density (Figure 78a). Figure 78b is a higher magnification bright field micrograph further illustrating the preference for the deformation to avoid the larger γ' precipitates. This same unusual behavior has been reported by Copley and Kear (Reference 104) for the superalloy, Mar-M200. These authors went on to explain their observations in terms of a dynamic theory of coherent precipitation hardening which they developed. In their formulation, the largest contribution to the critical resolved shear stress (CRSS) of a nickel-base superalloy comes from the antiphase boundary energy (APB) of the ordered phase. Therefore, the resistance to dislocation motion is



$g[002]$



(a)

1 um



$g[111]$



(b)

1 um

Figure 75. a) High Dislocation Density of 0.90 $\times 10^8$ Test at Elevated Temperature $[110]$ Z.A.; b) Lower Dislocation Density Under Same Test Conditions as Above, $[110]$ Z.A.

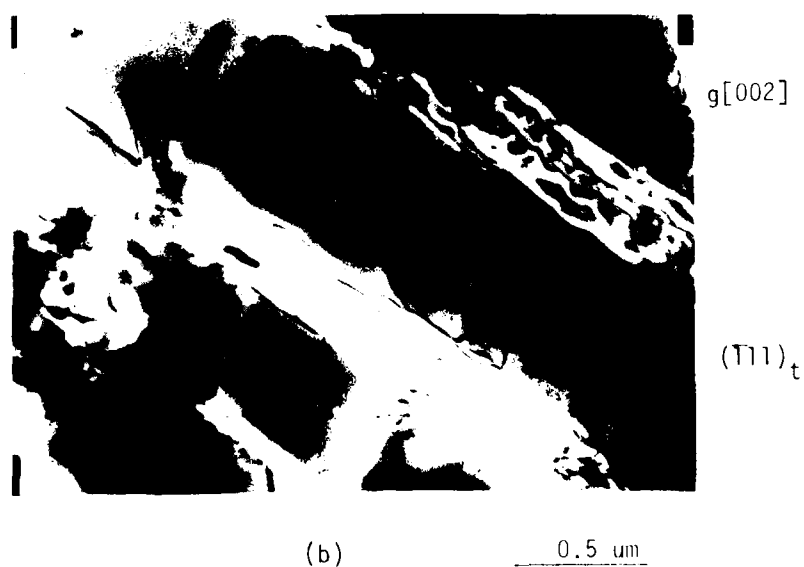
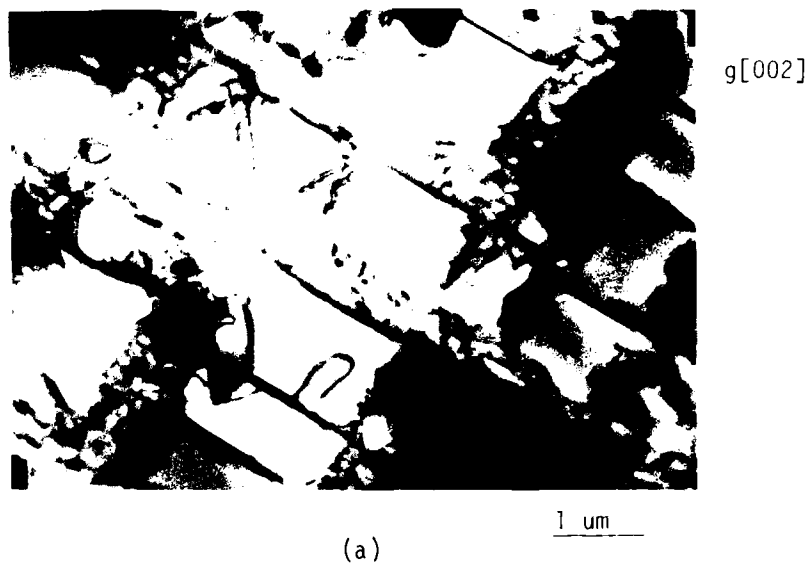


Figure 76. a) $[001]$ Superlattice Reflection of γ' Precipitates Showing Dislocation Concentration After Fatiguing at 0.90 $\Delta\sigma_t$, $[110]$ Z.A.; b) Bright Field Micrograph of Dislocations Shearing γ' Precipitate Along the Trace of the (111) Plane, $[110]$ Z.A.

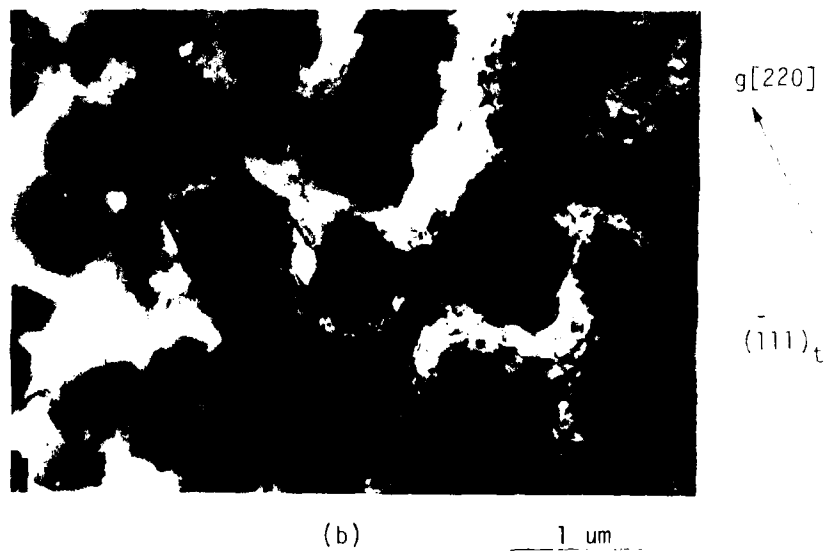
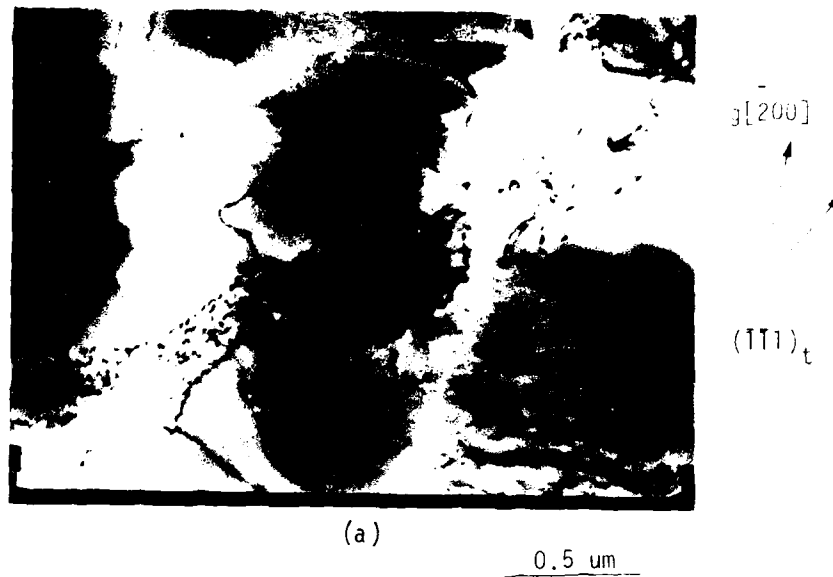


Figure 77. a) Band of Dislocations Along the Trace of the (111) Plane at Elevated Temperature, $[001]$ Z.A.; b) Array of Dislocations Located Preferentially in the Matrix Phase, $[100]$ Z.A.

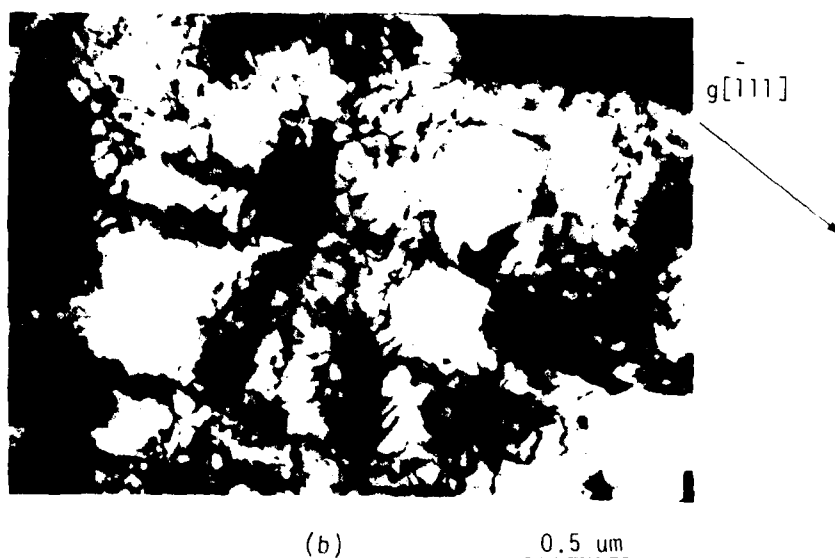
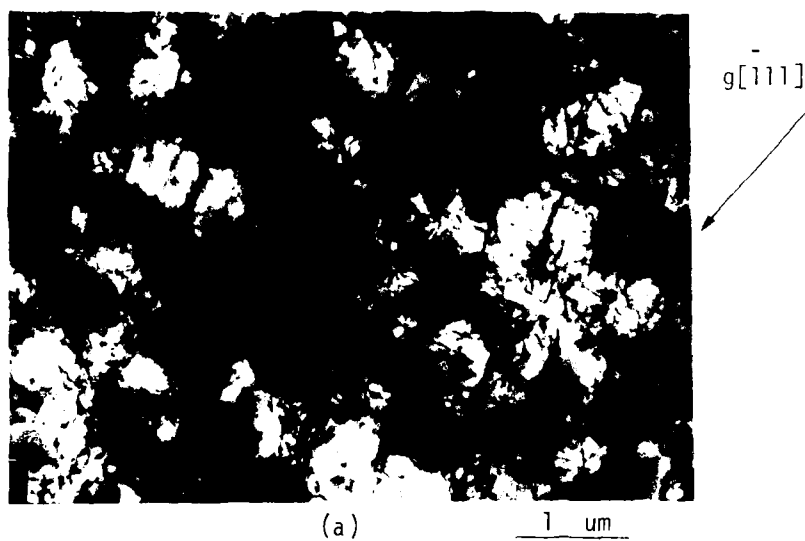


Figure 78. a) Wavy Slip Character of High Temperature Test at 1.10 Aet, [110] A.A.; b) Higher Magnification of Above Showing Lower Dislocation Density of the Larger Cooling γ' Precipitates, [110] Z.A.

greatest at the γ - γ' interface, and once dislocations pass into the γ' precipitate they travel quickly through the particle. Thus the observation that dislocations are concentrated in the γ phase simply reflects the slow step in the motion of the dislocations at the interface. This theory also successfully predicts the temperature dependence of the yield stress of the superalloy, Mar-M200 by including separate terms for the critical resolved shear stress of the γ and γ' phases.

2. ROOM TEMPERATURE

The deformation mode at room temperature was considerably different than the high temperature behavior. Specifically, the slip was now very heterogeneous and characterized by intense planar slip bands. Figure 79a is a bright field micrograph of a specimen fatigued at room temperature at $0.5\% \Delta\epsilon_t$; intense planar slip bands along $\{111\}$ planes are evident throughout the microstructure. A dark field superlattice reflection at higher magnification, Figure 79b, better illustrates the intensity of the γ' shearing as reflected by the large offsets in the precipitates along $\{111\}$ traces.

For the lower strain range test of $0.6\% \Delta\epsilon_t$, the deformation was again heterogeneous and planar, however, the intense bands were present in fewer grains and often the areas of greatest dislocation density were near MC carbides, as had been previously noted at elevated temperature. Figure 80 shows an example of intense planar slip bands near the edge of a carbide particle. The intensity of the slip at low strain ranges was most likely the reason why Stage I surface initiation still dominated the failure process at $0.60\% \Delta\epsilon_t$ in AF2-1DA, and as a result no surface-subsurface transition was observed at room temperature.

3. SUMMARY

This TEM analysis has shown that there was a distinct difference between room temperature and elevated temperature deformation in the superalloy, AF2-1DA. At room temperature, slip was planar and very

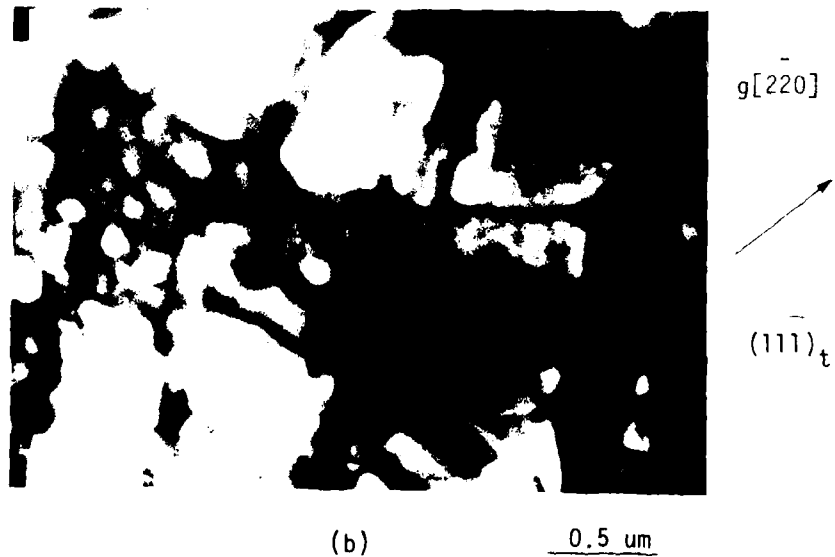
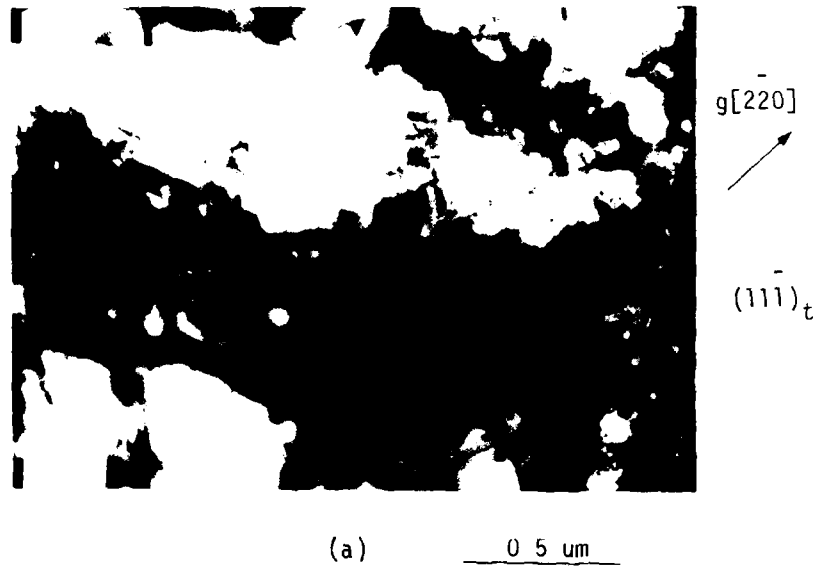


Figure 79. a) Planar Slip Character of the Room Temperature Deformation at 1.1% $\Delta\epsilon_t$ [001] Z.A.; b) Dark Field Superlattice Reflection Showing Shearing of the γ' Precipitates at Room Temperature Along the Traces of the (111) Plane, [110] Z.A.

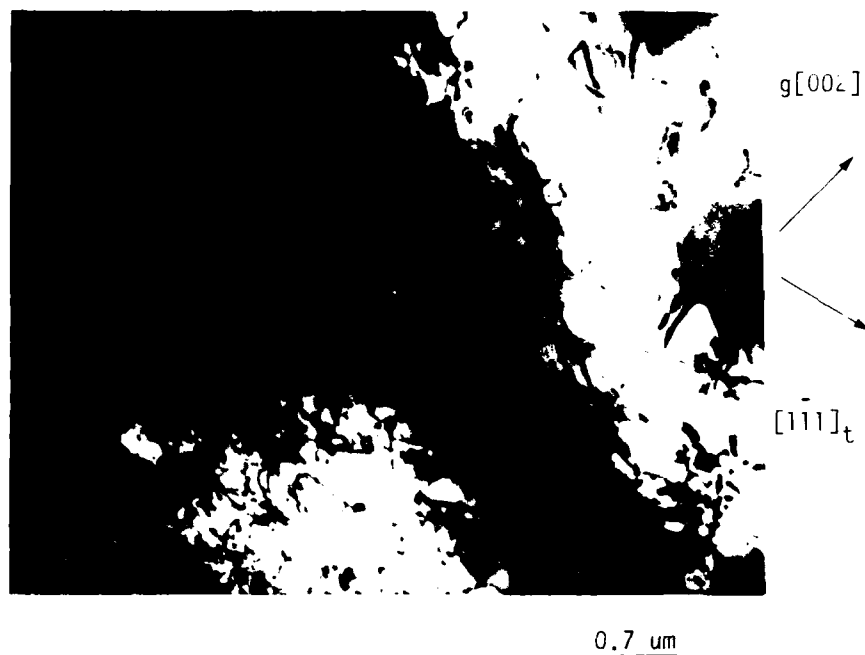


Figure 80. Intense Planar Deformation Apparently Originating at a Carbide at Low Strain Range, [110] Z.A.

AFWAL-TR-80-4063

heterogeneous, such that intense slip bands were present even at low strain ranges ($0.6\% \Delta \epsilon_t$). At elevated temperature, the deformation was wavy and more homogeneous. While there was also a tendency for dislocations in this temperature regime to form in bands at lower strain ranges, the deformation below the SST was comparatively diffused even around stress concentrations such as carbides.

SECTION XII

DISCUSSION

1. INTRODUCTION

The experimental results of this investigation have shown that at high temperature fatigue crack nucleation in nickel base superalloys is significantly influenced by slip behavior, defect population, and creep deformation. In particular, there have been three main findings of this study: first, at high temperature there was a transition in the initiation site of the dominant crack from a surface or near surface location to a subsurface site as the total strain range was reduced; second, crack nucleation at room temperature occurred by a different mechanism than at elevated temperature, and with no transition to subsurface initiation over the strain ranges tested, and finally, there was a significant creep-fatigue interaction in those alloys when tested with the incorporation of a tensile dwell cycle.

Each of these observations will be reviewed and analyzed, and their implications will be discussed. The discussion will specifically emphasize the fact that fatigue in a smooth bar specimen is comprised of two phases, crack initiation and crack propagation, and, therefore, the influences of deformation behavior and microstructural discontinuities on fatigue can be understood in terms of how these two factors effect crack initiation and propagation. The discussion will also be based on the premises that crack initiation is the result of highly localized plastic deformation (Reference 2), and crack propagation is controlled by the crack tip stress intensity (Reference 108) and the environment (Reference 42).

2. SURFACE-SUBSURFACE TRANSITION (SST)

This study has documented the critical influence of defects on the crack initiation process. Except for the AF2-1DA specimens that failed from surface initiated cracks, a specific discontinuity was identified at the fatigue crack origins for all the specimens tested. An SST in the

nucleation site of the dominant fatigue crack has been shown to exist, and since this type of SST has also been observed for other high strength P/M superalloys (Reference 96), it appears that this is a generic type of behavior, at least for this class of materials. While both surface and subsurface crack initiations have been reported in the literature for a wide range of alloys, there has been no known study which has explained why internal initiation can occur instead of the more commonly observed surface nucleation for certain test conditions. As noted earlier, de Kajinczy (Reference 3, 60, 61) has published considerable data for crack initiation of various steels and found no trends for the presence of internal crack initiation. He did state, however, that defects at the specimen's surface had a larger notch effect than defects located in the interior. Although this statement is rather general since it does not define notch effect in terms of stress concentration or stress intensity, the basic idea of an enhanced stress level at the specimen's surface will be an important one in our subsequent development.

To determine what conditions control the fatigue process and in particular, which are responsible for the SST in initiation site, several special tests were performed to investigate the effects of various parameters on the initiation mode. The effect of the environment was first tested. Remember that Gell and Leverant (Reference 26) observed internal crack initiation at low strain ranges for the directionally solidified superalloy, Mar-M200. The transition in nucleation site was attributed to surface oxidation which blunted small surface cracks in the low strain range regime. Since two of the high temperature, high vacuum tests were aborted because of mechanical malfunctions in this study, the effect of environment was not unequivocally established. However, the conclusion was reached that oxidation was not solely responsible for the change in initiation site of the dominant crack from the surface to an internal location (SST). A more thorough analysis of this question will presently be considered.

It has already been shown in Section VI that despite their differences in initiation mechanisms, AF-115 and AF2-1DA exhibited the change from

surface or near surface initiation to subsurface initiation at approximately the same total strain range. However, if the external environment was responsible for this change in nucleation site (SST), these two alloys would have been expected to have had contrasting behaviors. This is because crack nucleation at a near surface pore in AF-115 occurred approximately 10-20 μm below the surface and, therefore, a crack from such a pore in AF-115 was not subject to the influences of surface oxidation until it grew out to the specimen's surface. At this point, the crack would have an effective length of approximately 100 μm , including the pore diameter. The effect of oxidation on a 100 μm crack in AF-115 would be expected to be significantly different from its effect on a 1-2 μm surface microcrack in AF2-1DA which would be subject to the influences of environment immediately upon nucleation.

It has also been shown that no surface or near surface cracks were observed on the nickel-plated cross sections of AF-115 and AF2-1DA specimens that had been fatigued at strain ranges below the SST. For AF-115, this shows that below the SST, cracks at near surface pores never initiated, as opposed to the observations of Gell and Leverant (Reference 26) who reported that surface cracks initiated and were then blunted. As was previously noted, near-surface pores were not subjected to an air environment, and, therefore, the termination of cracking at near surface pores cannot be attributed to oxidation. In support of this conclusion, secondary cracking for AF-115 and AF2-1DA, both at the specimen's surface and internally, was described earlier in this report to decrease as the total strain range decreased (Section VI, 2.c.). Therefore, the termination of crack initiation at a certain strain range appears to be related more to a change in plastic strain level than to any surface interaction.

Finally, the one valid ultra high vacuum test at a strain range below the SST failed from an internal inclusion, precisely the same type of initiation mode found in the high temperature air atmosphere tests. This result along with the other observations that have been discussed strongly indicate that surface oxidation was not responsible for the

changes in crack initiation observed over the strain ranges tested, and, therefore, the environment was not solely responsible for the SST. It is, however, likely that the environment did affect the propagation phase of fatigue and therefore may still of had some influence on the surface-subsurface transition. This will be considered in a following discussion.

In summary, it has been shown that the crack initiation behavior cannot be explained in terms of environmental influences, and in Section VIII it was also demonstrated that two other factors that were especially tested, surface residual stresses and the strain ratio which controls the mean stress of a test, were not responsible for the SST. Recall that the elimination of surface residual machining stresses and changing the fatigue cycle to a fully-reversed strain cycle with no appreciable mean stress still resulted in subsurface initiations at strain ranges below the SST, as expected from the baseline tests.

Having eliminated these factors from primary consideration, it does appear that the existence of a SST can be better rationalized from an extension of de Kajinczy's idea that there is a difference in notch effect at surface and internal defect sites. The following analysis will take this approach, and will involve considering individually the fatigue process at the specimen's surface and at a subsurface site, and in each case, separating the process into the crack initiation and crack propagation phases. More specifically, this analysis will include: a) a review of the observations of crack initiation in this study, b) an analytical assessment of the stress and strain concentrations at various defects, c) definition of a crack initiation criterion, d) an analysis of crack propagation effects on fatigue, and e) a review of the results of this research in view of the factors listed above. From this approach it is hoped to also determine the relative influences of defect size, shape, and population on the fatigue process.

a. Observations of Crack Initiation

In this section, the observations of fatigue cracking at elevated temperature in both AF-115 and AF2-1DA will be reviewed with particular attention to the modes of secondary cracking. These observations will then be discussed in terms of plastic strain localization as the controlling process for crack nucleation.

As previously noted, there were many secondary cracks in each test specimen which initiated at various defects in addition to the dominant cracks which caused failure. The observations of secondary cracking for both alloys in this study were consistent; at strain ranges well above the SST, extensive cracking occurred both at the surface and internally at defects, and as the strain range was reduced so were the number of surface and internal initiation sites. Finally, below the SST there were no surface or near surface cracks, and only a very limited number of internal cracks which were invariably initiated at inclusions. These observations are significant in that they show that cracking at high strain ranges, above the SST, occurred at all defects with no apparent regard for location in the specimen, while at low strain ranges initiation occurred only at the most acute defects located in the interior of the specimen. This latter observation indicates that the acute shape of the subsurface defects may have been as necessary a requirement to cause initiation as was the defect's location below the surface. The fact that the number of secondary cracks decreased as the total strain range decreased, and that defect shape was important in subsurface initiation suggests that the initiation process was controlled by plastic strain concentration as has been hypothesized in this analysis.

The SST in failure location has been shown in Figures 24 and 25 to occur at a specific total strain range, and although the data are somewhat limited, the strain range corresponding to the transition point appears to vary with the alloy and the defect population. The SST strain ranges have been determined to be: 0.65% for AF2-1DA, between 7.0% and 0.6% for AF-115, and between 0.9% and 0.7% for AF-115-LD. An equally

important parameter associated with the transition point is the normalized stress range ($\Delta\sigma/\sigma_{y.s.}$) which provides a measure of the extent of general yielding in the specimen. The normalized stress range is, therefore, also a measure of the nominal plastic strain level in the specimen, and it has been utilized in other studies to provide a gauge of the localized plastic strain fields at defects (Reference 67). For AF2-1DA, the value of the normalized stress range at the SST was 1.24, while for AF-115 it occurred between 1.17 and 0.95, and for the AF-115-LD material it was between 1.29 and 1.17. The most striking point here is that the AF2-1DA alloy and the AF-115-LD material had a similar defect population, i.e., nonmetallic inclusion, no pores or HfO_2 inclusions, and they also had nearly equal values of the normalized stress range at the transition from surface to subsurface initiation. This result supports the suggestion that the SST may be related to a critical measure of localized plastic strain which has already been described as controlling the general crack initiation process. This result also supports the conclusions that neither the environment nor any other surface effect solely governs the SST.

Since the concept of strain localization appears critical to the existence of the SST, the relationship of defect character to plastic strain concentration will be discussed in the following section.

b Strain Concentration at Defects

The calculation of plastic strain concentrations at defects and other discontinuities in materials subject to general yielding is presently a formidable task, and existing data are limited. A qualitative appreciation for the magnitude of these localized strains can be obtained, however, by first examining the data for elastic strain concentrations which have been well established in the literature and then relating them to the available data for the elastic-plastic case. To accomplish this, Harkegard's (Reference 67) finite element analysis of plastic strains around defects in a elastic-plastic plate will be reviewed in this section along with the elastic solutions for similar problems found in the literature.

From Peterson's summary (Reference 65), the two-dimensional elastic stress concentration factors, K_t , for various defect geometries under tensile loading are:

Hole in an infinite plate	$K_t = 3.0$
Hole near a surface in semi-infinite plate; 200 μ diameter hole, 20 μ from edge	$K_t = 6.2$
Elliptical hole in an infinite plate	
b/a (length/thickness) = 3	$K_t = 7$
b/a = 10	$K_t = 21$

The K_t value indicates the magnitude of the increase in stress range at the discontinuity, so from these results an acute elliptical hole ($b/a = 10$) would be expected to be a much more effective stress concentrator than would be a spherical pore. In general, the stress concentration effect decreases as the root radius of the notch increases; that is, the stress concentration increases as the sharpness of the defect increases.

Although the elastic stress concentration values lose their quantitative significance when plastic yielding occurs, they would still be expected to indicate the relative order of severity for stress concentrations at different defects under elastic-plastic conditions. For the particular defects being studied in this investigation, a pore will be modeled as a spherical hole, a ceramic inclusion as an elliptical hole with (b/a) equal to 3.0, and a hafnium oxide inclusion as a sharp elliptical hole with a (b/a) ratio of 20, and as a result, the HfO_2 inclusion will be expected to be the most effective stress raiser, and the pore the least effective. For the cases of the HfO_2 and nonmetallic inclusions, no factors have been included in this analysis to account for the presence of an inclusion in or adjacent to the cavity. This decision is based on the metallographic observations of early inclusion-matrix decohesion for both the HfO_2 and ceramic inclusions, and particle

fracture for the metallic inclusions. Thus, there are no compatibility requirements which would restrict the elliptical cavities from expanding or compressing during fatigue. Similar approximations have been previously used successfully (Reference 63).

As described in the Literature Review, the results of Harkegard's (Reference 67) analysis support these same trends in stress concentration for the case of defects in an elastic-plastic medium. His finite-element calculations have shown that the equivalent plastic strain at the edge of a sphere at a load of $0.7 \sigma_{y.s.}$ was equal to the elastic strain at yield for the particular material conditions studied, while at the same load, the local plastic strain at the elliptical cavity was 4.5 times as great. Thus, the localized plastic strains that develop at defects can be many times the nominal value, and the strain concentrations at elliptical cavities (inclusions) are significantly greater than at spherical voids (pores) in the elastic-plastic case.

c. Criterion for Crack Initiation

Having established a more quantitative appraisal of the magnitude of the plastic strain concentrations at various defects, a criterion for crack nucleation needs to be developed in order to apply this information to the crack nucleation process. Harkegard (Reference 67) has proposed a simple model based on ductility exhaustion to determine the number of fatigue cycles necessary to nucleate a stable crack. He assumes that the number of cycles governed by the equivalent plastic strain range through:

$$N_f = (D/\Delta \epsilon_p^e)^2 \quad (1)$$

where D is a constant characterizing the ability of the material to resist repeated plastic strain, and $\Delta \epsilon_p^e$ is the calculated equivalent plastic strain range. This relationship is analogous to the Coffin-Manson (Reference 105) relationship where D is identified with the tensile ductility defined by:

$$D = -1 \ln (1 - R.A.) \quad (2)$$

R.A. here denotes the reduction of area obtained from a conventional tensile test. This formulation does not imply, however, that the fatigue lives will conform to Coffin-Manson behavior.

Harkegard applied this initiation criterion to his data for different defect geometries assuming $D = 1.0$, and the results are contained in a graph of normalized load range versus cycles to initiation, N_i , Figure 81. These results show that at a high normalized stress range (> 2.0), Harkegard's model predicted very rapid crack initiation at both the sphere and the elliptical cavity, and as the load range was reduced the predicted values for the number of cycles to crack initiation increased. At particular levels of normalized stress range, crack initiation from spheres and elliptical cavities requires such a large number of cycles (10^8) that these stress ranges can be considered as effective endurance limits. For Harkegard's data, the endurance limit for initiation from a sphere was at a normalized stress range of 1.0, while for the elliptical cavity it was approximately 0.7. Thus, these data predict that at a normalized stress range above 1.0, initiation can occur at both spheres and elliptical cavities, while at a normalized stress range between 1.0 and 0.7, cracks would nucleate only at elliptical cavities.

Although these quantitative results are not expected to apply directly to the superalloys under study, the importance of Harkegard's work is that it has shown that the magnitude of the localized plastic strain concentration at a defect in an elastic-plastic body is a function of the defect geometry and the far-field stress range, and when the plastic strain concentration at the defect is less than some critical value, crack initiation will not occur. For AF-115, then, these results would predict that at high stress ranges cracking would occur at both inclusions and pores, but as the stress range is reduced there would be a stress level at which cracks would no longer initiate at pores although they would still nucleate at the more acute inclusions. This, of course, is in agreement with the experimental observations reported earlier, where secondary cracking in AF-115 at pores both near the surface and in the specimen's interior was shown to terminate at the same stress range as the SST was observed.

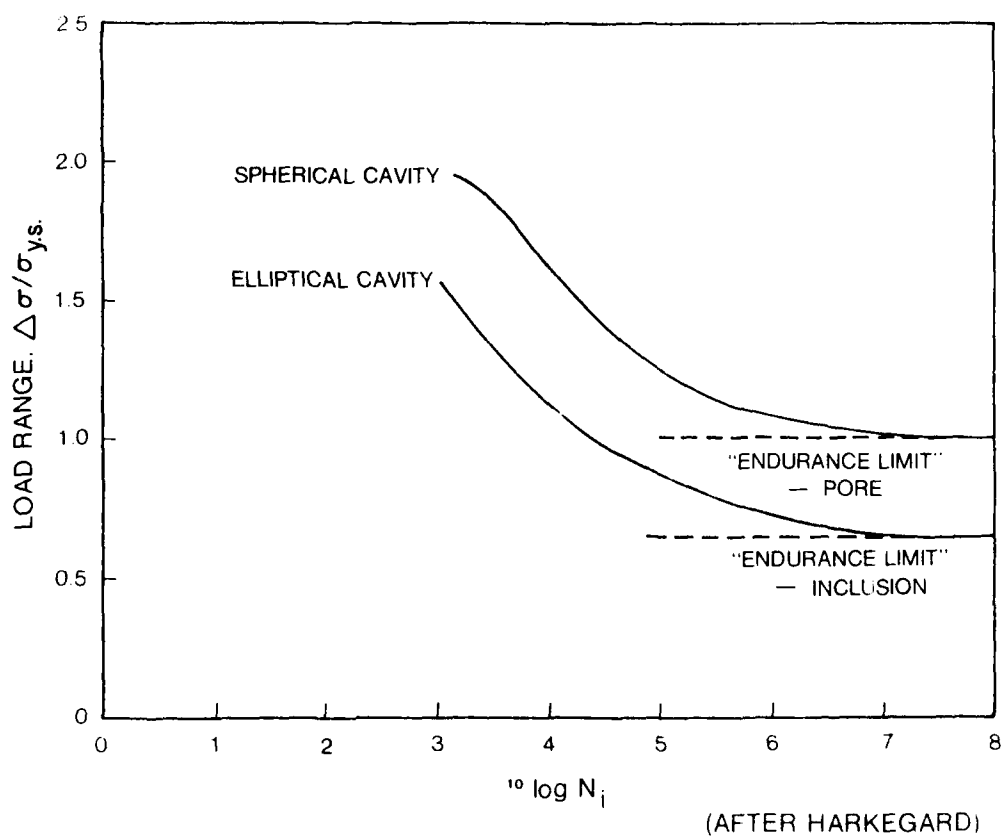


Figure 81. Crack Initiation Life Versus Normalized Stress Range (Harkegard, Reference 65)

In summary, crack initiation has been shown to be dependent on localized plastic strain which in turn is a function of defect geometry. It has also been shown that in AF-115 the SST can be related to the stress level at which cracking no longer occurs at the highly populous pores but still occurs at the more acutely shaped inclusions.

Despite the success of this theory to predict the fatigue initiation behavior of AF-115, the analysis has not addressed the case of surface crack initiation in AF2-1DA and AF-115-LD since for these no dominant defect was associated with the nucleation process. As previously stated, the origins of Stage II surface initiation in AF2-1DA were believed to be small inclusions, carbides, and other microstructural defects which were too small to be identified in most cases. It is significant that this type of initiation, associated with submicron size defects, occurred only at the specimen's surface, while all internal cracks nucleated at large inclusions greater than 100 μm in length.

The specimen's surface has been identified through the literature as the sole site of crack nucleation in the absence of large defects (Reference 2). In some instances this has been related to the environment (References 2, 106) but in other cases the presence of minor surface irregularities coupled with the fact that slip is easier on the surface has resulted in the surface being a preferred location for initiation (Reference 2). In this regard, Cottrell has shown that dislocation sources at the surface can be activated at one-half the stress needed to activate internal sources (Reference 107). Thus, the surface is a site of localized plastic strain concentration in the same way that pores and inclusions are, and therefore, the surface can be considered to have been the dominant defect for AF2-1DA and AF-115-LD at high strain ranges just as near-surface pores were the dominant defects for AF-115. As a result, in this context we will consider the surface as being a defect and will also refer to the surface as a location on the specimen. To help reduce the confusion over this differentiation, the words defect and location will be included with the use of the word surface.

Since the surface (defect) is a strain concentrator just as pores and inclusions, it too should have an "endurance limit" for crack initiation associated with it. Indeed, in AF2-1DA and AF-115-LD, surface (defect) cracking occurred at high stress ranges, and as the stress range was decreased there was a certain stress level at which cracks no longer initiated at the surface (defect). This stress range was the same as reported for the transition from SST. So, the localized plastic strain concentration seems to control surface (defect) initiation in the same way as it controls crack nucleation from a pore. An illustrated summary of the results presented in this section is shown in Figure 82.

Above the SST, crack initiation occurred at all defects (pores, inclusions, surface) both near the surface and in the interior of the specimen. This was because the plastic strain concentration at all these defects was greater than the threshold value needed for initiation. Below the SST, however, the plastic strain concentration at the surface (defect) and around pores was not great enough to nucleate a crack, but cracking still occurred at both HfO_2 and other nonmetallic inclusions which had larger localized strain concentrations due to their more acute shape. Since there were relatively few inclusions of this type in most specimens, they were expected statistically to be found in the bulk of the specimen, rather than at the surface. Thus, fatigue at low strain ranges (below SST) resulted in subsurface nucleation not because the interior of the specimen was a preferred site for initiation as compared to the surface (location), but because the only "sharp" defects capable of initiating cracks were found in the bulk of specimen. Therefore, this theory also suggests that if a statistically significant number of specimens were fatigued at strain ranges below the SST, one or more should fail from an inclusion at the surface. The number of specimens needed would be related to the probability of having an acute, properly oriented defect very near the surface.

This analysis has thus demonstrated that there is a stress range below which cracking at the surface (defect) and at pores no longer occurs, while initiation can still take place at acute, properly

SECONDARY FATIGUE CRACKING

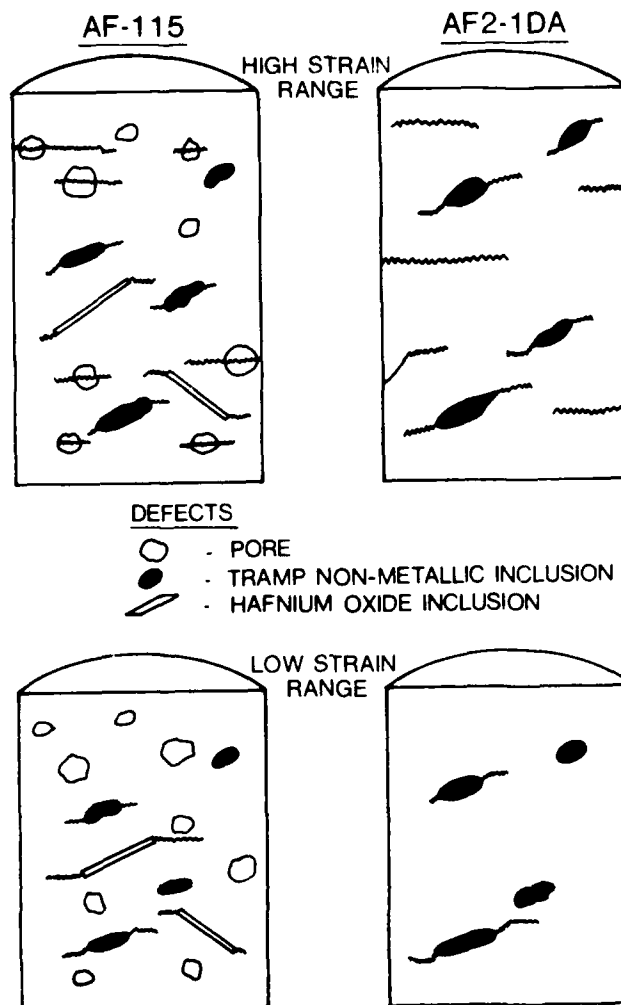


Figure 82. Summary of the Observations of Secondary Cracking in AF-115 and AF2-1DA at Elevated Temperature

oriented inclusions (Reference 67). However, the analysis has not given a complete reason why the dominant crack always originated at or near the specimen's surface (location) at high strain ranges (above SST) when, in fact, it has been shown that cracks initiated at most defects, both surface (location) and internal in this strain range regime. This observation will be explained by now considering the crack propagation phase of fatigue and those factors which influence it.

d. Crack Propagation

Research on fatigue crack propagation has shown that the two factors which most significantly affect crack growth are the stress level at the crack tip (Reference 108) and the environment (Reference 42). These parameters will now be considered to help explain the observations of a SST.

In this study there are limitations in our ability to quantitatively describe the crack tip stresses under elastic-plastic conditions. For this reason, the problem will be addressed first assuming LEFM, and then the analysis will be extended qualitatively to the elastic-plastic case. The stress distribution near the tip of a sharp fatigue crack in a linear elastic material can be described by the stress intensity factor, K , which has been analytically developed by Irwin (Reference 109). For many engineering materials, including nickel-base superalloys, linear elastic fracture mechanics (LEFM) can be used to approximate the stress intensity at the crack tip over a range of loading conditions even beyond local yielding by including plastic zone correction factors which account for plasticity at the crack front (References 110, 111). As an extension of this capability, the cyclic stress intensity range, ΔK , has been successfully used to correlate fatigue crack growth data in superalloys at high temperatures, but at loads well below the yield stress where the plastic zone sizes around the crack are relatively small. Figure 83 shows actual crack propagation data for the alloy AF2-1DA plotted as crack advance per cycle, (da/dn) versus K ; note the sigmoidal shape of curve which is typical of high strength nickel-base superalloys

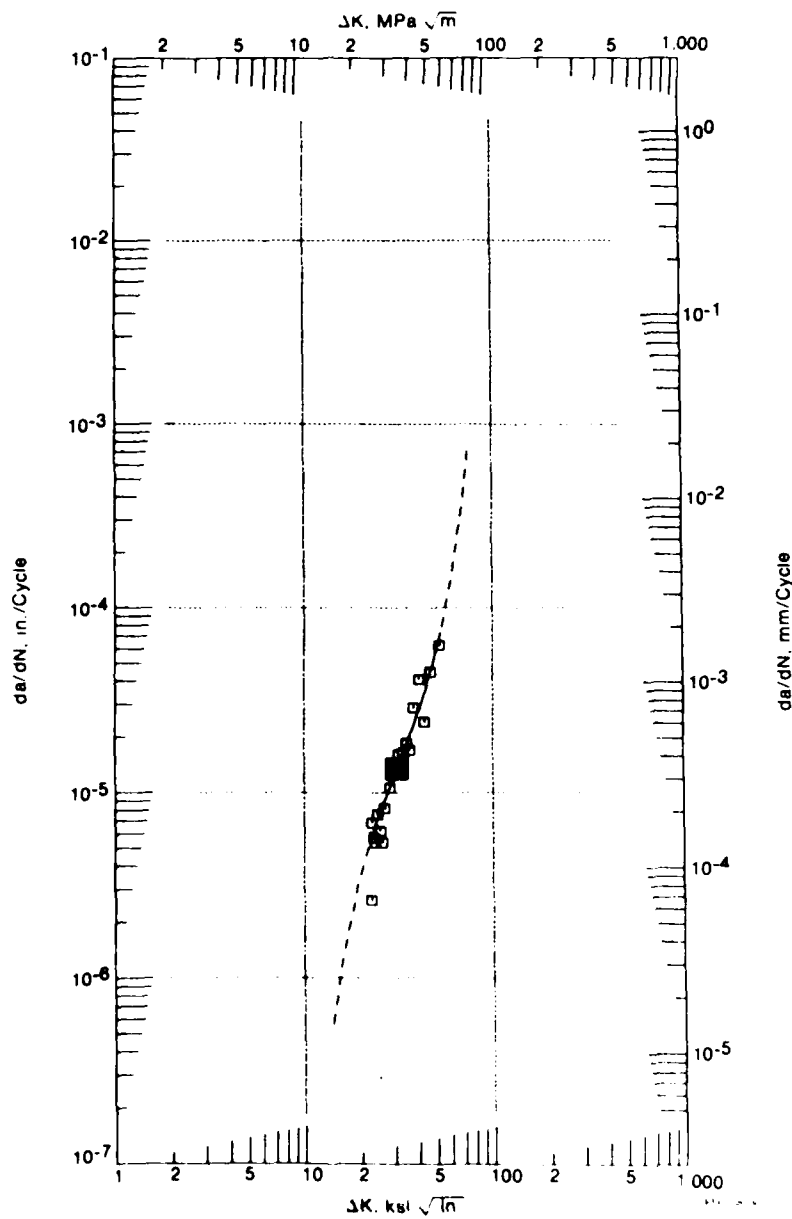


Figure 83. Crack Growth Data for AF2-1DA at 649°C, 0.17 Hz, A = 0.82 (R = 0.1) (Reference 126)

The stress intensity factor, K , is a function of crack length and component geometry, and K -calibrations have been derived for many geometries. To explain the SST behavior, it is important to compare the crack tip stresses for a surface crack with that for an internally initiated crack. First, calculations of the stress intensities for both cases have been made assuming LEFM. The solution for an internal circular crack in a round bar (Figure 84a) is shown in Appendix III to be:

$$K_I = \sigma_{\text{net}} \sqrt{\pi a} \quad (.65) \quad (3)$$

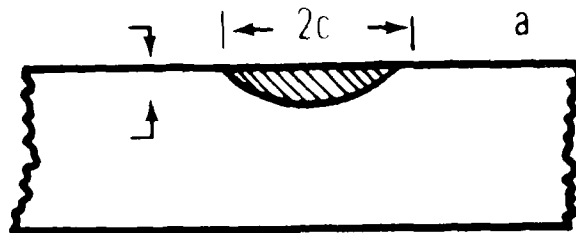
a = half the crack diameter

There is, however, no simple solution for the case of a surface crack in a round bar, but for small cracks the problem can be approximated as a surface flaw in a infinite body (Figure 84b). The solution for this problem, also described in Appendix C is:

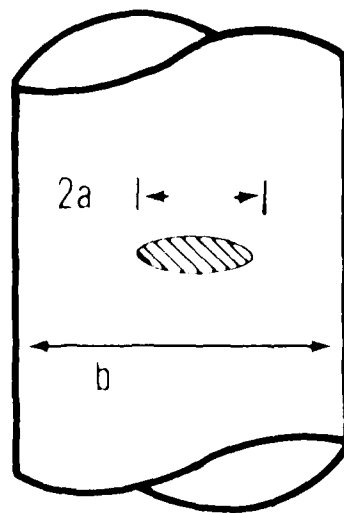
$$K_I = 1.1 \sigma \sqrt{\pi} \sqrt{\frac{a}{2.25}} \quad (4)$$

a = total crack length

Calculations for both crack geometries are also presented in Appendix C for the stress intensities at different crack lengths. The results show that the stress intensity factor for the surface crack is approximately 1.4 times greater than that for an internal crack of the same size. For example, a .010 cm deep surface crack in AF2-1DA would have a K equal to 11.9 MPa $\sqrt{\text{m}}$ (10.8 ksi $\sqrt{\text{in}}$) whereas the value for a .01 cm diameter internal crack would be only 7.4 MPa $\sqrt{\text{m}}$ (6.7 ksi $\sqrt{\text{in}}$). A surface crack half as deep, .005 cm, would still have a greater K than the .010 cm internal crack. Thus, LEFM predicts that if cracks of equal size and shape initiate at the same time, and one is located at the surface of the specimen (edge crack) and the other is located internally, then the surface crack will grow faster than the internal crack. Analytically, this result is due to the fact that a surface crack is less restrained than one internal, therefore, the effective crack length is doubled as compared to the internal crack, and the stress intensity is thus



A) SURFACE FLAW



B) INTERNAL CRACK

Figure 84. Illustration of a) An Internal Crack in Round Bar;
b) A Surface Flaw in an Infinite Body

equivalently increased by a factor of $\sqrt{2}$. It should also be noted that although there is only a 40% difference in stress intensity for the sample given above, the effect on crack growth may be many times this. This is because in the low ΔK range, near the threshold value for crack propagation, ΔK_{th} , small increases in ΔK can result in large changes in crack growth due to the steep slope of the crack growth curve (Figure 83).

The above analysis has assumed linear elastic conditions. The fatigue cycles in this study, however, included general yielding (although the plastic strain range was generally less than 25% of the total strain range), and under these conditions the quantitative results predicted by LEFM are not valid. An approach which accounts for the increased plasticity at the crack tip is the path independent J integral (References 112, 113) which has been extended to represent crack propagation behavior (References 114, 127, 128, 129). Results of this work suggest that although the quantitative results predicted by LEFM may not be directly applicable to the elastic-plastic case, the comparative relationships should still apply for differences between surface (location) and internal cracks since K is just a particular case of J analysis (Reference 127). That is, for the problem of plastic strain cycling, a surface crack will still have a greater stress intensity at the crack tip than will an internal crack of equal size and therefore the surface crack would be expected to grow faster.

Besides the crack tip stress intensity, another factor which has been shown to significantly influence crack propagation rates is the environment (Reference 42). In the literature review section, the effect of the environment on fatigue crack propagation was examined, and the review showed, in part, that an air environment at elevated temperature significantly increased the crack propagation rates for nickel-base superalloys as compared to results obtained in vacuum (Reference 42, 43). This detrimental effect on crack growth rates was attributed to the specific effect of oxidation, and the increases in crack propagation were shown to be particularly large in the small ΔK regime (Reference 45).

Considering environmental influences on surface (location) and internal cracking at elevated temperature, surface cracks would be expected to have greater crack propagation rates than would internal cracks since surface (location) cracks are exposed to oxidation, and internal cracks grow in the effective vacuum of the solid. The differences in crack propagation rates would also be expected to be greatest at low ΔK values, the regime of most concern in this study.

Having established the more significant influences on both the crack initiation and crack propagation phases of the fatigue process, the observations of a SST in failure location can now be explained. At low strain ranges, below the SST, cracks initiated only at the more acute inclusions since the plastic strain concentrations at the surface (defect) and at pre-existing pores were not greater than the threshold values needed to nucleate a stable crack. Due to their small population, however, the more acute inclusions were only located in the bulk of the specimen, below the surface and, therefore, failure resulted from a subsurface origin. At higher strain ranges above the SST, cracks initiated at most defects (pores, inclusions, surface) at a relatively small fraction of the total fatigue lives. Cracks located at or very near the specimen's surface (location), however, had greater crack growth rates than did the internal cracks due to the effect of oxidation and to the greater stress intensity associated with a surface flaw, and these cracks were first to grow to critical size. As a result, the dominant crack responsible for failure originated at or near the specimen's surface (location).

e. Review of AF-115 and AF2-1DA Data

The analysis to this point has shown that in order to successfully model fatigue behavior it is necessary to separate out the components of life due to crack initiation and crack propagation. At the higher strain ranges, initiation occurs very rapidly and the majority of life is controlled by crack propagation rates which are a function of crack

AD-A093 509

AIR FORCE WRIGHT AERONAUTICAL LABS WRIGHT-PATTERSON AFB OH F/6 11/6
THE EFFECT OF DEFECTS ON THE FATIGUE INITIATION PROCESS IN TWO --ETC(U)

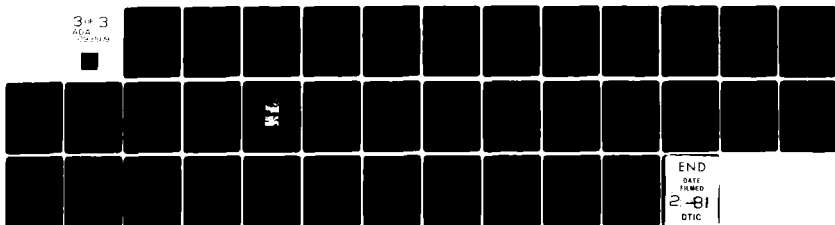
SEP 80 J M HYZAK

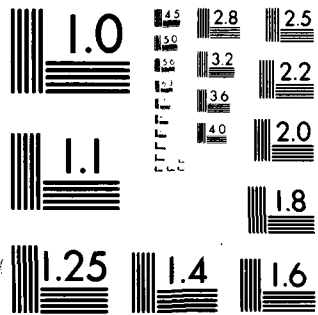
UNCLASSIFIED

AFWAL-TR-80-4063

NL

3-3
AUG
1980





MICROCOPY RESOLUTION TEST CHART

NATIONAL BUREAU OF STANDARDS-1963-A

location,* initial flaw size, and the environment. As the strain range is reduced, initiation is expected to involve a more significant fraction of the fatigue life, and as a result, defect shape, the factor which has been shown to control plastic strain concentration effects and therefore, crack initiation, should be more important.

These factors can help clarify some of the data for AF-115 and AF2-1DA. As previously described there was a significant difference in the fatigue lives for the two heats of AF-115, one with a high and one with a low defect population (Figure 48). In the high strain range regime, the low defect AF-115 tests lasted twice as long as did the baseline AF-115 alloy tests, and at the lower strain ranges this difference was increased to a factor of five. The improved fatigue properties of the AF-115-LD alloy at high strain ranges can be directly attributed to differences in crack propagation lives since initiation occurs very rapidly in this strain range region. Since both materials had similar strength levels, it is assumed that the crack propagation properties, (da/dn) vs ΔK , were nearly equal for both heats of material, and, therefore, the differences in fatigue lives can be attributed to the differences in size of the initial flaws. In the original heat of AF-115, which had a large population of pre-existing pores, the length of a newly initiated crack would be on the order of a pore diameter (70-100 μm), whereas the embryonic surface cracks in the AF-115-LD alloy, which were not associated with any large identifiable defect, would presumably be much smaller. Since the driving force for crack propagation, the crack tip stress intensity, increases with crack length for this type of loading, the smaller crack would take considerably longer to grow to failure. In fact, at high strain ranges, the difference in life of the two heats of AF-115, which was approximately 900 cycles at a total strain range of $1.1\% \Delta\epsilon_t$, can theoretically be equated to the number of cycles it takes a small surface crack in the AF-115-LD material to grow to be the size of a pore in AF-115.

*Defect location can be related statistically to the defect population.

At lower strain ranges, since the metallic and nonmetallic inclusions which caused failure were of generally the same size, the differences in life can be mostly attributed to the differences in crack initiation time; recall also, that initiation comprises a larger fraction of the total life in this region than at high strain ranges. Specifically, the increase in life of the AF-115-LD alloy was due to the greater number of fatigue cycles needed to initiate a crack from a nonmetallic inclusion as compared to nucleating a crack from a more acute HfO_2 inclusion in AF-115 since the plastic strain concentration at the nonmetallic inclusion was not as great as at the HfO_2 inclusion.

The difference in the strain concentration effects of the HfO_2 inclusions and the tramp nonmetallic inclusions was illustrated by the variation in initiation mode associated with these two defects. The cracks from HfO_2 inclusions initiated in a Stage II mode, whereas the cracks from the less acute nonmetallic inclusions originated first in a Stage I mode and after growth of approximately one grain diameter, these cracks changed to Stage II propagation. Stage II cracking is generally associated with a greater stress intensity at the crack tip than is Stage I cracking (Reference 6).

The same general explanation applies to the comparison of the AF2-1DA fatigue properties with those of the high porosity AF-115 alloy. The fatigue lives of the AF-115 alloy would be expected to be greater than those for AF2-1DA because AF-115 had a significantly higher yield stress and, therefore, the plastic strain levels were less than for AF2-1DA at a given total strain range. The data in Figure 48 show, however, that in the high strain range regime the two alloys had comparable fatigue lives, and in the lower strain range region the AF2-1DA tests lasted longer than the AF-115 tests. The lower than expected fatigue properties for the AF-115 alloy can be attributed to its high defect content in the same ways as above; in the high strain ranges the large pore size shortened the crack propagation lives, and in the longer life regime the acute HfO_2 inclusions accelerated crack initiation.

In summation, these results have shown that defects detrimentally affect the fatigue behavior of high strength P/M superalloys. Differences in fatigue lives between different alloy heats are directly relatable to differences in their defect population and to the specific characteristics of the defects which can affect different phases of the fatigue process. At high strain ranges, most defects were capable of initiating cracks, but the location and size of the defects determined the subsequent crack growth rate which in turn controlled most of the life. Cracks that initiated at defects that were larger in size and were located close to the specimen's surface had greater stress intensities, and led to shorter fatigue lives. At low strain ranges, however, the shape of the inclusions was found to be the most important characteristic since the shape determined the relative magnitude of the localized strain concentration at the defect, the factor ultimately responsible for crack initiation. In this regime, the initiation phase of fatigue was particularly significant since it is believed to account for a larger fraction of the fatigue life than at higher strain ranges, and more importantly because it determined if indeed fatigue cracking would occur. It has been shown that conditions existed where crack initiation from particular defects did not take place since the strain concentrations were below the critical value required for nucleation.

It should be noted that although the defect shape was found to be of critical importance at the lower strain ranges, the size and location of the defects must also be considered in any subsequent analysis. As discussed above, these two factors influence the crack propagation phase of fatigue which can still be a significant portion of the total life.

Since this analysis has been based on the general principles of strain localization and stress intensity, these same general patterns would be expected to apply to other alloy systems. The particular regions of the fatigue curve that would be affected by specific defects, however, would probably change. Factors such as the defect concentration, defect character, microstructure, environment, slip character, and the constitutive behavior of the alloy would all bear on the final

initiation character. The constitutive behavior would be particularly important, since it would largely determine the propensity for strain localization in a given alloy.

3. EFFECT OF TEMPERATURE ON INITIATION MECHANISMS

The second major observation of this investigation was that the mechanism of room temperature crack initiation differs significantly from that at elevated temperature. It was observed that for both alloys at room temperature cracks initiated in a Stage I fashion along planar slip bands, which in turn originated at the surface or at near surface pores. Initiation occurred in this fashion at all the strain ranges tested, to values as low as $0.44\% \Delta \epsilon_t$. In contrast to this behavior, elevated temperature crack initiation generally occurred in a Stage II mode, with an associated surface-subsurface transition in the location of the dominant fatigue origin. From the results of the metallographic observations and the thin foil microscopy, it appears that the differences in initiation mode at room and elevated temperatures are related to the differences in slip behavior of these alloys in the different temperature regimes. This hypothesis will be investigated for the AF2-1DA alloy since thin foil analysis was not accomplished for the AF-115 material. In this section, the predominant initiation mechanisms in each temperature regime will be reviewed and then will be related to the observed slip behavior.

Room temperature crack initiation occurred in a Stage I mode along intense planar slip bands. In several instances, cracking was shown to be concentrated in parallel bands oriented at a 45° angle with respect to the tensile axis, and in fact, cutting of the γ' precipitates was observed in the slip bands that initiated cracks. The intense planar nature of the deformation was particularly apparent from the optical microscopy observations of etched slip bands found throughout the gauge section of the high strain test (Figure 64).

These observations were consistent with the results of the thin foil study. In general, the deformation at room temperature was planar and very heterogeneous. Even at low strain ranges ($0.60\% \Delta\epsilon_t$), intense planar deformation was observed in areas adjacent to strain concentrators such as MC carbides. Many examples of intensive shearing along $\{111\}$ slip planes in the γ' precipitates were found through the specimens.

The propensity for Stage I slip at room temperature can, therefore, be related to the heterogeneous nature of the planar slip in this room temperature regime. The intense localization of such deformation into slip bands for alloys with ordered precipitates has been attributed in the literature to localized softening of the slip band due to shear of the ordered precipitate. The subject has been addressed in detail by Laird and Calabrese (References 115, 116, 117) and Stoltz and Pineau (Reference 118). The proposed progression of events in this process was basically the same in each treatment. In the case of sheared precipitates, there is localized strain softening in the slip band which, in turn, promotes additional deformation in the same band. This results in intensive strain localization and subsequent crack nucleation along the slip trace. The original softening of the slip band was attributed to mechanical disordering of the precipitates which made subsequent shearing easier.

This explanation for the intense planar nature of the slip at room temperature is supported by the constitutive behavior of AF2-1DA at room and elevated temperature, as observed in this investigation. Although not previously discussed, the AF2-1DA test specimens cyclically softened an appreciable amount during the fatigue life at room temperature, whereas at elevated temperature the cyclic softening was nominal. For example, at room temperature and at a cyclic strain range of $0.6\% \Delta\epsilon_t$, the load range of the AF2-1DA test decreased over 6.5%; at elevated temperature, however, the maximum change in stress range was less than 1% over its entire life. Therefore, it appears that the heterogeneous concentration of deformation in planar bands can be attributed to the

cyclic softening of the slip bands, and as a result, deformation even in the low strain ranges was concentrated enough to cause Stage I surface cracking.

At elevated temperature, however, deformation was generally more wavy and more homogeneous than at room temperature, particularly at the higher strain ranges. In the lower strain range regime, although the average dislocation density was small, there were several thin foil observations of dislocation banding, and in many of these cases those dislocation bands were seen in the vicinity of MC carbides. It was also observed that the deformation was concentrated mostly in the γ phase and seemed to avoid the larger γ' precipitates. The reason for the deformation to be observed mostly in the matrix phase at elevated temperature has already been discussed, and is probably due to the fact that the resistance to dislocation motion is greatest at the γ - γ' interface, and once dislocations pass into the γ' precipitates they travel quickly through the particle.

This more wavy and homogeneous type of deformation at elevated temperature was associated with Stage II crack initiation in the higher strain range regime. As previously noted, this mode of initiation occurred at the specimen's surface, and limited observations of the Stage II cracking morphology in both alloys showed that the Stage II cracks propagated mainly in the γ matrix phase with little shearing of the larger precipitates. The mechanism for Stage II initiation is still, however, uncertain. It could possibly be the result of environmental interactions at the specimen's surface which cause the crack tip to sharpen, or it may be a result of the wavy slip behavior of the superalloys at elevated temperature. It is apparent, though, that Stage I initiation was retarded in this temperature regime, and that the more classical initiation mechanisms associated with wavy slip behavior were also not observed. As has been discussed, Laird and Duquette (Reference 106) in their review of the mechanisms of crack initiation stated that nucleation in wavy slip materials generally occurs by the formation of extrusions and intrusions, as a result of the development of persistent slip bands. However, nickel-base superalloys do not develop persistent

slip bands due to their high volume fraction of γ' precipitates (Reference 2). So, although the mechanism of Stage II initiation cannot be specifically defined at this time, it certainly appears to be different from the Stage I mechanism observed at room temperature and from the more classical mechanisms proposed in the literature.

In summary, the differences in initiation mechanism at room and elevated temperatures can be attributed to differences in slip behavior. At room temperature, the deformation was planar and very heterogeneous with shear cracking occurring in intense planar bands in a Stage I mode. The concentration of deformation in planar bands was attributed to cyclic softening of the shear bands, and the intensity of this deformation, even at low strain ranges, resulted in surface initiation below the elevated temperature SST.

At higher temperatures, the deformation was much more wavy than at room temperature and at the high strain ranges the deformation was homogeneous which may have contributed to the State II initiation. In the lower strain range regime (below SST), the total dislocation density was relatively small, but localized banding of dislocations near large defects, such as inclusions, promoted Stage I crack initiation from subsurface inclusions.

4. CREEP-FATIGUE INTERACTION

In Section IX it was shown that specimens tested with a tensile dwell cycle at 760°C exhibited creep-fatigue damage that was characterized by internal cracking at defects and along grain boundaries normal to the tensile axis. Compressive dwell specimens, however, showed no creep damage and failed in the same manner as the creep-free continuously cycling tests. It was also observed that compressive dwell tests lasted fewer cycles than did the tensile dwell tests at the same total strain range. It has been hypothesized that this behavior is a result of the large mean stresses that developed in the cyclic dwell tests, such that although the tensile dwell cycle is more damaging, the rate of damage

accumulation in the compressive dwell tests was greater due to the larger maximum tensile stress value. This theory will be further developed in this section.

It was previously explained that there was a large shift in the position of the hysteresis loops relative to the tensile stress axis for the 760°C strain dwell tests, and this appears to have had a significant effect on the fatigue life. Since these tests were strain controlled, the strain was held constant during the dwell period, and the stress was allowed to relax. Due to the stress relaxation, the hysteresis loops developed a bias in the opposite direction to the dwell so that the tensile dwell tests developed a compressive mean stress and the compressive dwell tests developed a tensile mean stress. This behavior has been illustrated in Figure 63. The major significance of this stress shift is that the values of the maximum tensile stress associated with these tests were also altered accordingly, so that a tensile dwell test had a significantly lower tensile stress than did the corresponding compressive dwell test at the same total strain range. (See data in Appendix B).

We know that resultant crack growth rates are a function of the stress intensity range, ΔK or ΔJ , which, in turn, are a function of the load range. It had also been shown in the literature that in both the elastic and the elastic-plastic cases the load range over which the crack is open defines the effective ΔK or ΔJ value, and as a first approximation, the crack is only open during the tensile portion of loading (References 120, 121). As a result of this, the effective driving force for crack propagation in a dwell test is proportional to the maximum tensile stress. From this result, cracks in compressive dwell tests would grow faster than would cracks in tensile dwell tests because of their higher effective tensile stress. Also, due to their greater value of maximum tensile stress, compressive dwell tests would fail at smaller crack sizes than would tensile dwell tests fatigued at the same total strain range (Reference 113). So although cracks in tensile dwell tests performed at 760°C would be expected to initiate more rapidly and in greater number than cracks in compressive dwell tests due to the

extensive creep-fatigue cracking associated with a tensile hold cycle, the compressive dwell tests failed first as a result of faster crack propagation rates and failure at smaller critical crack sizes. This result not only explains the data contained in Figures 19 and 20, but it also emphasizes the fact that in order to most effectively analyze LCF data, the initiation and propagation phases of life must be considered independently.

Two AF2-1DA cyclic dwell tests were also performed at a lower temperature of 649°C, and their behavior is also shown in the graph in Figure 21. Although, at first, these two tests do not appear to behave in the same fashion as the tests at 760°C since the compressive dwell test lasted longer than the tensile dwell test, these results are consistent with the explanation of life based on maximum tensile stresses; at this temperature, however, the tensile dwell test did not develop as large a stress bias as at 760°C, and therefore its life was shortened. The dependence of the fatigue lives on the maximum tensile stress for tests at both 760°C and 649°C will be illustrated in the following figure.

To better illustrate the effect of dwell periods on the crack initiation phase of the fatigue life, the data in Figures 19 and 21 have been replotted in Figures 85 and 86 as maximum tensile stress versus cycles to failure. Comparing the tests at the same value of maximum tensile stress has the effect of eliminating much of the difference in life due to crack propagation. Figures 85 and 86 show the data plotted in this manner along with the best fit lines for the 760°C and 649°C continuously cycling tests at 20 cpm; at this frequency the occurrence of creep damage was suppressed. When presented in this form the data are more easily understood; the graphs show that at a fixed temperature the fatigue lives decreased as the tensile dwell period increased, and, therefore, exposure to creep damage is shown to reduce the fatigue life, as expected. It can also be seen in Figure 85 that the five minute tensile dwell test at 649°C had a shorter life than the 20 cpm creep-free tests, but that the reduction in life was small compared to that of the five minute tensile dwell test at 760°C. This result, of course, would be expected since creep is a thermally activated process, and

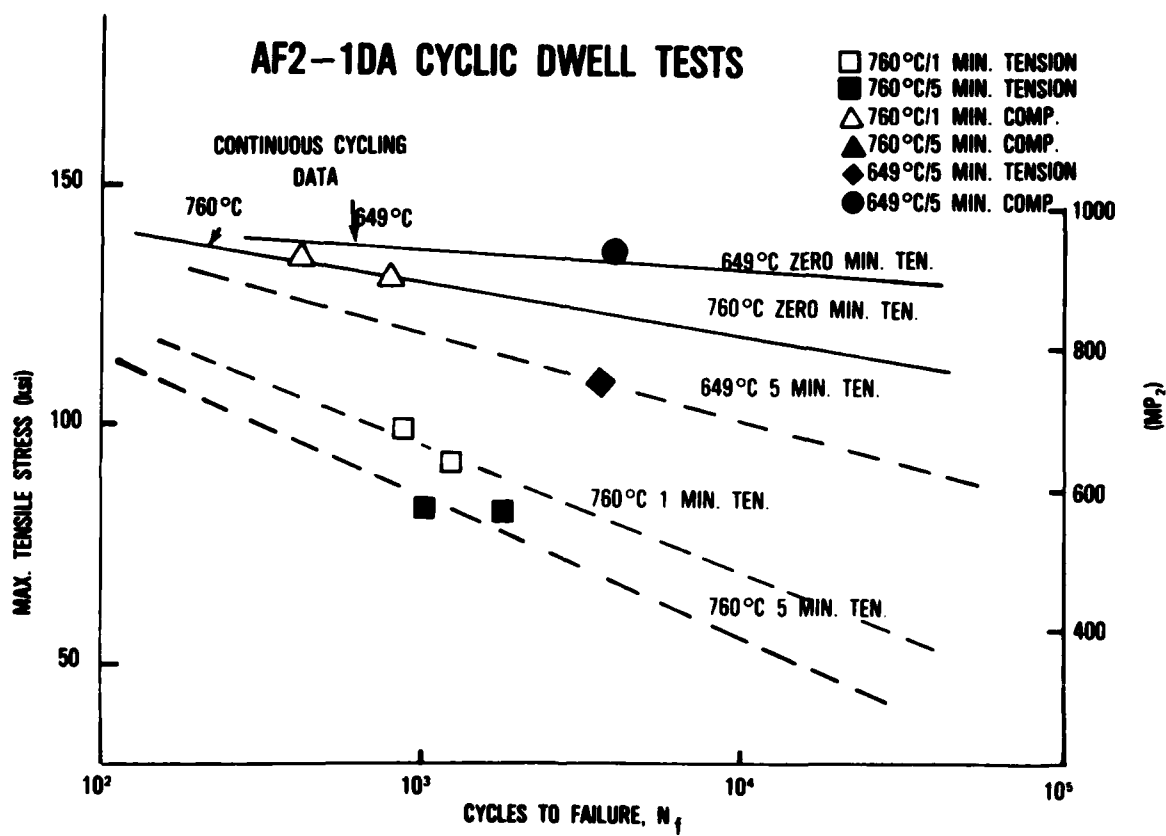


Figure 85. AF2-1DA Cyclic Dwell Data Plotted as Maximum Tensile Stress Versus Cycles to Failure

AF-115 CYCLIC DWELL TESTS

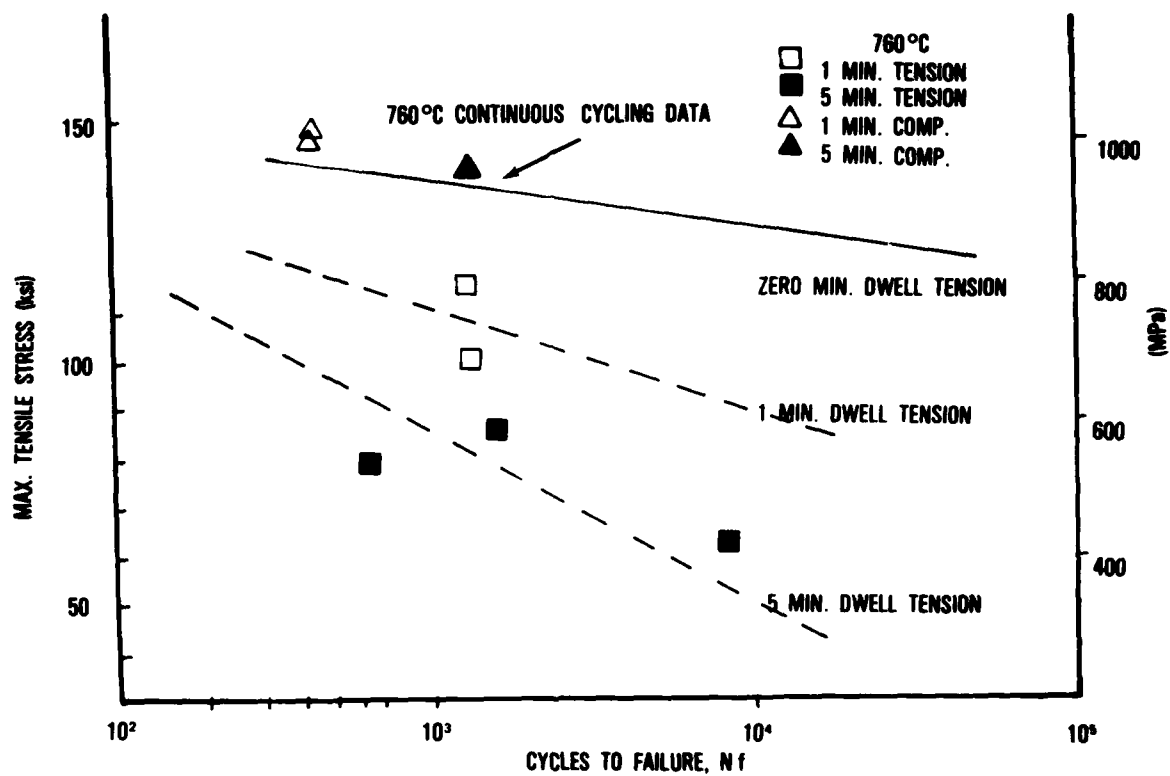


Figure 86. AF-115 Cyclic Dwell Data Plotted as Maximum Tensile Stress Versus Cycles to Failure

therefore creep effects should be greater at a higher temperature. In Figures 85 and 86, the dashed lines have been drawn through the limited tensile dwell data to suggest trends that have been observed in a similar study by Hyzak and Bernstein (Reference 80). It is important to note that the compressive dwell data fall along the 20 cpm creep-free fatigue lives for the respective temperatures. This indicates that compressive dwell tests incurred no creep damage during the tests. This result agrees with the fractographic observations which showed that the initiation mechanisms for the compressive dwell tests were the same as for the continuously cycling tests.

In summary, there was a significant creep-fatigue interaction observed at elevated temperature in both alloys for tensile dwell cycles, and there was no evidence of creep damage found in the compressive dwell test specimens. When the fatigue lives were compared at equal maximum tensile stress, tensile dwell tests had significantly shorter fatigue life than compressive hold test, and the lives of the tensile dwell tests decreased with increasing temperature and dwell period. These data are in agreement with the metallographic observations previously described in Section VI. Test specimens fatigued under a tensile dwell cycle exhibited a considerable amount of intergranular creep-type cracking in the interior of the specimen; cracks initiated both at defects and along grain boundaries normal to the tensile axis. The failure process for the tensile dwell tests was proposed to involve the link-up of surface initiated cracks with the internal creep cracks. Specimens fatigued under a compressive dwell cycle exhibited no intergranular cracking and cracks initiated in the same mode as for continuously cycling tests.

When the cyclic dwell data were compared instead as a function of total strain range rather than maximum tensile stress, the tensile dwell tests had larger lives than the compressive hold tests. This anomaly was resolved and attributed to significant mean stresses which developed in these tests.

SECTION XIII

SUMMARY

Microstructural defects have been previously shown to significantly affect fatigue crack initiation, but there have been few experimental studies performed to systematically determine the relative influences of defect size, shape, and population. It was, therefore, the purpose of this investigation to examine the effect of such defect characteristics on the crack initiation and early crack growth processes for two high strength P/M nickel-base superalloys. These alloys were tested over a range of temperatures and strain ranges to study the effect of defects in regimes where the deformation behavior differed. Cyclic dwell tests were also performed to investigate possible creep-fatigue interactions at elevated temperatures. Both scanning and transmission electron microscopy were utilized to determine the origins of the fatigue cracks that caused failure (dominant crack) in each specimen, and observations were also made of the secondary cracks that initiated independently in each specimen, but did not cause the ultimate failure. TEM thin foil analysis was also employed to observe the deformation behavior of one of the alloys both at room and elevated temperatures.

The P/M superalloys that were studied in this program were AF-115 and AF2-1DA. These alloys had the contrasting defect populations essential to the purpose of the study. The AF-115 alloy contained a large population of pores (20-100 μm), and a lesser number of hafnium oxide and tramp nonmetallic (ceramic) inclusions which ranged in size up to 120 μm in length. The AF2-1DA material contained appreciably no pores or hafnium oxide inclusions, but did have a similar population of tramp inclusions as the AF-115. A limited number of tests were also performed on specimens from another heat of AF-115, identified as AF-115-LD. This heat of alloy also contained only tramp nonmetallic defects.

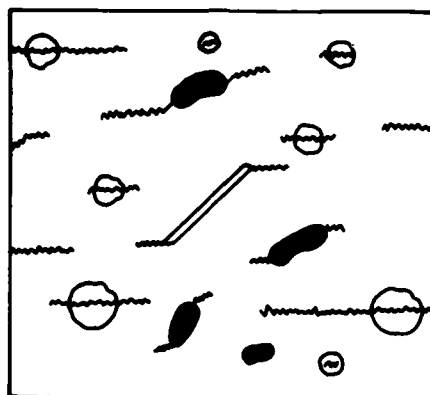
At elevated temperature (649°C, 760°C) where the majority of the testing was performed, there was a transition in the origin of the crack that caused failure from a surface or near-surface site to a location

well below the specimen's surface; this surface-subsurface transition was termed the SST. The SST occurred at approximately the same strain range for AF-115 and AF2-1DA. For AF-115 above the SST strain range, in the high strain range regime, the dominant crack initiated in a Stage II mode from a near-surface pre-existing defect, predominantly pores. In the lower strain range regime, the cracks initiated well below the specimen's surface at the more acutely shaped hafnium oxide inclusions. For AF2-1DA, at high strain ranges, initiation occurred at the specimen's surface in Stage II mode; the origins of the dominant cracks were usually too small to identify but were believed to be submicron size inclusions and carbides. Below the SST, the dominant cracks in AF2-1DA originated at tramp nonmetallic inclusions in the interior of the specimens.

In addition to the dominant cracks which were responsible for specimen failure, many secondary cracks were also observed on polished and etched cross-sections of failed specimens. For both alloys at high strain ranges, secondary cracking occurred both at the surface and at subsurface locations which were generally either HfO_2 or nonmetallic inclusions. Below the SST strain range, there were no surface initiated cracks, and very few cracks in the interior of the specimen; these latter cracks were invariably initiated at the more acutely shaped inclusions. In summary, at high strain ranges cracking occurred both at the surface and in the interior of the specimen, although the crack that caused failure always originated at or very near the surface. In the low strain range regime, both the dominant and secondary cracks only initiated in the specimen's interior.

In explaining the SST behavior, it was necessary to separate the fatigue process into two phases: crack initiation and early growth, and crack propagation in the plastic strain field to failure. The former is believed to be controlled by plastic strain concentrations, and the latter by the stress intensity at the fatigue crack tip. Based upon this approach to the problem, a summary of the process responsible for the SST is illustrated in Figure 87. In the high strain range regime, above the SST strain range, crack initiation occurred easily at most surface and subsurface defects, at a small fraction of the specimen's

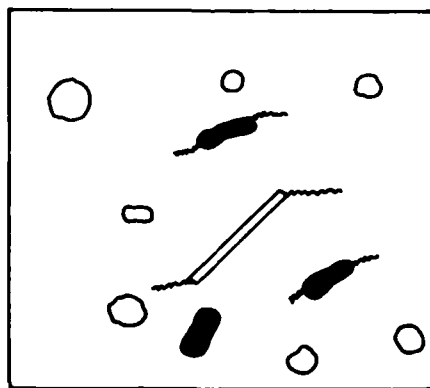
INITIATION TRANSITION



HIGH STRAIN RANGE

INITIATION AT MOST DEFECTS
PROPAGATION DETERMINES LIFE

— DEFECT SIZE, LOCATION
MOST IMPORTANT



LOW STRAIN RANGE

INITIATION CRITICAL EVENT

— DEFECT SHAPE MOST IMPORTANT

Figure 87. Summary Illustration of the Fatigue Processes for both Superalloys Above and Below the SST

total life. As a result, crack propagation controlled the major portion of the fatigue life in the regime. It was explained that surface cracks promoted failure in these cases because surface cracks propagated more rapidly than subsurface cracks of the same size. This was due to the influence of the oxidizing atmosphere at the specimen's surface, and also because surface cracks have a greater stress intensity than do internal cracks. Since crack propagation was the more critical phase of the fatigue process in this strain range regime, defect size and defect location relative to the specimen's surface were considered the most important defect characteristics, because both directly influenced the level of the stress intensity at the crack tip. Defect location, of course, can be related to the relative population, of the defect, i.e., pores were the origins of the dominant cracks in AF-115 not because they were more detrimental than inclusions but because they were more populous and, therefore, they had a greater probability of lying near the surface.

In the lower strain range regime, the plastic strain concentrations at pores in AF-115, and at small surface defects in AF2-1DA were not great enough to initiate cracks at these defects, as had been possible at the higher strain ranges. As a result, initiation only occurred at the more acutely shaped inclusions which had greater strain concentration effects; due to their small population these defects were most often located in the interior of the specimens. Since, in this case, crack initiation was more critical in determining the dominant fatigue origin, defect shape, which determined the magnitude of the localized plastic strain, was considered the most important defect characteristic.

Fatigue tests were also performed at room temperature where the deformation behavior was considerably different than at elevated temperature. The slip at room temperature was planar and very heterogeneous, while at higher temperature the deformation was wavy and more homogeneously distributed. This important difference is shown in Figure 88. The planar nature of the slip at room temperature resulted in Stage I crystallographic crack initiation at the specimen's surface

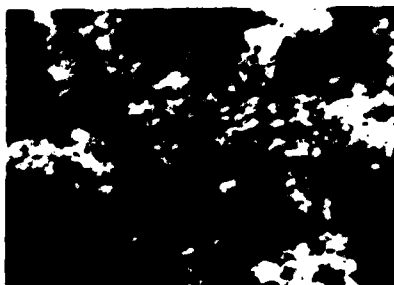
AF2—1DA SLIP BEHAVIOR

ROOM
TEMPERATURE



PLANAR
HETEROGENEOUS

ELEVATED
TEMPERATURE



WAVY
HOMOGENEOUS

Figure 88. Change in Slip Behavior with Temperature a) Planar Slip at Room Temperature; b) Wavy Slip at Elevated Temperature

in AF2-1DA, and at near-surface pores in AF-115. These modes of crack initiation were observed at all the strain ranges tested. The reason that an SST was not observed at room temperature was due to the heterogeneous planar nature of the deformation and, as a result, the strain concentration in localized areas even at the low strain ranges was still great enough to cause failure from the less acute defects at the specimen's surface.

Finally, a number of cyclic dwell tests were performed at elevated temperatures to determine the nature and the magnitude of a creep-fatigue interaction in both alloys. There was a significant creep-fatigue interaction observed in both alloys for tensile dwell cycles, and there was no evidence of creep damage found in the compressive dwell test specimens. When the fatigue lives were compared at equal maximum tensile stress, tensile dwell tests had significantly shorter fatigue life than compressive hold tests, and the lives of the tensile dwell tests decreased with increasing temperature and dwell period. These data are in agreement with the metallographic observations previously described in Section IX. Test specimens fatigued under a tensile dwell cycle exhibited a considerable amount of intergranular creep-type cracking in the interior of the specimen; cracks initiation both at defects and along grain boundaries normal to the tensile axis. The failure process for the tensile dwell tests was proposed to involve the link-up of surface initiated cracks with the internal creep cracks. This process is depicted schematically in Figure 89. Specimens fatigued under a compressive dwell cycle exhibited no intergranular cracking and cracks initiated in the same mode as for continuously cycling tests.

When the cyclic dwell data were compared as a function of total strain range rather than maximum tensile stress, the tensile dwell tests had longer lives than the compressive hold tests. This was attributed to significant mean stresses which developed in these tests.

The fatigue initiation processes of two high strength nickel-base superalloys have been studied, and they have been shown to be dependent

FAILURE PROCESS — TENSILE DWELL TEST

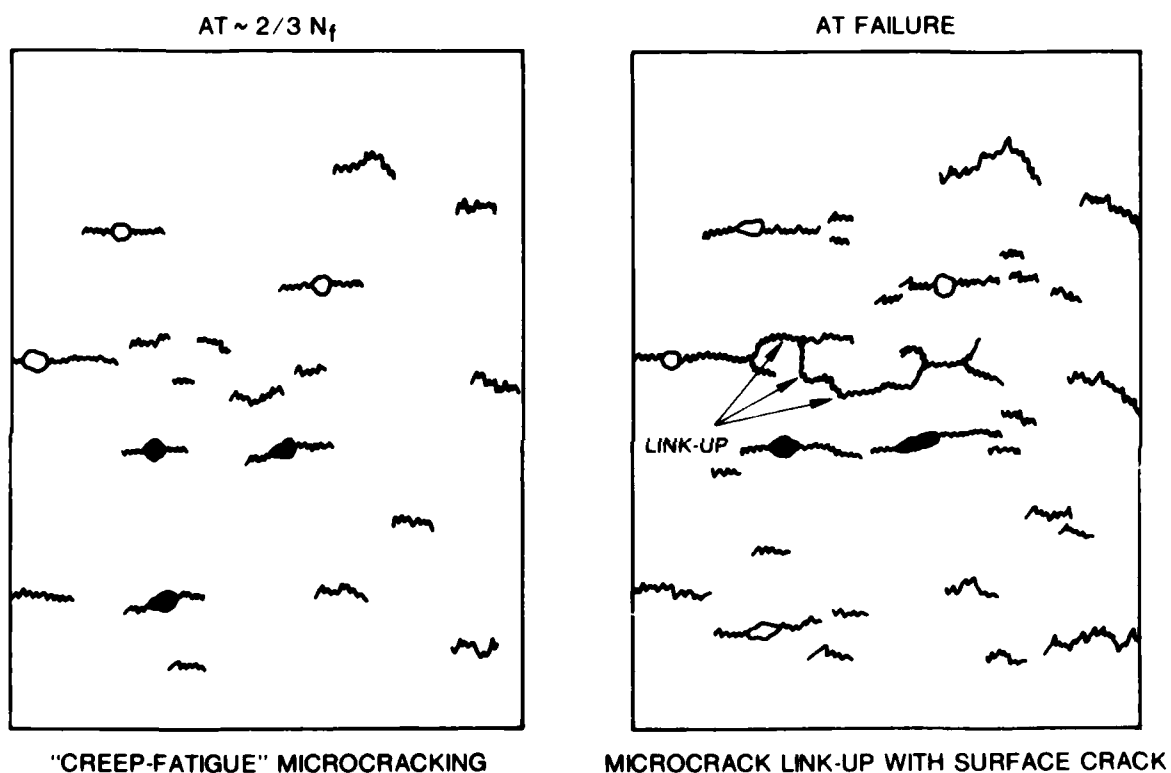


Figure 89. Schematic Illustration of the Failure Process in Tensile Dwell Tests, Microcrack Initiation and Link-Up

AFWAL-TR-80-4063

on the slip behavior, the environment, and the defect concentration. In particular, the size, shape, and population of pre-existing defects have been shown to influence the crack nucleation and crack propagation phases of fatigue in different ways.

SECTION XIV

SUGGESTIONS FOR FUTURE WORK

The following areas are proposed as extensions of research related to this thesis:

1. The present work has shown that there was an SST in the origin of the crack that caused failure for high strength P/M superalloys. The research has also shown that this was due in large part to the relative strain concentration effects of differently shaped defects. The results, however, only included tests that lasted less than 50,000 cycles. It would therefore be of interest to extend these results farther into the high cycle fatigue region. In this regard it would be important to determine if the alloy would have an endurance limit when cracking no longer occurred at inclusions, or if another mechanism, perhaps environmentally assisted at the surface would then control initiation.

2. It is believed that the conclusions drawn from this study concerning the effects of defect size, shape, and population on the fatigue nucleation process are general in nature; that is, these same relationships should apply to other systems. In order to test this premise, the fatigue initiation processes in several other alloys need to be studied. The work should include other engineering systems such as the aluminum alloys, titanium alloys, and steels. The program should also cover both P/M alloys, and more conventional cast and wrought alloys.

3. The mode of fatigue crack initiation at elevated temperature for both AF2-1DA and AF-115 was described as being Stage II, noncrystallographic. As previously mentioned, this mechanism of crack nucleation is not usually observed for structural alloys. It was also described that at elevated temperature, the deformation behavior of the superalloys was wavy and generally homogeneous. It would be valuable to determine what the mechanism of Stage II initiation is in this case, and how it is

AFWAL-TR-80-4063

related to the deformation behavior of the alloys at high temperatures. It is also possible, however, that surface oxidation plays the major role in Stage II initiation, and this should be determined.

4. With the large volume of data available relating to the SST and to secondary cracking, an analytical program should be undertaken to try to predict these results. This would also serve as a check on the theories presented herein.

REFERENCES

1. M. Gell and G. R. Leverant, Fatigue at Elevated Temperature, ASTM STP 520, 1973.
2. J. C. Grosskreutz, Metal Fatigue Damage, S. S. Manson, ed., ASTM STP 495, 1971.
3. F. de Kazinczy, JISI, 207, 1970, p. 851.
4. L. F. Coffin, Jr., Fatigue at Elevated Temperature, ASTM STP 520, 1973, p. 5.
5. 1976 ASME MPC Symposium on Creep-Fatigue Interactions, R. M. Curran, ed., MPC-3, ASME, New York, 1976.
6. C. H. Wells, C. P. Sullivan, and M. Gell, Metal Fatigue Damage, S. S. Manson, ed., ASTM STP 495, 1971.
7. C. Laird, Fatigue Crack Propagation, ASTM 415, American Society for Testing and Materials, 1967, p. 131.
8. P. Neumann, H. Vehoff, and H. Fuhlrott, Fracture 1977, Proc. 4th International Conference on Fracture, 2, Waterloo, Canada, 1977, 1313.
9. R. F. Decker and C. T. Sims, The Superalloys, C. T. Sims and W. C. Hagel, eds., Wiley & Sons, 1972, p. 52.
10. C. H. Wells and C. P. Sullivan, Trans. ASM., 58, 1967, p. 391.
11. C. H. Wells and C. P. Sullivan, Trans. ASM., 60, 1967, p. 217.
12. C. H. Wells and C. P. Sullivan, Trans. ASM., 61, 1968, p. 149.
13. G. P. Sabol, T. F. Hengstenberg, D. M. Moon, Electron Microscopy and Structure of Materials, Univ. Calif. Press, Berkeley, 1972, p. 753.
14. F. E. Organ and M. Gell, Met. Trans., 2, 1971, p. 943.
15. G. R. Leverant and M. Gell, Met. Trans., 6A, 1975, p. 367.
16. M. Gell and G. R. Leverant, Trans. AIME, 242, 1968, p. 1869.
17. M. Gell and G. R. Leverant, Ordered Alloys, Proc. Third Bolton Landing Conf., Claiborne's Publishing Div., Baton Rouge, 1970.
18. G. R. Leverant, M. Gell, and S. W. Hopkins, Mater. Sci. Eng., 8, 1971, p. 125.

REFERENCES (Continued)

19. G. R. Leverant, M. Gell, and S. W. Hopkins, Proc. 2nd International Conf. Strength of Metals and Alloys, ASM, Metals Park, 1970, 3, p. 1141.
20. J. M. Oblak and B. H. Kear, Electron Microscopy and Structure of Materials, Univ. of Calif. Press, Berkeley, 1972, p. 566.
21. B. H. Kear, A. F. Giamei, G. R. Leverant, and J. M. Oblak, Scripta Met., 3, 1969, p. 123.
22. B. H. Kear, A. F. Giamei, G. R. Leverant, and J. M. Oblak, Scripta Met., 3, 1969, p. 445.
23. S. M. Copley and B. H. Kear, Trans. AIME, 239, 1967, p. 977.
24. P. H. Thornton, R. G. Davies, and T. L. Johnston, Met. Trans., 1, 1970, p. 207.
25. C. H. Wells, Acta. Met., 17, 1969, p. 443.
26. M. Gell and G. R. Leverant, Fracture, Second International Conf. Fracture, Brighton, P. L. Pratt, ed., 1969, p. 565.
27. M. Gell and G. R. Leverant, Trans. TMS-AIME, 242, 1968, p. 1869.
28. D. J. Duquette, M. Gell, and J. W. Piteo, Met. Trans., 1, 1970, p. 3107.
29. M. B. McNeil and J. C. Grosskreutz, Phil. Mag., 16, 1968, p. 115.
30. D. H. Avery and W. A. Backofen, Fracture of Solids, Interscience, New York, 1962, p. 339.
31. J. C. Williams, A. W. Thompson, and R. G. Baggerly, Scripta Met., 8, 1974, p. 625.
32. D. J. White, Proc. Institute of Mech. Eng. Applied Mech. Group, 184, 1969-1970, p. 223.
33. M. R. Archter, Fatigue Crack Propagation, ASTM STP 415, 1967, p. 181.
34. L. F. Coffin, Jr., Met. Trans., 2, 1971, p. 3105.
35. L. F. Coffin, Jr., Trans. ASM, 56, 1963, p. 339.
36. L. F. Coffin, Jr., International Conf. on Corrosion Fatigue, 1971, Storrs, Conn.
37. G. F. Paskiet, D. H. Boone, and C. P. Sullivan, J. Inst. Metals, 100, 1972, p. 58.
38. F. E. Fujita, Fracture of Solids, Interscience Publ., New York, 1963, p. 657.

REFERENCES (Continued)

39. G. J. Danek, Jr., H. H. Smith, and M. R. Achter, Proc. ASTM, 61, 1961, p. 775.
40. M. R. Achter, Proc. Inst. Environ. Sci., 1963, p. 385.
41. M. Gell and D. J. Duquette, Corrosion Fatigue, NACE, 2, 1972, p. 366.
42. M. O. Speidel, High Temperature Materials in Gas Turbines, Sahm and Speidel, eds., Elsevier Scientific Publishers, New York, 1974, p. 207.
43. R. B. Scarlin, Fracture 77, 2, Pergamon Press, New York, 1977, p. 849.
44. W. J. Mills and L. A. James, J. Engr. Matls. and Tech., Trans. ASME, 101, 1979, p. 205.
45. L. A. James and R. L. Knecht, Met. Trans., 6A, 1975, p. 109.
46. J. S. Hirschhorn, Introduction to Powder Metallurgy, American Powder Metallurgy Institute, 1969.
47. A. E. Kravic, SAE Paper 690236, International Eng. Congress, Detroit, 1969.
48. G. Bockstiegel and C. A. Blande, Powder Met. International, 8, 1976, p. 155.
49. S. H. Williams and R. Haynes, Powder Met., 16, 1973, p. 387.
50. R. Haynes, Powder Met., 13, 1970, p. 465.
51. V. Gallina and G. Mannone, Powder Met., 11, 1968, p. 73.
52. D. Eylon and N. Birla, Met. Trans. A, 8A, 1977, p. 367.
53. S. Bashir, P. Taupin, and S. D. Antolovich, "Low Cycle Fatigue of As-HIP and HIP+ Forged Rene 95," Met. Trans., In Press.
54. J. C. Grosskreutz and G. G. Shaw, Fracture, Second International Conf. Fracture, Brighton, 1969, p. 620.
55. C. Q. Bowles and J. S. Schijve, International Journ. Fract., 9, 1973, p. 171.
56. W. L. Morris, O. Buck, and H. L. Marcus, Met. Trans., 7A, 1976, p. 1161.
57. J. Lankford, International Metals Review, 1977, p. 221.
58. J. Lankford, Eng. Fract. Mech., 9, 1977, p. 617.
59. J. Lankford, Int. Journ. of Fract., 12, 1976, p. 155.

REFERENCES (Continued)

60. F. de Kazinczy, J. Iron and Steel Instit., 207, 1969, p. 40.
61. F. de Kazinczy, Jernkont. Ann., 150, 1966, p. 493.
62. M. R. Mitchell, J. Eng. Matl. and Tech., Trans. ASME, 1977, p. 329.
63. M. R. Mitchell, Fracture Control Program Report No. 23, College of Engineering, Univ. of Illinois, 1976.
64. H. Neuber, Theory of Notch Stresses, Translated from the German (Kerbspannunglehre, 1937) by F. A. Raven, J. N. Edwards, Ann Arbor, Michigan, 1946.
65. R. E. Peterson, Stress Concentration Factors, Wiley & Son, New York, 1974.
66. D. V. Edmonds and C. J. Beevers, J. Matl. Science, 3, 1968, p. 457.
67. G. Harkegard, Engr. Fract. Mech., 6, 1974, p. 795.
68. Probabilistic Aspects of Fatigue, ASTM STP 511, R. A. Heller, ed., American Society for Testing and Materials, 1971.
69. E. Epremian and R. F. Mehl, Symposium on Fatigue with Emphasis on Statistical Approach - II, ASTM STP, 137, 1952.
70. F. A. McClintock, Metal Fatigue, Ed. G. Sines and J. L. Waisman, McGraw-Hill, New York, 1959, p. 112.
71. J. L. Swedlow and G. B. Sinclair, "Two Cases of Inclusion-Inclusion Interaction in a Ti Alloy," Dept. of Mechanical Engineering Report SM-77-7, Carnegie-Mellon University, 1977.
72. N. F. Fiore and D. R. Diercks, J. Eng. Matls. and Tech., Trans. ASME, 99, 1977, p. 29.
73. J. Waring, Met. Trans., 6, 1975, p. 1367.
74. J. Waring, B. Tomkins, and G. Summer, Fatigue at Elevated Temperature, ASTM STP 520, 1973, p. 123.
75. R. A. T. Dawson, W. J. Elder, G. J. Hill, and A. T. Price, Thermal and High Strain Fatigue, The Metals and Metallurgy Trust, London, 1967, p. 239.
76. C. H. Wells and C. P. Sullivan, Fatigue at High Temperature, ASTM STP 459, 1968, p. 59.
77. E. Smith and J. T. Barnby, Metal Science Journal, 1, 1967, p. 1.
78. J. Gittus, Thermal and High Strain Fatigue, The Metals and Metallurgy Trust, London, 1967, p. 142.

REFERENCES (Continued)

79. M. F. Day and G. B. Thomas, "Characterization of Low Cycle Fatigue by the Strainrange Partitioning Method," AGARD CP-242, 1978, p.
80. J. M. Hyzak and H. L. Bernstein, "Characterization of Low Cycle Fatigue by the Strainrange Partitioning Method," AGARD CP-243, 1978; also published as AFML-TR-78-174, Air Force Materials Laboratory, 1978.
81. D. McLean, J. Inst. Metals, 85, 1956-1957, p. 468.
82. H. D. Williams, Acta Met., 16, 1968, p. 771.
83. F. Garafalo, Fundamentals of Creep and Creep Rupture, MacMillian New York, 1965, p. 241.
84. D. McLean, Mechanical Properties of Metals, Wiley & Son, New York, 1962, p. 327.
85. R. Raj, J. Eng. Matl. and Tech., Trans. ASMA, 1976, p. 132.
86. S. S. Manson, Fatigue at Elevated Temperature, ASTM STP 520, American Society for Testing and Materials, 1978, p. 744.
87. L. F. Coffin, Jr., 1976 ASME-MPC Symposium on Creep-Fatigue Interaction, MPC-3, ASME, New York, 1976, p. 349.
88. W. J. Ostergren, 1976 ASME-MPC Symposium on Creep-Fatigue Interaction, MPC-3, ASME, New York, 1976, p. 179.
89. S. Majumdar and P. S. Maiya, 1976 ASME-MPC Symposium on Creep-Fatigue Interaction, MPC-3, ASME, New York, 1976, p. 179.
90. "Time Dependent Fatigue of Structural Alloys - A General Assessment (1975)," W. L. Greenstreet, ed., Oak Ridge National Laboratory Report ORNL 5073, 1977.
91. H. L. Bernstein, "An Evaluation of Four Current Models to Predict Creep-Fatigue Interactions in Rene 95," AFML-TR-79-4114, 1979.
92. "Analysis of Prediction Methods for Time-Dependent Fatigue Crack Initiation in Nickel-Base Superalloys," NMAB-347, National Materials Advisory Board, National Academy of Sciences, 1979.
93. J. L. Bartos, "Development of a Very High Strength Disk Alloy for 1400°F Service," AFML-TR-74-187, 1974.
94. B. A. Cowles, D. L. Sims, and J. R. Warren, "Evaluation of the Cyclic Behavior of Aircraft Turbine Disk Alloys," NASA Report CR-159409, 1978.
95. V. Shahani and H. G. Popp, "Evaluation of Cyclic Behavior of Aircraft Turbine Disk Alloys," NASA Report CR-159433, 1978.

REFERENCES (Continued)

96. B. A. Cowles, Pratt & Whitney Aircraft, GPD; Personal Communication.
97. S. S. Manson, Experimental Mechanics, 5, 1965, p. 193.
98. J. Schijve, Fatigue Crack Propagation, ASTM STP 415, American Society for Testing and Materials, 1967, p. 415.
99. G. C. Smith, Proc. Royal Society, A-242, 1957, p. 189.
100. P. Neumann, Acta Met., 22, 1974, p. 1155.
101. R. J. Bucci, P. C. Paris, R. W. Hertzberg, R. A. Schmidt, and A. F. Anderson, Stress Analysis and Growth of Cracks, American Society for Testing and Materials, ASTM STP 513, 1971, p. 125.
102. J. H. Westbrook, G. Bellows, M. Field, and J. F. Kahles, The Superalloys, Ed. C. T. Sims and W. C. Hagel, Wiley & Sons, New York, 1972, p. 557.
103. Residual Stress Measurements by X-Ray Diffraction, M. E. Hilley, Ed., SAE J784a, Soc. of Automotive Engrs., 1971.
104. S. M. Copley and B. H. Kear, Trans. AIME, 239, 1967, p. 984.
105. S. S. Manson, Thermal Stresses and Low Cycle Fatigue, McGraw-Hill, New York, 1966.
106. C. Laird and D. J. Duquette, Corrosion Fatigue, NACE-2, 1972, p. 88.
107. A. H. Cottrell, Dislocations and Plastic Flow in Crystals, Oxford, Clarendon Press, 1953, p. 86.
108. J. R. Rice, Fatigue Crack Propagation, ASTM STP 415, American Society for Testing and Materials, 1967, p. 247.
109. G. R. Irwin, Structural Mechanics, Proceedings of 1st Navel Symposium, Pergamon Press, 1960, p. 557.
110. F. A. McClintock and G. R. Irwin, Applied Fracture Mechanics, ASTM STP 381, American Society for Testing and Materials, 1965, p. 84.
111. D. S. Dugdale, J. Mech. Phys. Sol., 8, 1960, p. 100.
112. J. R. Rice, J. Appl. Mech., Trans. ASME, 1968, p. 370.
113. J. A. Bagley and J. D. Landes, Fracture Toughness, ASTM STP 514, American Society for Testing and Materials, 1971, p. 1.
114. D. F. Mowbray, Cracks and Fracture, ASTM STP 601, American Society for Testing and Materials, 1976, p. 33.

REFERENCES (Concluded)

115. C. Calabrese and C. Laird, *Matl. Sci. and Engr.*, 13, 1974, p. 141.
116. C. Calabrese and C. Laird, *Matl. Sci. and Engr.*, 13, 1974, p. 159.
117. C. Calabrese and C. Laird, *Met. Trans.*, 5, 1974, p. 1785.
118. R. E. Stoltz and A. G. Pineau, *Matl. Sci. and Engr.*, 34, 1978, p. 275.
119. J. C. Grosskreutz, *Phys. Stat. Sol.*, 47(b), 1971, p. 359.
120. W. Elber, *Engr. Fract. Mech.*, 2, 1970, p. 37.
121. W. Elber, Damage Tolerance in Aircraft Structures, ASTM STP 486, American Society for Testing and Materials, 1971, p. 230.
122. G. R. Irwin, *J. Appl. Mech.*, 29, Trans. Amer. Soc. Mech. Eng., 84, Series E, 1962.
123. P. Benthern and W. T. Koiter, Methods of Analysis of Crack Problems, G. C. Sih, ed., Noordhoff International, 1972.
124. C. F. Tiffany and J. N. Masters, Applied Fracture Mechanics, ASTM STP 381, American Society for Testing and Materials, 1964.
125. B. D. Cullity, Elements of X-Ray Diffraction, Addison-Wesley, Reading, Mass., 1967.
126. D. L. Sims, "Evaluation of Crack Propagation in an Advanced P/M Superalloy, AF2-1DA," AFML Technical Report, to be published.
127. P. C. Paris, Fracture Mechanics In The Elastic-Plastic Regime, ASTM STP 631, American Society for Testing and Materials, 1977, p. 3.
128. T. H. Topper and M. H. El Haddad, *Canadian Met. Quart.*, 18, 1979, p. 207.
129. N. E. Dowling, Cracks and Fracture, ASTM STP 601, American Society for Testing and Materials, 1976, p. 19.
130. F. Rotvel, "Symposium on Random Load Fatigue", AGARD-CP-118, 1972.

APPENDIX A
NOMINAL COMPOSITION OF SUPERALLOYS; WT. PERCENT

Alloy Designation	C	Mn	Si	Cr	Ni	Co	Mo	W	Nb	Fe	Ti	Al	B	Zr	Other
(Cast Alloys)															
Alloy 713C	0.12	-	-	12.5	bal	-	4.2	-	2.0	-	0.8	6.1	0.012	0.10	-
IN-100	0.18	-	-	10.0	bal	15.0	3.0	-	-	-	4.7	5.5	0.014	0.06	1.0V
Mar-M200	0.15	-	-	9.0	bal	10.0	-	12.5	1.0	-	2.0	5.0	0.015	0.005	-
(Wrought Alloys)															
Nimonic 80A	0.06	0.10	0.70	19.5	bal	1.1	-	-	-	-	2.5	1.3	-	-	-
Nimonic 90	0.07	0.50	0.70	19.5	bal	18.0	-	-	-	-	2.4	1.4	-	-	-
René 95	0.15	0.10	0.10	14.0	bal	8.0	3.5	3.6	3.5	0.13	2.5	3.6	0.012	0.04	-
Udimet 500	0.08	-	-	18.0	bal	18.5	4.0	-	-	-	2.9	2.9	0.006	0.05	-
Udimet 700	0.08	-	-	15.0	bal	18.5	5.2	-	-	-	3.5	4.3	0.030	-	-

APPENDIX B
FATIGUE DATA

LEGEND

20cpm	Continuously cycling, 20 cpm frequency
0.2cpm	Continuously cycling, 0.2 cpm frequency
60cpm	Continuously cycling, 60cpm frequency
1-0	Cyclic dwell, 1 minute hold in tension
5-0	Cyclic dwell, 5 minute hold in tension
0-1	Cyclic dwell, 1 minute hold in compression
0-5	Cyclic dwell, 5 minute hold in compression

AF-115 Data	200 series	As HIP
	700	
	900	
	500 series	HIP & Forged

AF2-1DA Data	100 series	Pancake 1
	200 series	Pancake 2

AF-115

SPEC. NO.	TYPE OF TEST	A-RATIO	TOTAL STRAIN -RANGE (%)	CYCLES TO FAILURE	INEL. STRAIN -RANGE (%)	MAX. TENSILE STRESS (KSI)	MAX. COMPR. STRESS (KSI)	RELAXED TENSILE STRESS (KSI)	RELAXED COMPR. STRESS (KSI)	TIME TO FAILURE (HOURS)	ELASTIC* MODULJS	TEMP (F)
701	20CPM	+1	1.10	626	.13000	137.6	110.5	0.00	0.00	.52	25.3	1400
201	20CPM	+1	.90	883	.05000	137.0	85.3	0.00	0.00	.74	24.0	1400
702	20CPM	+1	.90	1226	.05000	135.7	89.0	0.00	0.00	1.02	26.9	1400
703	20CPM	+1	.80	3422	.03000	137.4	56.2	0.00	0.00	2.85	24.4	1400
202	20CPM	+1	.70	2153	.02000	133.6	40.0	0.00	0.00	1.79	24.5	1400
707	20CPM	+1	.70	6036	.01500	132.1	43.7	0.00	0.00	5.00	25.2	1400
905	20CPM	+1	.60	13463	.01500	134.5	12.6	0.00	0.00	11.22	23.9	1400
705	20CPM	+1	.60	14472	.01000	130.3	23.9	0.00	0.00	12.06	25.4	1400
709	20CPM	+1	.50	18820	.01700	123.0	4.0	0.00	0.00	15.68	25.5	1400
712	20CPM	+1	.51	27723	.01500	119.6	11.5	0.00	0.00	23.10	24.9	1400
706	.2 CPM	+1	1.30	215	.26000	141.9	140.4	0.00	0.00	17.92	25.1	1400
203	.2 CPM	+1	1.10	73	.30000	104.0	100.8	0.00	0.00	6.08	23.1	1400
708	.2 CPM	+1	1.00	524	.10500	130.3	111.5	0.00	0.00	43.67	25.4	1400
901	.2 CPM	+1	1.00	680	.09500	137.7	104.0	0.00	0.00	56.67	25.7	1400
906	.2 CPM	+1	.90	929	.10000	115.8	92.6	0.00	0.00	77.42	24.8	1400
704	.2 CPM	+1	.90	1495	.08000	123.5	95.6	0.00	0.00	124.58	25.2	1400
710	.2 CPM	+1	.80	3178	.11000	106.5	78.9	0.00	0.00	264.80	25.8	1400
907	.2 CPM	+1	.71	2908	.09500	89.6	67.4	0.00	0.00	242.30	23.7	1400
711	.2 CPM	+1	.70	3848	.04000	103.8	59.4	0.00	0.00	316.40	23.3	1400
914	1-0	+1	1.00	1270	.13000	114.6	141.8	12.00	0.00	22.23	26.9	1400
917	5-0	+1	1.00	1553	.14600	85.6	145.7	14.00	0.00	130.71	24.6	1400
918	5-0	+1	.80	2504	.14000	61.8	129.4	11.10	0.00	208.33	26.2	1400
912	5-0	+1	.80	8082	.10500	61.9	131.7	9.98	0.00	673.50	25.5	1400
915	0-1	+1	1.00	419	.15500	147.7	101.2	0.00	7.18	7.33	27.1	1400
916	0-5	+1	.80	1310	.04850	139.7	53.9	0.00	2.99	109.17	24.6	1400
204	20CPM	+1	1.10	1096	.07000	155.6	115.6	0.00	0.00	.91	24.8	1200
908	20CPM	+1	.90	2501	.02000	152.6	75.7	0.00	0.00	2.10	24.8	1200
205	20CPM	+1	.80	2860	.02000	147.7	65.1	0.00	0.00	2.38	26.3	1200
909	20CPM	+1	.70	4082	.01000	140.5	40.5	0.00	0.00	3.40	25.4	1200
206	20CPM	+1	.60	20808	.02000	140.0	20.8	0.00	0.00	17.34	26.2	1200
207	.2 CPM	+1	1.10	495	.06000	151.4	119.5	0.00	0.00	41.25	25.2	1200
911	.2 CPM	+1	.90	1387	.06500	149.1	91.4	0.00	0.00	115.58	27.6	1200
208	.2 CPM	+1	.80	4085	.03000	155.7	50.7	0.00	0.00	340.42	26.5	1200
209	20CPM	+1	.90	9000	.03500	159.6	115.1	0.00	0.00	7.50	31.0	70
210	20CPM	+1	.60	12672	.00600	154.5	36.1	0.00	0.00	10.56	31.8	70
718	60CPM	+1	.44	51156	.00010	134.0	5.1	0.00	0.00	14.02	31.0	70
520	20CPM	+1	1.10	468	.11000	140.2	108.1	0.00	0.00	.39	25.4	1400
507	20CPM	+1	.90	763	.04500	141.6	81.9	0.00	0.00	.64	25.0	1400
502	20CPM	+1	.90	1172	.03500	156.6	86.5	0.00	0.00	.98	26.4	1400
508	20CPM	+1	.80	2068	.03500	142.3	56.9	0.00	0.00	1.72	24.9	1400
509	20CPM	+1	.70	5920	.02500	136.4	38.6	0.00	0.00	4.93	25.0	1400
503	20CPM	+1	.70	7221	.01500	142.2	39.9	0.00	0.00	6.02	24.5	1400
505	20CPM	+1	.60	17257	.01000	138.6	12.8	0.00	0.00	14.40	24.1	1400
510	20CPM	+1	.60	21302	.01500	126.5	25.7	0.00	0.00	17.75	25.0	1400
518	20CPM	+1	.50	130215	.01000	101.2	17.4	0.00	0.00	108.50	24.1	1400

* x 10⁶ psi

AF-115 (Concluded)

SPEC. NO.	TYPE OF TEST	A- RATIO	TOTAL STRAIN -RANGE (%)	CYCLES TO FAILURE	INEL. STRAIN -RANGE (%)	MAX. TENSILE STRESS (KSI)	MAX. COMPR. STRESS (KSI)	RELAXED TENSILE STRESS (KSI)	RELAXED COMPR. STRESS (KSI)	TIME TO FAILURE (HOURS)	ELASTIC* MODULJS	TEMP (F)
516	.2 CPM	+1	1.30	80	.25000	140.4	134.0	0.00	0.00	6.67	24.0	1400
512	.2 CPM	+1	1.10	220	.11500	139.2	122.0	0.00	0.00	18.30	25.0	1400
504	.2 CPM	+1	1.10	274	.14000	133.1	119.5	0.00	0.00	22.83	24.1	1400
513	.2 CPM	+1	.90	1097	.16000	96.4	84.5	0.00	0.00	91.42	23.9	1400
506	.2 CPM	+1	.90	1593	.09000	119.3	85.5	0.00	0.00	135.92	24.0	1400
514	.2 CPM	+1	.80	2474	.11000	84.6	91.0	0.00	0.00	206.20	24.3	1400
515	.2 CPM	+1	.70	4059	.07000	92.2	75.9	0.00	0.00	338.25	25.9	1400
526	1-0	+1	1.00	1293	.12000	99.8	135.7	11.00	0.00	22.63	24.8	1400
528	5-0	+1	1.00	625	.19250	79.0	151.7	19.20	0.00	52.60	25.4	1400
527	0-1	+1	1.00	420	.14250	147.7	96.8	0.00	6.99	7.36	25.2	1400

* x 10⁶ psi

AF2-1DA

SPEC. NO.	TYPE OF TEST	A-RATIO	TOTAL STRAIN -RANGE (%)	CYCLES TO FAILURE	INEL. STRAIN -RANGE (%)	MAX. TENSILE STRESS (KSI)	MAX. COMPR. STRESS (KSI)	RELAXED TENSILE STRESS (KSI)	RELAXED COMPR. STRESS (KSI)	TIME TO FAILURE (HOURS)	ELASTIC* MODULUS	TEMP (F)
202	20CPM	+1	1.30	285	.29000	141.9	145.2	0.00	0.00	.24	25.8	1400
122	20CPM	+1	1.10	688	.13000	131.6	123.3	0.00	0.00	.57	25.2	1400
208	20CPM	+1	1.10	732	.21000	127.2	116.1	0.00	0.00	.61	26.5	1400
219	20CPM	+1	.90	1640	.07500	127.2	99.4	0.00	0.00	1.37	25.5	1400
207	20CPM	+1	.80	2693	.07000	122.5	75.1	0.00	0.00	2.24	26.3	1400
224	20CPM	+1	.75	3465	.03500	124.4	59.7	0.00	0.00	2.90	25.6	1400
225	20CPM	+1	.70	3365	.03500	123.7	64.0	0.00	0.00	2.82	27.4	1400
201	20CPM	+1	.70	7104	.02000	123.3	56.4	0.00	0.00	5.92	25.7	1400
215	20CPM	+1	.64	10448	.01500	123.3	39.7	0.00	0.00	8.70	26.1	1400
211	20CPM	+1	.64	13228	.03400	119.3	44.9	0.00	0.00	11.00	25.2	1400
121	20CPM	+1	.65	14823	.02000	110.5	47.4	0.00	0.00	12.35	24.3	1400
209	20CPM	+1	.60	26638	.01500	112.1	44.2	0.00	0.00	22.20	25.9	1400
213	20CPM	+1	.60	47974	.01500	103.8	47.7	0.00	0.00	39.98	25.3	1400
221	20CPM	+1	.55	50260	.01500	112.1	31.0	0.00	0.00	41.88	26.7	1400
205	20CPM	+1	.50	84724	.01600	115.3	15.9	0.00	0.00	70.60	27.0	1400
231	.2 CPM	+1	1.30	358	.39000	128.0	123.7	0.00	0.00	29.80	24.8	1400
232	.2 CPM	+1	1.10	608	.32000	114.1	111.3	0.00	0.00	50.67	27.6	1400
204	.2 CPM	+1	1.10	630	.25000	119.3	115.3	0.00	0.00	52.50	26.2	1400
233	.2 CPM	+1	.90	1173	.17000	110.5	91.5	0.00	0.00	97.75	26.0	1400
210	.2 CPM	+1	.80	2346	.12000	103.4	81.5	0.00	0.00	195.50	24.7	1400
228	.2 CPM	+1	.70	3442	.04000	98.6	60.4	0.00	0.00	286.80	23.8	1400
239	1-0	+1	1.00	771	.18000	99.4	132.4	15.90	0.00	13.49	26.0	1400
125	5-0	+1	1.00	1221	.21000	92.2	130.9	16.30	0.00	101.80	26.2	1400
107	5-0	+1	.85	1036	.12000	82.5	130.6	13.60	0.00	86.33	26.6	1400
241	5-0	+1	.85	1794	.12000	82.3	125.3	10.70	0.00	149.50	25.8	1400
235	0-1	+1	1.00	433	.19000	135.2	92.2	0.00	13.50	7.25	25.6	1400
243	0-5	+1	.85	802	.09000	131.2	71.6	0.00	6.80	66.80	25.3	1400
230	20CPM	+1	1.15	731	.16000	142.1	142.1	0.00	0.00	.61	27.7	1200
212	20CPM	+1	1.00	1326	.12000	137.1	124.3	0.00	0.00	1.10	27.6	1200
238	20CPM	+1	.94	2015	.04500	132.9	115.4	0.00	0.00	1.68	26.8	1200
237	20CPM	+1	.90	3345	.03000	136.1	81.4	0.00	0.00	2.79	24.7	1200
222	20CPM	+1	.85	3817	.02000	131.7	83.9	0.00	0.00	3.18	25.2	1200
203	20CPM	+1	.71	6137	.01300	128.0	70.8	0.00	0.00	5.10	27.7	1200
216	20CPM	+1	.66	9706	.01500	131.3	59.9	0.00	0.00	8.89	28.0	1200
234	20CPM	+1	.62	29662	.00800	130.0	47.5	0.00	0.00	24.70	28.0	1200
218	20CPM	+1	.57	38402	.01000	131.7	23.2	0.00	0.00	32.10	26.7	1200
217	.2 CPM	+1	1.00	902	.08000	147.7	117.8	0.00	0.00	75.20	27.1	1200
236	.2 CPM	+1	.80	4819	.03800	136.5	58.7	0.00	0.00	401.58	24.0	1200
242	5-0	+1	.85	3641	.04000	109.0	115.8	5.20	0.00	303.42	26.4	1200
244	0-5	+1	.85	4005	.03000	135.7	69.9	0.00	2.00	333.75	23.7	1200
119	20CPM	+1	.90	6539	.14000	140.4	121.6	0.00	0.00	5.45	33.3	70
120	20CPM	+1	.60	47406	.01200	142.9	44.0	0.00	0.00	39.50	31.0	70

*X 10⁶ psi

APPENDIX C STRESS CONCENTRATION FACTOR CALCULATIONS

SURFACE FLAW

Irwin (Reference 122) has described the opening stress intensity solution for a part-through elliptical crack (surface flaw) as shown in Figure 84a as:

$$K_I = A \sigma \sqrt{11} \sqrt{\frac{a}{Q}} \quad (C-1)$$

where A, Q constants

σ farfield tensile stress

a crack depth.

For the particular case of a flaw with an aspect ratio, $a/2c$, equal to 0.5 and an applied stress equal to the yield stress, the solution is (Reference 123):

$$K_I = 1.1 \sigma \sqrt{\pi} \sqrt{\frac{a}{2.25}} \quad (C-2)$$

Using this equation, the values of the stress intensity factors for surface cracks of various lengths have been calculated using values for the farfield tensile stress of 903 MPa and 1027 PMA for AF2-1DA and AF-115, respectively. The results are contained in Table C-1.

INTERNAL CRACK

The opening stress intensity solution for an internal circular crack in a round bar (Figure 84b) has been determined to be (Reference 124):

$$K_I = \sigma_{\text{net}} \sqrt{\pi a} F_1 (a/b)$$

AFWAL-TR-80-4063

where $F_1 (a/b)$ is the shape factor. For $(a/b) = .032$, the solution reduced to

$$K_I = \sigma_{\text{net}} \sqrt{\pi a} (.65)$$

The stress intensity values for a .010 inch crack at stresses equal to the yield stress are presented in Table C-1.

TABLE C-1
STRESS INTENSITY CALCULATIONS

	a, Crack Depth		K_I^*	
	<u>cm (inches)</u>		<u>MPa \sqrt{m}, (ksi \sqrt{in})</u>	
SURFACE CRACK				
AF2-1DA	.010	(.004)	11.9	(10.8)
	.0025	(.001)	5.9	(5.4)
	.005	(.002)	8.4	(7.6)
AF-115	.010	(.004)	13.5	(12.3)
	.0025	(.001)	6.7	(6.1)
	.005	(.002)	9.5	(8.7)
INTERNAL CRACK				
AF2-1DA	.010	(.004)	7.4	(6.7)
AF-115	.010	(.004)	8.5	(7.7)

* K_I calculated using farfield stress level equal to the yield stress for the alloy at 760°C.